To the University of Wyoming:

The members of the Committee approve the thesis of Kedar A. Malusare presented on 3/13/2014.

Dr. Ray S. Fertig, Chairperson

Dr. Victor E. Ginting, External Department Member

Dr. Mark. R. Garnich

APPROVED:

Paul A. Dellenback, Head, Department of Mechanical Engineering.

Dr. Khaled A.M. Gasem, Dean, College of Engineering and Applied Science.

Malusare, Kedar A., <u>Energy Conserving Stresses to Predict Composite Failure</u>, M.S., Department of Mechanical Engineering, May,2014.

The complexity of the multiple failure mechanisms exhibited by unidirectional fibrous composites makes failure prediction a daunting challenge for the analyst. One approach to better identify failure mechanisms has been the use of volume average constituent stresses of the composite and directly predicting constituent failure. However, the total strain energy is not conserved by volume average constituent quantities (stresses and strains). To address this, this missing energy, termed interaction energy, was quantified as a function of loading, material properties, and fiber volume fraction. It was concluded that the stress/strain fluctuations of the matrix constituent were the major cause of interaction energy. Consequently, an energy conserving matrix stress metric was developed to attempt to improve failure load predictions. This energy consistent matrix stress was then used with an existing failure theory to predict failure loads of unidirectional fiber reinforced laminae subjected to biaxial and tri-axial load states.

ENERGY CONSERVING STRESSES TO PREDICT COMPOSITE FAILURE

by

Kedar A. Malusare

A thesis submitted to the Department of Mechanical Engineering

and the University of Wyoming

in partial fulfillment of the requirements

for the degree of

MASTER OF SCIENCE

in

MECHANICAL ENGINEERING

Laramie, Wyoming

May, 2014

UMI Number: 1561307

UMI

Dissertation Publishing

UMI 1561307

ProQuest®

DEDICATION PAGE

I would like to dedicate this thesis to my parents Anant and Jyoti Malusare and my younger brother Omkar Malusare.

ACKNOWLEDGEMENTS

I would like to thank my advisor Dr. Ray Fertig for believing in my abilities and giving me the opportunity of pursuing research in the field of composites materials. I would also like to thank Dr. Mark Garnich and Dr. Victor Ginting for providing their valuable inputs to this thesis. Last but not the least, I would like to thank my companion Aditi Anand. Without her support, my journey through research would have indeed been very difficult.

TABLE OF CONTENTS

LIST OF FIGURES

ix

LIST OF TABLES

1. Introduction to composite materials

1.1 What are composite materials?

Composite materials are defined as heterogeneous mixtures that are obtained by bonding two or more homogeneous phases. A careful observation would reveal that composite materials have always been present in nature. Perhaps the most commonly used composite material that is present in nature is wood, which has long fibers of cellulose that provide strength that are held together by a much weaker substance called lignin which acts as the glue that bonds and holds the fibers in place (Rowell, 2012). Other natural composites include bones, teeth and plant leaves. Recent studies on spider silk have shown that it also is a composite consisting of a gel core enfolded by a solid hollow structure (Mukhopadhyay and Sakthivel, 2005; Vollrath et al., 1996). This suggests that Mother Nature has been far ahead of humans in exploiting the benefits of composites. The beginning of manmade composite materials can be traced back to the early Egyptian civilization c. 4000 B.C. (Herakovich, 2012). They made papyrus paper by laying strips from the fibrous papyrus plant into two layers with each layer at right angles to the other. In addition, they made bricks from mud and then reinforced them with straw to provide strength (Nicholson and Shaw, 2000). Over time other manmade composite materials like concrete and papier-mâché were produced and used all over the world. In 1939, continuous glass fibers were produced commercially (Knox, 1982) for high temperature electrical applications . After two more decades fibers from boron (Talley, 2004) and carbon (Timot, 1961) were produced. The history of modern composite materials thus begins in the second half of the 20th century when lightweight fibers were embedded in polymeric resins to obtain novel materials having superior material properties and durability.

1.2 Advantages of fibrous composite materials

Compared to conventional homogeneous metals, fibrous composites offer many advantages that make them attractive alternatives for designers to consider. Unquestionably, the most cited advantage of fibrous composites is their high specific stiffness and high specific strength as compared to conventional engineering materials. These properties translate into significant improvement in performance and reduction in consumption of energy. Unlike isotropic engineering materials like metals, properties of composites are often anisotropic. As a result composite materials can be designed to have desired properties in one direction without having to overdesign in other directions, which leads to significant weight savings. Use of composites also increases fatigue life and corrosion resistance of final products (Herakovich, 2012). Due to these advantages composite materials have found applications in various industries like aerospace, automotive, sports, wind energy, and athletic and recreational equipment.

1.3 Unidirectional fiber reinforced polymers

Unidirectional fiber reinforced polymers (UD FRPs) are a special class of composite materials that are produced by embedding long, lightweight fibers in a polymeric resin called the matrix. The most commonly used fibers include glass and carbon/graphite which are inlaid in thermoset epoxies. A unidirectional lamina, the most basic form of continuous fiber reinforced polymers is shown in Fig. 1. The lamina or ply is a flat arrangement of unidirectional fibers in a matrix. The fibers are the principal load carrying entities and are generally very strong and stiff as compared to the matrix. The matrix provides support and protection to the fibers. Another important function of the matrix is to provide a means of distributing load among and transmitting load between the fibers. The stiffness and strength of the lamina in the fiber
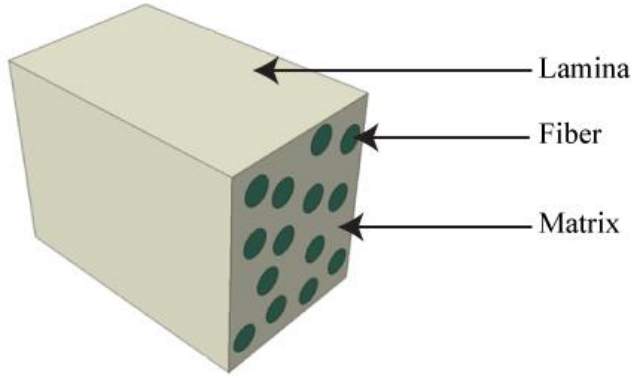
Figure 1: Unidirectional lamina

direction is typically much greater than in the transverse directions. Generally, the properties of a

unidirectional lamina are orthotropic, with different properties in the material principal

directions. The three-dimensional elastic constants for an orthotropic unidirectional lamina

consist of the following independent in-plane and through thickness properties:

$E_1, E_2, E_3, G_{12}, G_{13}, G_{23}, \nu_{12}, \nu_{13}$ and ν_{23} where 1, 2 and 3 represent the three mutually independent

material directions. It is usually assumed that a unidirectional fiber reinforced lamina can be

treated as being transversely isotropic which reduces the independent elastic constants to five

since $E_2 = E_3$, $G_{12} = G_{23}$, $\nu_{12} = \nu_{13}$ and $G_{23} = E_2 / 2(1 + \nu_{23})$. Transverse isotropy also reduces the

independent strength values to six as compared to nine for fully orthotropic materials. These are

longitudinal and compressive strengths S_{1T}, S_{1C}, transverse tensile and compressive strengths

S_{2T}, S_{2C}, longitudinal shear strength S_{12} and transverse shear strength S_{23}. In practical

applications, laminates with fibers oriented in only one direction are a rarity. Even though

unidirectional laminates (fibers oriented only in one direction) are extremely strong and stiff in

the fiber direction, they are very weak in the transverse direction and under shear loads because the load is carried by the much weaker polymer matrix. In order to make the final product stronger in the non-fiber directions, unidirectional laminae with fibers oriented in different directions are stacked on top of one another and the final layup is called a composite laminate as shown in Fig. 2. The resulting laminates are much stronger in the non-fiber directions and also have a higher shear load carrying capacity than their constituent laminae considered individually.
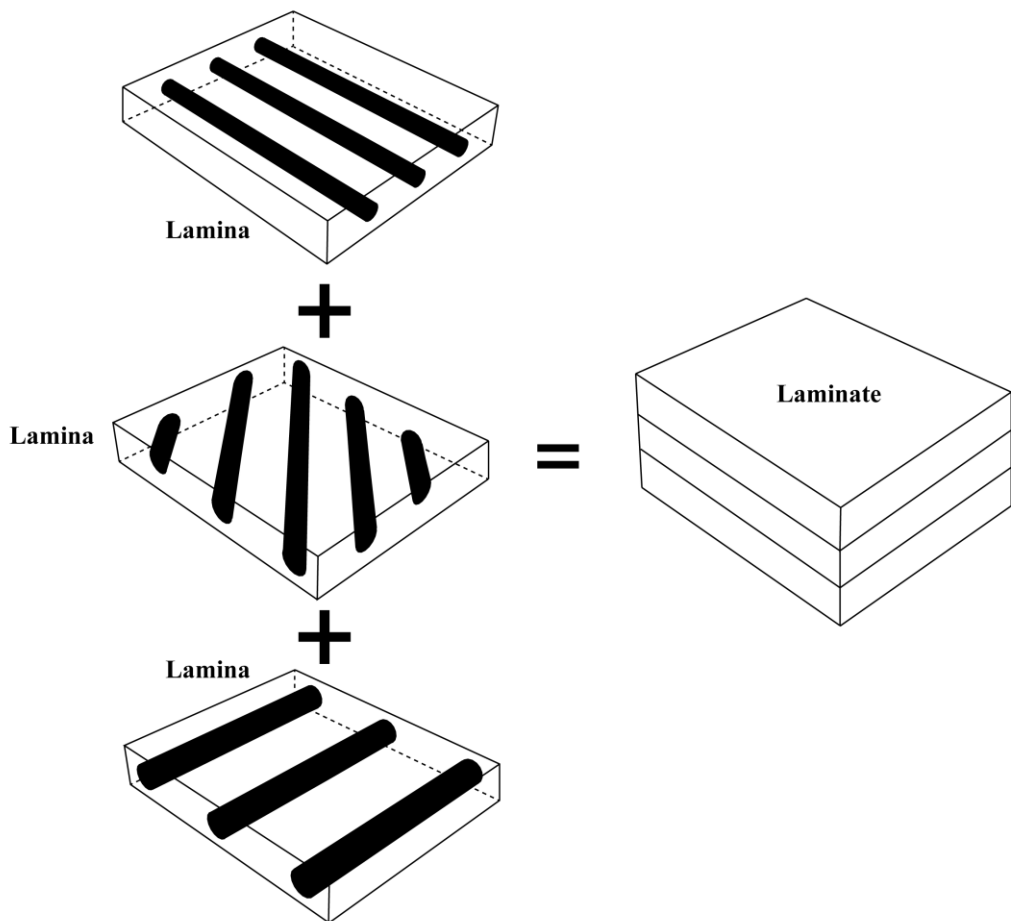
Figure 2: Synthesis of a laminate from individual laminae

1.4 Failure of unidirectional fiber reinforced polymers

Failure in unidirectional (UD) fiber reinforced polymers may occur due a variety of mechanisms at the constituent level including: fiber fracture, fiber buckling (kinking), fiber splitting, fiber pullout, fiber/matrix debonding, matrix cracking and matrix yielding. Fiber fracture involves breaking of the continuous fibers into two or more distinct segments and is the most catastrophic of failure mechanics since the fibers are the primary load-carrying agents in UD fiber reinforced polymers. This type of fiber failure is typically due to tensile stress in the fiber direction. Fiber fracture accompanied by fiber/matrix debonding causes fiber pullout. Axial compressive loading causes buckling of the fibers. Matrix cracking results from transverse or shear loads that exceed the strength of the matrix. Since UD fiber reinforced polymers are widely used in many applications it is very important to understand composite failure mechanisms to improve safety and reliability of composite products. The majority of failure theories analyze a composite laminate on a ply-by-ply basis. These theories try to predict the failure of one of the plies of the laminate which is termed as first ply or initial failure after which, the properties of the failed lamina are degraded such that its load carrying capacity is significantly decreased and the remaining un-failed laminae carry more loads. Final or catastrophic failure occurs when all the laminae of the laminate have failed and the laminate can no longer support any load. Based on the type of quantities that the failure methodologies use, they can be classified into mesomechanics based or micromechanics based. Mesomechanics based failure techniques use quantities (stresses/strains) that are averaged over the entire volume of the lamina to assess failure. A major drawback of using volume average lamina quantities is that they do not accurately represent the true stress/strain state in the constituents of the lamina. As shown in Fig. 3 a composite lamina was subjected to a transverse load of 40 MPa, which generated stresses in

5

the fiber and matrix constituents. The volume average stress in the transverse direction in the fiber constituent is about 46 MPa and is about 32 MPa in the matrix constituent. Moreover, the stresses in the longitudinal and the through thickness directions in the constituents was non-zero
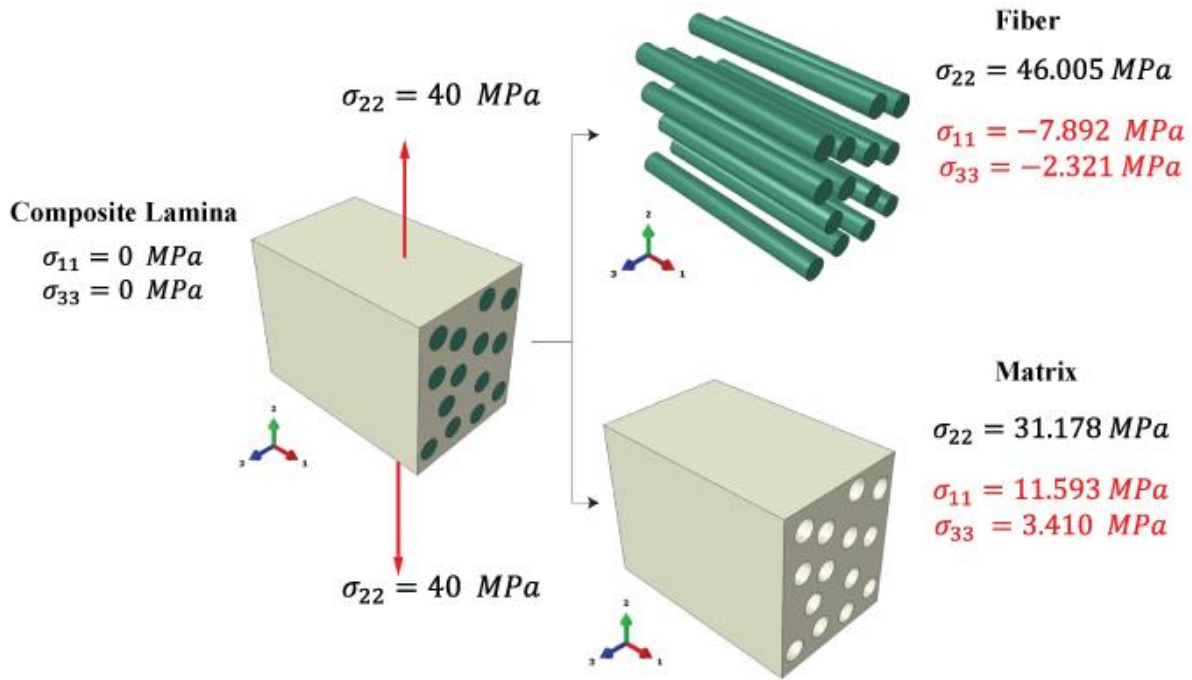
Figure 3: Difference in volume average lamina stresses and constituent level stresses

even in the absence of such volume average stresses in the lamina. These stresses are self-equilibrating and so do not appear on the lamina scale. This suggests that volume average constituent stresses as opposed to volume average lamina stresses are much more accurate in describing the true stress/strain state in the constituent. Since failure of a lamina initiates at the constituent level, it is important to predict failure of the constituent to assess failure of a lamina. Moreover, since constituent level stresses more accurately describe the stress/strain state in the

constituents, volume average constituent level stresses are a better choice than lamina-averaged stresses for failure prediction.

1.5 A Representative Volume Element (RVE)

In real microstructures of unidirectional fiber reinforced composites, fibers are distributed randomly in the matrix. Figure 4(a) shows an SEM image (De Oliveira et al., 2009) with the fibers colored gray that are distributed randomly in the matrix which is colored black. In the theoretical analysis of composite materials, a Representative Volume Element (RVE), also called

| (a) | (b) | (c) |
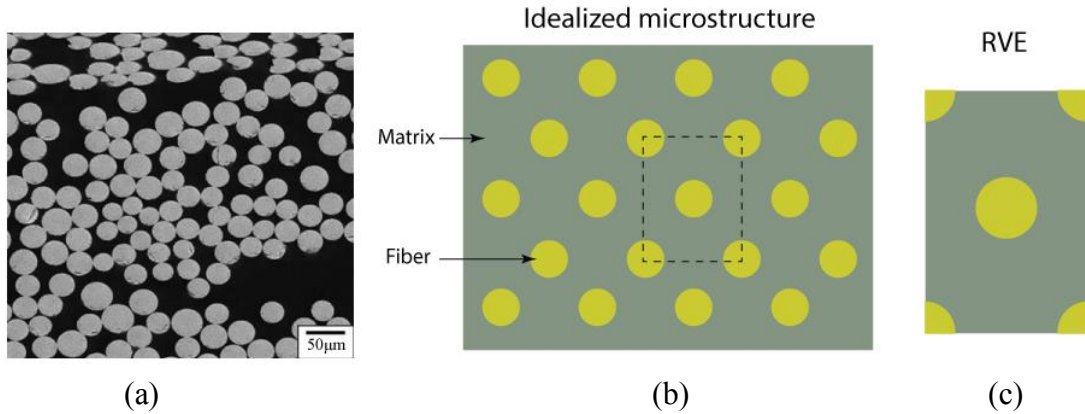
Figure 4: Idea of a Representative Volume Element

a unit cell, can be defined as the smallest volume over which the measurements of average stress and strain and properties like fiber volume fraction, moduli etc. will yield a values that are representative of the whole of the composite (Hashin, 1983; Hill, 1963). For the work in this thesis, it was assumed that the fibers were packed in a hexagonal array in the matrix as shown in Fig. 4(b) and a Representative Volume Element (RVE) of this idealized microstructure as shown in Fig. (c) was used to study the behavior of unidirectional fiber reinforced composites. To produce homogeneous fields, the RVE was subjected to periodic boundary conditions (Appendix

7

A). The use of an RVE with hexagonal fiber packing not only offered significant reduction in computational costs but provided similar volume average quantities as compared to an RVE with a random distribution of fibers.

1.6 Distribution of stresses and strain in the constituents of a composite material

Figure 5 shows comparison of volume average stresses in the RVEs of a homogeneous material like steel and an in-homogeneous composite material consisting of fibers made of carbon that are embedded in an epoxy matrix. Both the RVEs were subjected to a transverse load of 10 MPa and volume average stresses were computed. The volume average stress in the
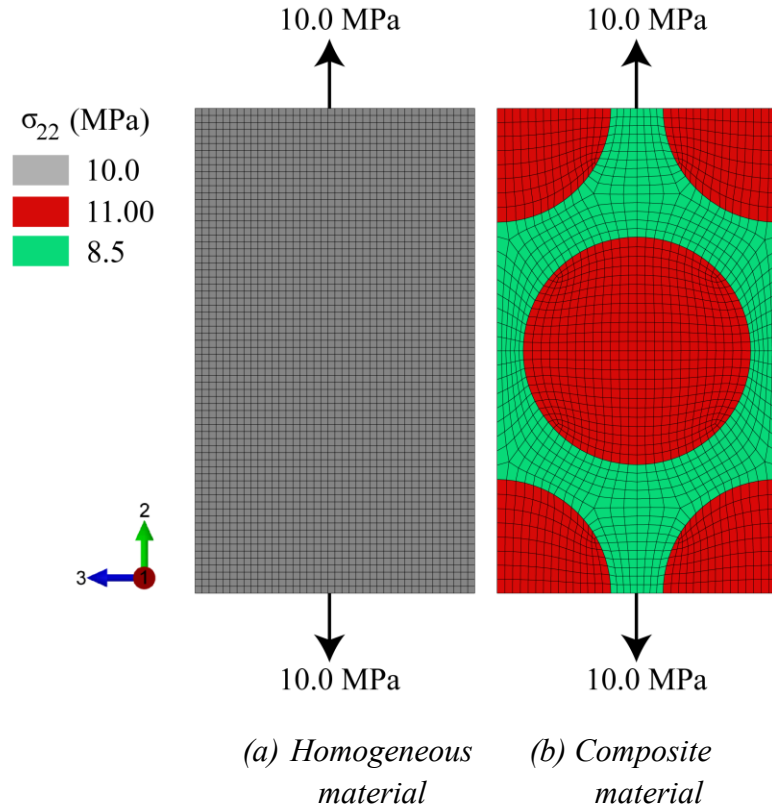
Figure 5: Comparison of volume average stresses in a homogeneous and a composite material

load direction in the homogeneous material equals the applied load but for the in-homogeneous material, the volume average stress in the load direction is different for the two constituents of the composite material. A more careful observation of the stress state in microstructure as shown in Fig. 6 reveals that even in the constituents, the actual stresses in the load direction are not constant as suggested by the volume average constituent stresses. The volume average stresses
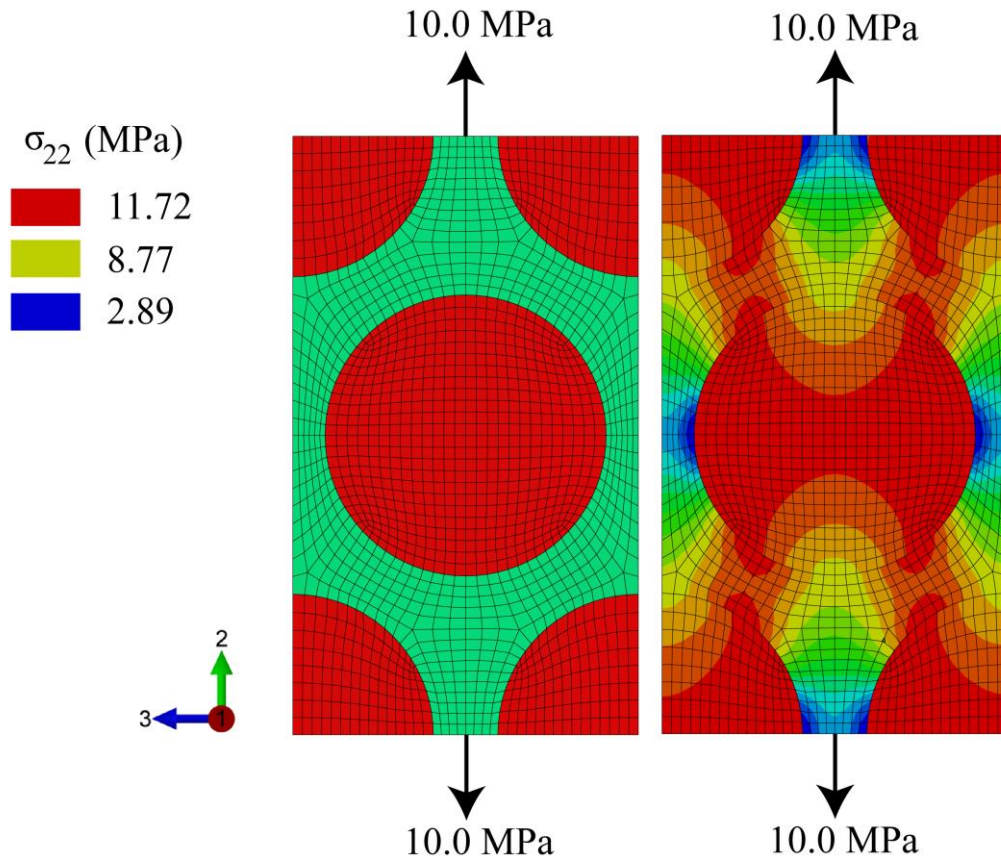
Figure 6: Comparison of constituent volume average stresses and the actual distribution of stresses in the RVE

are also not able to capture the fluctuations in the through thickness direction as shown in Fig. 7 which may play a role in promoting failure. Thus we can conclude that volume average

9

constituent quantities do not acknowledge these fluctuations and as a result, the strain energy

computed from the constituent volume average quantities may not account for all the strain

energy of the composite which raises a question of their accuracy in failure load predictions.
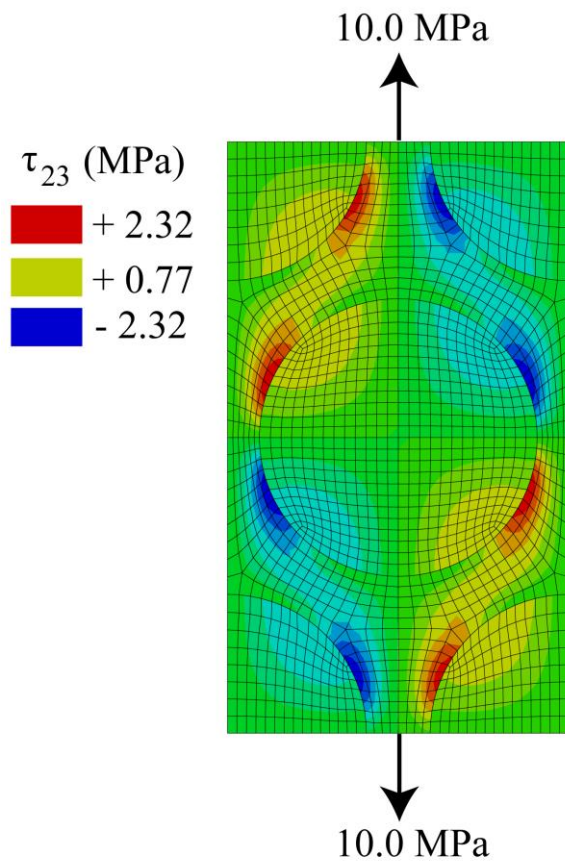
Figure 7: Fluctuation of shear stress in the through thickness
direction

1.7 Objective

The thesis of this work is *that an energy consistent constituent -level stress metric exists that accounts for stress fluctuations within each constituent and can be used for failure prediction.* The goal of this work is to test this hypothesis and, if the stress metric exists, to develop a method for computing it and using it to predict constituent-level failure in composites.

2. *Literature review*

2.1 Early approaches for predicting failure loads of composite materials

A failure theory is a methodology that is used to predict the conditions under which materials fail when subjected to various types of loads. In mathematical terms, a failure theory is expressed in the form of an inequality and failure of the material is said to occur when one equality is satisfied. The concept of a failure theory is better explained by considering the example of von Mises failure criterion which can be expressed as

$$\frac{\sqrt{\dfrac{(\sigma_I - \sigma_I)^2 + (\sigma_{II} - \sigma_{III})^2 + (\sigma_I - \sigma_{III})^2}{2}}}{S_y} \geq 1 \tag{2.1}$$

where σ_I, σ_{II} and σ_{III} are principal stresses and S_y is the uniaxial yield strength of the material. According to the von Mises failure criterion, a material fails when Eq. (2.1) is satisfied. Since it assumes the materials to be homogeneous and isotropic, it can be applied to conventional engineering materials like metals. However, since composites are in-homogeneous and highly anisotropic, the von Mises failure criterion cannot be directly applied to these materials. Fibrous composites exhibit a range of complex failure behaviors and a variety of theories have been proposed to predict their failure. The maximum stress failure criterion is the earliest and one of the simplest failure theories that was applied to predict the strength of composites (Burke, 1983; Gerstle and Reedy, 1985; Nahas, 1986). It can be expressed as

$$\left| \frac{\sigma_i}{S_i} \right| \geq 1 \tag{2.2}$$

where $i = 11,22,\ldots23$, σ_i is the stress in i-direction and S_i is the strength in i-direction. It is a non-interactive failure theory that is used to assess failure for a composite ply. According to this theory, a composite ply fails when the magnitude of stress in any direction exceeds its corresponding limit in that direction. This theory evaluates the failure state of the composite lamina based on a single value of stress in that lamina and does not take into consideration the state of multi-axial loading or the effects of the combinations of different stress components on the onset of failure. Although, the maximum stress failure criterion is capable of distinguishing between various lamina failure modes, it cannot explicitly separate fiber and matrix constituent failure. The non-interactive nature of the theory undermines its accuracy for predicting failure loads of composite materials under a multi-axial state of stress.

The maximum strain failure criterion is identical to the 'maximum stress' failure criterion except that the former accounts for some of the interactions between the stresses that are attributable to the Poisson's effects in the material (i.e., stresses in the fiber and through-thickness directions will affect the strain in the transverse-direction). It can be expressed as

$$\left| \frac{\varepsilon_i}{\varepsilon_i^{max}} \right| \geq 1 \tag{2.3}$$

where $i = 11,22,\ldots23$, ε_i is the strain in i-direction and ε_i^{max} is the maximum allowable strain in i-direction. The 'maximum strain' theory, as the name suggests, evaluates the state of failure of a lamina based on strains in that composite lamina. Even though both the failure criteria are simple and may sound primitive, they are often used either in their original or modified forms by many structural analysts today.

Non-interactive failure criteria like the maximum stress and maximum strain assess failure based on a single component of stress and strain respectively. However, under a biaxial/triaxial load state, the stress components may interact in which case the non-interactive failure theories may overpredict the failure loads. Gol'denblat and Kopnov (Gol'denblat and Kopnov, 1965) were one of the first to suggest the use of a quadratic interactive or tensor polynomial failure criteria with the use of stress tensors for glass reinforced plastics. For the first time a failure theory considered interactions of various stress components of the lamina to evaluate damage in composites. Tsai-Wu (Tsai and Wu, 1971) adopted a similar approach and came up with a simplified equation similar to Gol'denblat and Kopnov's which can be expressed as

$$F_i \sigma_i + F_{ij} \sigma_i \sigma_j \geq 1 \qquad (2.4)$$

where $i, j, k = 1, 2, ..6$; F_i and F_{ij} are strength tensors. Their quadratic, interactive, stress-based failure criteria used lamina level stress to determine the loads at which a composite ply fails. Lamina strengths were used to determine coefficients of stress components. However, neither of the two theories could distinguish between lamina failure modes or between fiber or matrix constituent failure. Moreover, neither theory was based on actual physical phenomena. With the availability of new experimental test data, there arose a need for failure theories that were not completely empirical but also had some physical significance.

Hashin (Hashin, 1980) proposed a stress-based failure criteria for composite materials that considered a multi-axial stress state for matrix dominated failure modes and a uniaxial stress state in the fiber direction for fiber dominated failure modes which can be expressed as

Fiber failure in tension
$$\left(\frac{\sigma_{11}}{S_{11}^+}\right)^2 + \alpha\left(\frac{\sigma_{12}}{S_{12}}\right)^2 \geq 1 \qquad (2.5)$$

Fiber failure in compression
$$\left(\frac{\sigma_{11}}{S_{11}^-}\right)^2 \geq 1 \qquad (2.6)$$

Matrix failure in tension
$$\left(\frac{\sigma_{22}}{S_{22}^+}\right)^2 + \alpha\left(\frac{\sigma_{12}}{S_{12}}\right)^2 \geq 1 \qquad (2.7)$$

Matrix failure in compression
$$\left(\frac{\sigma_{23}}{2S_{23}}\right)^2 + \left[\left(\frac{S_{22}^-}{2S_{23}}\right)^2 - 1\right]\frac{\sigma_{22}}{S_{22}^-} + \left(\frac{\sigma_{12}}{2S_{12}}\right)^2 \geq 1 \qquad (2.8)$$

where σ_{ij} is the stress component on the i-coordinate surface in the j-direction, S_{ij}^+ and S_{ij}^- are tensile and compressive strengths respectively and α is a user-specified parameter. Hashin, similar to his predecessors, used lamina level stresses to predict failure in a composite ply. The theory identified four different modes of failure of a composite ply: tensile fiber failure, compressive fiber failure, tensile matrix failure and compressive matrix failure. A major drawback of this theory is the need to specify an independent parameter to determine fiber or matrix tensile failure in the ply which has to be determined from experimental data. Thus in the absence of any experimental evidence, this value may be arbitrarily chosen between an allowable range of 0 to 1 which makes accuracy of 'blind' predictions made by the theory questionable.

Christensen (Christensen, 1997) also formulated a failure criteria which used lamina level stresses to identify failure in composite plies which can be expressed as

Fiber failure criterion
$$\left(\frac{1}{S_{22}^+} - \frac{1}{S_{22}^-}\right)\sigma_{11} + \frac{\sigma_{11}^2}{S_{22}^+ S_{22}^-} \geq 1 \tag{2.9}$$

Matrix failure criterion
$$\left(\frac{1}{S_{22}^+} - \frac{1}{S_{22}^-}\right)(\sigma_{22} + \sigma_{33}) + \frac{1}{S_{22}^+ S_{22}^-}(\sigma_{22} + \sigma_{33})^2 + \frac{1}{S_{23}^2}(\sigma_{23}^2 - \sigma_{22}\sigma_{33}) + \frac{1}{S_{12}^2}(\sigma_{12}^2 + \sigma_{13}^2) \geq 1 \tag{2.10}$$

The theory recognized failure as either fiber or matrix dominated. Unlike Hashin, Christensen considered multi-axial stress state for both fiber and matrix constituent failure. His theory did not involve an independent parameter that required correlation with test data and yet was general since it provided failure mode predictions for both the fiber and matrix constituents. Over time numerous other failure theories were proposed but none of the existing failure theories could provide accurate and meaningful predictions for the entire spectrum of loadings encountered in a composite structure. To confirm the then current state-of-the of predicting failure and damage in fiber reinforced polymers, Hinton and Soden launched a study called the 'World Wide Failure Exercise' (WWFE) (Hinton and Soden, 1998). This failure benchmark was aimed at comparing failure predicting capabilities of various leading composite failure theories from around the world for a variety of experimental test data. The first failure exercise was deemed a success and was then followed by two other exercises (Hinton and Kaddour, 2012; Kaddour et al., 2013). The text in the following sections contains a brief discussion of some of the important failure methodologies from the First and Second World Wide Failure Exercises.

2.2 World Wide Failure Exercise – I

The first World Wide Failure Exercise (WWFE-I) contains a detailed assessment of nineteen failure methodologies for predicting the deformation and failure response of polymer composite laminates when subjected to complex states of stress. Of all the nineteen failure techniques, the theories of Zinoviev(Zinoviev et al., 1998, 2002), Bogetti (Bogetti et al., 2004a, 2004b), Puck (Puck and Schürmann, 1998, 2002), Cuntze (Cuntze, 2004; Cuntze and Freund, 2004) and Tsai (Kuraishi et al., 2002; Liu and Tsai, 1998) were ranked highest with regards to accuracy of failure prediction (Soden et al., 2004). These leading theories along with some other micromechanical failure techniques from WWFE-1 are discussed in the following text.

Zinoviev (Zinoviev et al., 1998) used a non-interactive maximum stress failure criterion to determine failure mechanisms and took appropriate post-initial failure action. He used ply level stresses to predict failure loads on the lamina. Since the theory is based on the maximum stress criterion, it is not able to distinguish between various constituent-failure modes. The post-initial failure degradation model involved a gradual drop in the properties of the lamina. The final elastic and the shear moduli of the damaged lamina were degraded to a fraction of the original moduli depending on the strains on the laminate. The non-interactive nature of the failure criteria led to over-prediction of ultimate loads for certain loading combinations. In spite of assuming linear-elastic material properties, the stress-strain predictions of the theory were in close agreement with test data. The theory failed to predict the observed large deformations in one of the test cases and predicted an unrealistic open failure envelope in another test case. The Zinoviev theory used a simple maximum stress failure criterion but due to a well-controlled degradation model, the theory performed very well overall and appeared to be one of the best theories of the exercise.

Bogetti (Bogetti et al., 2004a) used a non-interactive maximum strain failure criterion to obtain failure envelopes for the available test data but unlike Zinoviev, Bogetti considered the non-linear behavior of the lamina under shear loads. To simulate progressive failure, the elastic/shear modulus of the failed lamina was set to zero and resultant loads were transferred to the un-failed laminae. Like Zinoviev's theory, this theory is also not capable of separating the various constituent-failure modes. The theory over-predicted the transverse compressive strength of one of the unidirectional laminae. For the same test case, the predictions in the biaxial tension and compression quadrants were much higher as compared to other theories. The theory gave good initial predictions for the non-linear stress-strain curves of multi-directional laminates. Owing to its simplicity and capability of predicting the wide range of test data features, it was ranked higher than other theories.

Puck's failure theory (Puck and Schürmann, 1998) is one of the most sophisticated theories of the failure exercise. It is an interactive failure theory which is able to differentiate between fiber and matrix constituent failures. Puck used both stresses and strains of the lamina as well as constituent properties of the lamina to assess failure. This failure theory has two fiber failure modes, the first being longitudinal tensile failure and second being longitudinal compressive failure. For the matrix constituent, Puck's theory provides three different kinds of modes, also known as 'inter- fiber failure modes'. The three modes which are termed A, B and C are distinguished by the orientation of fracture planes relative to the unidirectional fibers. It must be noted that lamina level properties were used by Puck to evaluate failure in individual composite plies. Progressive damage was achieved by a gradual degradation of the properties of the failed lamina. The final elastic and shear moduli and the Poisson's ratio of the failed lamina were assumed to be a fraction of the original lamina properties depending on the stress on the

laminate. The theoretical failure envelopes and stress-strain curves predicted by the theory were in very close agreement with the experiments except where large non-linear deformations were observed. Puck's failure theory has a large number of parameters to be determined which makes calibration very difficult.

Cuntze's (Cuntze, 2004) failure theory bears a strong resemblance to the failure modeling used by Puck but comparatively has fewer parameters which makes calibration easier. He used lamina level stresses to predict failure of composite plies. The theory recognized five failure mechanisms: Longitudinal tensile and compressive fiber-dominated failures and three matrix dominated failure modes also called 'inter-fiber failure modes'. The maximum stress criterion was used to assess failure state of the fibers. Unlike Puck, Cuntze assumed interaction between various failure mechanisms due to some probabilistic effects. The degradation of properties of the matrix constituent was based on experimentally obtained non-linear stress-strain curves of the lamina. The theory performed very well overall and provided quite accurate predictions for a variety of test data.

Liu and Tsai (Liu and Tsai, 1998) used Tsai's well know interactive failure criterion (Tsai and Wu, 1971) to predict strength of composites in the first World Wide Failure Exercise. After initial failure had occurred, they degraded the properties of the isotropic matrix by 85% and the effective properties of the failed lamina were computed using micromechanics. Their theory described the failure envelopes for unidirectional lamina better than any other theory. However, the theory predicted an enhancement in strength under compression-compression biaxial loading which was not verified due to lack of experimental test data. The predicted initial failure stresses for multi-directional laminates were in poor agreement with experimental data but the predicted shapes of the final failure envelopes agreed quite well with the experiments.

Owing to the assumption of linear elasticity, their theory could not predict the large non-linear strains observed in the test cases where high lamina shear was involved. Overall, due to its simplicity and good failure predicting capabilities, the Liu and Tsai failure theory was one of the best theories of the exercise.

Overall, approximately half of the theories of the First World Wide Failure Exercise relied on micromechanics in their formulation. Chamis's failure theory (Gotsis et al., 1998) used relations based on micromechanics to predict properties of the lamina from properties of its constituents using a computer code called 'Integrated Composite Analyzer (ICAN). ICAN required constituent level properties to compute several lamina level properties which were then used to assess failure using a modified distortion energy criterion. The computed lamina level properties like ply-stress components, ply-strengths, normal moduli of the ply and the Poisson's ratio of the ply were used to predict failure of the lamina. Another computer code 'Composite Durability Structural Analysis' (CODSTRAN) was used to degrade constituent properties after first ply failure and eventually predict catastrophic failure in multi-ply laminates. It must be noted that even though a simple modified distortion energy theory was used to assess failure at the lamina level, the process of obtaining the lamina properties using constituent properties was very complicated. For example, the ply-stress components were computed using an expression that contains more than fifteen terms. Moreover, the failure criteria used lamina level stresses as opposed to constituent level stresses to assess failure and so this technique failed to take full advantage of the power of micromechanical modeling. The Chamis failure theory did not explicitly provide the mode of failure but a close examination of the terms in the criterion can reveal if the damage is due to matrix or fiber constituent failure. The post initial degradation model replaced the modulus of the matrix to a negligible value after initial failure and the

resultant properties of the failed lamina were computed using micromechanics relations. The failure predictions for unidirectional laminae agreed with the experimental evidence but were very conservative for multi-directional laminates indicating a problem in post-initial failure modeling. The theory was not able to predict the observed nonlinear stress-strain curves. Chamis's failure theory is very complicated and involves a large number of variables making it difficult to work with. Moreover, the predictions were not as accurate as other theories dues to which it was ranked lower than the leading failure theories.

Huang's theory (Huang, 2004), is also micromechanics based and combines ideas like bridging model, plasticity and generalized maximum stress theory into a single failure modeling technique. The model consists of 'bridging matrices' that relate constituent level stresses to lamina level stresses. The various terms of these matrices were computed using both lamina and constituent level properties: fiber volume fraction, elastic and shear moduli, and Poisson's ratio. Fiber and matrix level stresses were then used to compute maximum and minimum principal stresses in the constituents and an equivalent stress was determined for each of the constituent using these principal stresses. The composite lamina was assumed to have failed if any of the two (fiber or matrix) equivalent stresses reached an ultimate stress value that corresponded to the strength of the constituent. For post initial failure modeling, Huang replaced all the constituent properties with a zero and assumed that the failed lamina did not take carry any load after it had failed. The theory predicted large values for uniaxial transverse tensile and shear strengths for the unidirectional laminae which differed significantly from the experimental data. The predictions of final strengths and deformation of multidirectional laminates was very low for some loading configurations. A unique feature of this methodology was the use of plasticity flow theory (Prandtl – Reuss flow theory) while calculating deformation and loads on the matrix

21

constituent enabling Haung to show matrix yielding while predicting failure loads. Overall, Haung's theory seems to be quite mature but needs improvement to enhance the assessment of failure.

Mayes and Hansen (Mayes and Hansen, 2004) used a failure theory that expressed the failure state of the composite material in terms of transversely isotropic stress invariants of the volume average stresses of the constituents. Their theory assumed that damage in a composite lamina begins at the constituent level which is why Mayes and Hansen used constituent level stress and strain data to predict failure of a constituent (fiber or matrix). A finite element code based on the Multicontinuum theory (Garnich and Hansen, 1997) was used to extract stress and strain field data for constituents of the composite. The theory had two separate criteria, one for fiber and the other for matrix constituent failure. The failure criteria are composed of stress invariants with appropriate coefficients that can be determined from composite strength data. Since it is very difficult to obtain some of constituent strengths experimentally, Mayes and Hansen used a numerical technique to obtain the same. Their degradation model employed a discrete reduction in the properties of the failed lamina by reducing all the moduli of the constituents to near zero values. The theory performed moderately well in predicting unidirectional lamina failure enveloped but failed to predict the maximum shear stresses observed in experiments under combined direct and shear loading. In spite of being an interactive stress based theory, the predicted failure envelope for biaxial tension and compression test was similar to that of non-interactive theories. This was due to the assumption that composite failure in the fiber direction is fiber dominated which led to neglecting the matrix constituent stresses in the fiber direction. Even though the final failure stresses predicted by their theory for multi-directional laminates were sometimes very low as compared to experiments, the

initial failure strengths of the same laminates were in better agreement with the test data. The stress-strain curves were also truncated at much lower strains that the final strains observed in experiments. Thus Mayes and Hansen tried to solve the complicated problem of composite failure prediction using a novel approach and have seemed to have paved the path for other researchers to look at constituent level behavior for assessing composite failure.

Some theories from WWFE-I were not completely based on micromechanics but used some properties of the constituents to predict final failure loads. Hart-Smith's theory (Hart-Smith, 2002) used constituent properties (fiber volume fraction, elastic moduli and Poisson's ratios of the fiber and matrix constituents) to compute final failure strains required for obtaining failure envelopes in the strain plane. These strain envelopes were then converted into appropriate failure stress envelopes. Rotem's failure technique (Rotem, 1998) used elastic modulus and strengths of the matrix constituent in his matrix failure criterion.

2.3 World Wide Failure Exercise – II

The second world wide failure exercise was set up to assess the maturity of failure criteria for predicting the failure strengths and deformation of unidirectional fiber reinforced composite materials subjected to tri-axial load states. A total of twelve failure theories were employed to solve twelve test cases. Of the twelve different methodologies, the failure theories of Carrere (Carrere et al., 2012, 2013), Cuntze (Cuntze, 2012, 2013), Pinho (Pinho et al., 2012, 2013) and Puck (Deuschle and Kröplin, 2012; Deuschle and Puck, 2013) were ranked highest due to their accurate predictions of failure strength and stress-strain curves of unidirectional

laminae and multidirectional laminates (Kaddour and Hinton, 2013). These failure theories and some important micromechanics based theories are discussed in the following text.

Carrere (Carrere et al., 2012) employed a micromechanical-based hybrid mesoscopic (MHM) 3D approach where a failure mechanism was formulated in terms of physical principles and introduced micromechanical aspects at the mesoscopic scale. His failure theory considered non-linear material behavior of the lamina and distinguished between two fiber failure modes and two matrix failure (called Inter Fiber Failure) modes. He used various parameters which described damage at the micro-scale along with lamina based quantities to predict first ply failure. Post initial failure modeling employed a gradual reduction in the properties of the failed lamina again with the use of parameters which describe the effect of damage at fiber/matrix constituent level. The failure model was able to capture the important features over the wide range of test data. It was one of the two theories that were able to predict fiber failure due to fiber kinking under compressive loads. Carrere's failure theory is very complicated and demands a lot of effort on the part of the analyst to provide meaningful results. However, Carrere was able to formulate a physically sound failure technique by taking the advantage of micromechanics and lamina based quantities which can prove to be a useful tool in understanding the failure behavior of fiber reinforced polymers.

Cuntze's failure theory (Cuntze, 2012) was established on the modeling capability called 'Failure Mode Concept (FMC)'. Based on nonlinear analysis, Cuntze's used an in-house MathCad code to explain the behavior of composite materials under triaxial load states. The theory incorporated five FMC modes of failure: two fiber failure modes and three matrix failure modes. The fiber failure modes employed the maximum stress failure criterion and the matrix failure modes used the stress invariants of the transversely isotropic lamina to asses and predict

failure of the lamina. After initial failure, the theory assumed softening behavior of the failed lamina and the effective moduli of the failed lamina were computed using stresses and available stress-strain data of the laminate. Unlike Carrere, Cuntze employed a much less rigorous approach to describe the failure behavior of composite materials. The predictions of the theory were in good agreement with the experimental evidence.

Deuschle and Kröplin (Deuschle and Kröplin, 2012) used the same mature failure theory which was employed by Puck (Puck and Schürmann, 1998) in the first World Wide Failure exercise with slight modifications to predict failure loads and deformation of fiber reinforced composites under tri-axial stress states. Originally, the theory was formulated based on the assumption that matrix failure can occur on planes parallel to the fibers which is indeed the case in UD composites. However for pure matrix, fracture may occur in a plane at any orientation and to capture this behavior, two more matrix failure modes were introduced. Overall, the predictions of their failure theory were in good agreement with the test data from the twelve test cases.

Pinho (Pinho et al., 2012) used physically-based constitutive modeling to formulate his theory and like all the other participants considered non-linear material properties of the lamina for predicting failure in fiber reinforced polymers. His failure theory used lamina level quantities to assess failure and distinguished between fiber and matrix failure modes. The fiber failure modes incorporated failure due to longitudinal tensile loads and fiber kinking/splitting due to compressive loads. A maximum stress failure criterion was used to predict fiber failure in longitudinal tension. Pinho concluded from various experiments on FRPs under compressive loads that matrix failure next to misaligned fibers was one of the driving forces behind fiber kinking. His theory used transverse tensile stresses as well as in-plane and through thickness

shear stresses of the lamina to predict buckling of fibers. Pinho computed the normal, transverse and longitudinal components of the traction in the fracture plane and used the same to predict matrix failure. For propagating failure, Pinho reduced the components of the traction vector acting on the fracture plane to zero such that the all the load is carried by un-failed laminae in the composite. Overall, Pinho's failure theory performed very well as compared to other theories. Unlike, some theories of the exercise which ranked very high, Pinho's theory is comparatively simple thus making it one of the best failure theories of the exercise.

Tsai-Ha's theory (Huang et al., 2012) in the second failure exercise is completely different than the failure methodology employed by Liu and Tsai (Liu and Tsai, 1998) in the first World Wide Failure Exercise. Huang et al. developed a new micromechanics based failure theory that used constituent level stresses to predict failure of a constituent. His model used a unit cell with hexagonally arranged fibers to extract 'Stress Amplification Factors' which relate lamina level stresses to constituent level stresses. The new approach was able to distinguish between two fiber failure modes, one matrix failure mode and one interface failure mode using constituent level stresses. The maximum stress failure criterion was used for predicting failure of fibers under longitudinal tensile and compressive loads. A modified distortion energy failure criterion was used to predict failure of the matrix constituent. A quadratic failure criterion was proposed which used tractions on the interface to predict initiation of damage at the fiber-matrix interface. They never used the interface failure criterion assuming that the bonding between the fiber and the matrix was sufficiently strong such that separation of the fiber-matrix interface did not occur. After initial failure of a ply, the matrix properties of the failed ply were degraded gradually depending on the stresses in the ply. The predictions of the theory were conservative for most of the test case and need several improvements. Even though Huang et al. explained the

26

use of the 'Stress Amplification Factors' to compute constituent level stresses from lamina level stresses, they have not explained the procedure in detail. Conservative predictions for the test case indicate that the theory may need a more robust progressive failure methodology. In spite of all these drawbacks, their theory is very simple and appears to have potential to grow into a much more robust failure modeling technique.

Nelson, Hansen and Mayes (Nelson et al., 2012) used a similar approach like the one in the first World Wide Failure exercise, in the second failure exercise with some major modifications to the matrix failure criterion and post initial failure modeling technique. They continued the use of constituent level stresses to predict failure loads on composites which were extracted from composite level stresses using a FE approach based on the Multicontinuum theory. A new matrix failure criterion was proposed which now incorporated the matrix constituent stresses in the longitudinal (fiber) direction. A coupling between shear and transverse compressive stresses was also added. The post initial failure approach adopted in the second failure exercise allowed gradual degradation of the properties of the matrix constituent. The modification of the matrix failure criterion has made calibration more difficult, as one of the invariants used in the criterion has no physical meaning. The model predicted large and unbounded strengths in various test cases that were analyzed. Contrary to the predictions of other theories, the model predicted an open envelope under tension-tension case for isotropic matrix. Although the failure theory is not as complicated as other failure methodologies, it has a lot of room for growth since overall its predictions were not as highly ranked as the best theory of the exercise.

In the second failure exercise, Haung (Zhou and Huang, 2012) used 3D laminate theory along with the original bridging model used in the first failure exercise to predict failure loads

and deformation of fiber reinforced polymers. Bridging matrices were used to compute constituent level quantities from lamina level quantities. The tensile failure criterion of the fiber and the matrix constituents was not changed but a new compressive failure criterion for the constituents was introduced. This new failure criterion, which took into account the enhancement of lamina strength due to tri-axial compressive loading, used principal stresses of the constituents to predict their compressive failure. In the new post initial degradation model, the modulus of the resin material in the failed lamina was reduced to one percent of its original magnitude. The modifications introduced by Haung in his failure theory did not improve its overall failure predicting capability.

The majority of failure theories in the WWFEs used lamina level quantities to assess failure state of the composite. Some of the theories were micromechanics based and used constituent level quantities to predict failure loads of the composite. The work in this thesis is primarily concerned with improving the measurement of volume average constituent level quantities that are used in failure modeling by micromechanical theories. The new stress metric that was obtained could be used in conjunction with any of the micromechanical failure methodologies that use volume average stresses in evaluating failure.

3. Interaction Energy

(The majority of this chapter has been accepted for publication in the AIAA Journal).

Complex interactions in fiber reinforced composites between multiple failure mechanisms have made accurate failure prediction a daunting challenge. One approach to better identify failure mechanisms has been the use of volume average constituent stresses in the composite to predict the onset and outcome of failure in individual constituents. However, this approach is shown here to not conserve strain energy in the composite, which could potentially affect the accuracy of failure prediction under certain loading conditions. The focus of this chapter is to develop an expression for the discrepancy in strain energy, termed the interaction energy, and to numerically evaluate the influence of constituent properties, fiber volume fraction, and load combinations on the magnitude of this energy.

3.1. Overview of volume average quantities used for composite failure load predictions

The use of composite materials in the wind and aerospace industries has grown dramatically in recent years, with composites comprising 50% or more of Boeing's 787 and Airbus's A380. With this increase in use has come a greater demand for design tools that can accurately predict damage initiation and propagation, durability, and remaining life. This has proven to be quite challenging due the range of complex failure behaviors exhibited by composites. Unlike conventional homogeneous materials like metals, the constituent undergoing failure may switch rapidly and the failure mechanisms within each constituent can vary widely depending on the loading. At the lamina level, tensile loads parallel to the fiber direction may

cause both fiber and matrix fracture. Under transverse loading, Mode I matrix cracking or fiber/matrix debonding may occur in tension, with a shear matrix failure occurring in compression. At the laminate level, delamination may occur, which will substantially affect the distribution of stresses in each lamina. The result of this complexity has been a large number of proposed composite failure theories with no clearly superior choice.

The First and the Second World-Wide Failure Exercises (WWFE I and WWFE II, respectively) have provided a much needed benchmark against which to compare the effectiveness of various composite failure theories for both glass- and carbon-fiber composites subject to complex loading configurations (Hinton and Kaddour, 2012; Hinton and Soden, 1998). One distinction among failure theories was the use of micromechanics in the prediction of failure, such that some measure of fiber and matrix constituent stresses were used to predict lamina failure rather than using lamina-level failure criteria to predict failure. Although none of the micromechanics based theories were judged in the benchmark exercises to exceed the performance of more established theories, they were assessed as evolving towards maturity (Kaddour and Hinton, 2013). The unique appeal of constituent-level failure theories is not simply in static failure prediction, but their potential for physics-based modeling and materials design efforts, such as the Materials Genome Initiative and Integrated Computational Materials Engineering.

The methods used to extract constituent stresses and strains from composite stresses typically utilize some form of a localization tensor to map composite stresses to constituent stresses, which may be evaluated at specific points (like peak stresses) or as volume average quantities. The use of constituent stresses at specific points is strongly dependent on the choice of representative volume element (RVE) for the composite microstructure. Any deviation from

the idealized structure may substantially alter the stress at a particular location. The use of volume average stresses is appealing because it is less sensitive to details of the microstructure; random fiber packing and idealized hexagonal fiber packing will yield nearly the same average constituent stresses and strains. However, the use of volume average constituent stresses and strains may not account for the total strain energy in a composite. For example, a careful inspection of the stress fields in a composite microstructure reveals the presence of shear stresses in the constituents even when the composite loading is purely transverse normal—these stresses, however, average to zero and therefore cannot be accounted for in any failure or material nonlinearity model. As a result, failure prediction under particular loading configurations may not be consistent with bulk constituent properties because a significant portion of the strain energy may be unaccounted for. The energy not accounted for when using volume average constituent stresses and strains is herein termed the interaction energy. To enhance physics-based composite failure prediction, all strain energy should be accounted for. The goal of this chapter is to provide a quantitative foundation for the development of constituent-level composite failure theories based on the conservation of strain energy across length scales. As such, the focus of this research is to quantify the magnitude of the interaction energy relative to the total strain energy for a variety of fiber volume fractions, matrix elastic properties, and complex multi-axial loading configurations. The reported results clearly indicate that a significant fraction of energy is unaccounted for under a variety of loading conditions in typical aerospace composite materials, but also suggest that this interaction energy could be readily incorporated into constituent failure criteria.

3.2. Theoretical Motivation

This section focuses on establishing the equations that can be used to quantify the interaction energy. Consider a RVE of a composite material consisting of fiber and matrix phases. Let U denote the strain energy of this composite under an arbitrary load state. Assuming a linear elastic material, this energy can be represented as

$$U = \frac{1}{2} \int_{V_C} \sigma_{ij}^C \varepsilon_{ij}^C \, dV_C \tag{3.1}$$

where σ_{ij}^C and ε_{ij}^C are the composite stresses and strains, respectively; repeated ij indices are summed, and integration performed over the entire volume of the composite V_c. For a periodic RVE subject to homogeneous boundary conditions as defined by Hashin (Hashin, 1983), Equation (3.1) can be readily written in terms of average composite properties (Sun and Vaidya, 1996)

$$U = \frac{1}{2} \left\langle \sigma_{ij}^C \right\rangle \left\langle \varepsilon_{ij}^C \right\rangle V_C \tag{3.2}$$

where the terms in the brackets denote volume average quantities. Strain energy may be separated into contributions from the fiber and the matrix constituents

$$U = U_f + U_m \tag{3.3}$$

such that

$$U_f = \frac{1}{2} \int_{V_f} \sigma_{ij}^f \varepsilon_{ij}^f \, dV_f \tag{3.4}$$

$$U_m = \frac{1}{2} \int_{V_m} \sigma_{ij}^m \varepsilon_{ij}^m \, dV_m \tag{3.5}$$

where the superscripts f and m denote quantities for fiber and matrix, respectively. In contrast to using average lamina stresses, summing the strain energies of the constituents computed using constituent volume average stresses does not account for all of the strain energy in the composite. To quantify this interaction energy the strains in each constituent are written in terms of a mean value $\langle \varepsilon_{ij} \rangle$ plus a fluctuation $\widetilde{\varepsilon}_{ij}$; similarly, the stresses are also written as a mean value $\langle \sigma_{ij} \rangle$ plus a fluctuation $\widetilde{\sigma}_{ij}$.

$$\varepsilon_{ij} = \langle \varepsilon_{ij} \rangle + \widetilde{\varepsilon}_{ij} \tag{3.6}$$

$$\sigma_{ij} = \langle \widetilde{\sigma}_{ij} \rangle + \widetilde{\sigma}_{ij} \tag{3.7}$$

For the fiber, Eqs. (3.6) and (3.7) are substituted into Eq. (3.4) to obtain

$$U_f = \frac{1}{2} \int_{V_f} \left(\langle \sigma_{ij}^f \rangle + \widetilde{\sigma}_{ij}^f \right) \left(\langle \varepsilon_{ij}^f \rangle + \widetilde{\varepsilon}_{ij}^f \right) dV_f \tag{3.8}$$

Expanding Eq. (3.8) yields

$$U_f = \frac{1}{2} \int_{V_f} \langle \sigma_{ij}^f \rangle \langle \varepsilon_{ij}^f \rangle dV_f + \frac{1}{2} \int_{V_f} \widetilde{\sigma}_{ij}^f \widetilde{\varepsilon}_{ij}^f \, dV_f + \frac{1}{2} \int_{V_f} \langle \sigma_{ij}^f \rangle \widetilde{\varepsilon}_{ij}^f \, dV_f + \frac{1}{2} \int_{V_f} \widetilde{\sigma}_{ij}^f \langle \varepsilon_{ij}^f \rangle dV_f \tag{3.9}$$

which on further simplification gives

$$U_f = \frac{1}{2} \langle \sigma_{ij}^f \rangle \langle \varepsilon_{ij}^f \rangle V_f + \frac{1}{2} \int_{V_f} \widetilde{\sigma}_{ij}^f \widetilde{\varepsilon}_{ij}^f \, dV_f \tag{3.10}$$

Because volume average quantities are constant and $\tilde{\sigma}_{ij}^{f}$ and $\tilde{\varepsilon}_{ij}^{f}$ are local fluctuations with averages that are identically zero. The matrix contribution is derived in a similar manner to give

$$U_m = \frac{1}{2}\left\langle \sigma_{ij}^m \right\rangle\left\langle \varepsilon_{ij}^m \right\rangle \mathcal{V}_m + \frac{1}{2}\int_{\mathcal{V}_m} \tilde{\sigma}_{ij}^m \tilde{\varepsilon}_{ij}^m d\mathcal{V}_m \qquad (3.11)$$

The strain energies in the fiber and matrix can then be written as

$$U_f = \frac{1}{2}\left\langle \sigma_{ij}^f \right\rangle\left\langle \varepsilon_{ij}^f \right\rangle \mathcal{V}_f + \Phi_f \mathcal{V}_f \qquad (3.12)$$

$$U_m = \frac{1}{2}\left\langle \sigma_{ij}^m \right\rangle\left\langle \varepsilon_{ij}^m \right\rangle \mathcal{V}_m + \Phi_m \mathcal{V}_m , \qquad (3.13)$$

where Φ_f and Φ_f are the fiber and matrix contributions to the interaction energy density, respectively given by

$$\Phi_f = \frac{1}{2\mathcal{V}_f}\int_{\mathcal{V}_f} \tilde{\sigma}_{ij}^f \tilde{\varepsilon}_{ij}^f d\mathcal{V}_f \qquad (3.14)$$

$$\Phi_m = \frac{1}{2\mathcal{V}_m}\int_{\mathcal{V}_m} \tilde{\sigma}_{ij}^m \tilde{\varepsilon}_{ij}^m d\mathcal{V}_m \qquad (3.15)$$

The interaction energy ΔU is thus related to the total strain energy and the energy computed from volume average constituent quantities via

$$U = U_f + U_m = \frac{1}{2}\left\langle \sigma_{ij}^m \right\rangle\left\langle \varepsilon_{ij}^m \right\rangle \mathcal{V}_m + \frac{1}{2}\left\langle \sigma_{ij}^f \right\rangle\left\langle \varepsilon_{ij}^f \right\rangle \mathcal{V}_f + \Delta U \qquad (3.16)$$

where

$$\Delta U = \Phi_f \mathcal{V}_f + \Phi_m \mathcal{V}_m . \qquad (3.17)$$

Substituting Hooke's law into Eq. (3.14) allows the interaction energy density to be written entirely in terms of strain fluctuations

$$\Phi_f = \frac{1}{2}\int_{V_f} C_{ijkl}\tilde{\varepsilon}_{ij}^f \tilde{\varepsilon}_{kl}^f dV_f = \frac{1}{2}\int_{V_f} C_{mn}\tilde{\varepsilon}_m^f \tilde{\varepsilon}_n^f dV_f \qquad (3.18)$$

where C_{mn} is the m,n component of the 6x6 fiber stiffness matrix. Assuming transverse isotropy and expanding Eq. (3.18) yields

$$2\Phi_f = \begin{bmatrix} C_{11}^f \left\langle \left(\tilde{\varepsilon}_1^f\right)^2 \right\rangle + C_{22}^f \left\langle \left(\tilde{\varepsilon}_2^f\right)^2 \right\rangle + C_{33}^f \left\langle \left(\tilde{\varepsilon}_3^f\right)^2 \right\rangle + 2C_{12}^f \left\langle \tilde{\varepsilon}_1^f \cdot \tilde{\varepsilon}_2^f \right\rangle + 2C_{13}^f \left\langle \tilde{\varepsilon}_1^f \cdot \tilde{\varepsilon}_3^f \right\rangle + \\ 2C_{23}^f \left\langle \tilde{\varepsilon}_2^f \cdot \tilde{\varepsilon}_3^f \right\rangle + C_{44}^f \left\langle \left(\tilde{\gamma}_4^f\right)^2 \right\rangle + C_{44}^f \left\langle \left(\tilde{\gamma}_5^f\right)^2 \right\rangle + C_{66}^f \left\langle \left(\tilde{\gamma}_6^f\right)^2 \right\rangle \end{bmatrix} \qquad (3.19)$$

The interaction energy density for the matrix can be similarly shown to be

$$2\Phi_m = \begin{bmatrix} C_{11}^m \left\langle \left(\tilde{\varepsilon}_1^m\right)^2 \right\rangle + C_{22}^m \left\langle \left(\tilde{\varepsilon}_2^m\right)^2 \right\rangle + C_{33}^m \left\langle \left(\tilde{\varepsilon}_3^m\right)^2 \right\rangle + 2C_{12}^m \left\langle \tilde{\varepsilon}_1^m \cdot \tilde{\varepsilon}_2^m \right\rangle + 2C_{13}^m \left\langle \tilde{\varepsilon}_1^m \cdot \tilde{\varepsilon}_3^m \right\rangle + \\ 2C_{23}^m \left\langle \tilde{\varepsilon}_2^m \cdot \tilde{\varepsilon}_3^m \right\rangle + C_{44}^m \left\langle \left(\tilde{\gamma}_4^m\right)^2 \right\rangle + C_{44}^m \left\langle \left(\tilde{\gamma}_5^m\right)^2 \right\rangle + C_{66}^m \left\langle \left(\tilde{\gamma}_6^m\right)^2 \right\rangle \end{bmatrix} \qquad (3.20)$$

Equations (3.19) and (3.20) quantify the interaction energy between fiber and matrix, but they contain a total of 18 terms. The focus of the subsequent modeling effort is to determine the significance of the interaction energy relative to the total strain energy, to investigate how the interaction energy may change as a function of loading and material properties, to evaluate the contribution of each of the 18 terms to interaction energy and to attempt to establish relative contribution of each constituent to the interaction energy.

3.3. Finite Element Modeling

A finite element model was developed and studied using Abaqus™ to investigate the magnitude of the interaction energy as a function of fiber volume fraction, elastic moduli of the constituents, and varying loading conditions. For the purpose of analysis, a representative volume element (RVE) of a hexagonal fiber packing was modeled, as shown in Fig. 8. Periodic boundary conditions were applied on all RVE edges, faces, and corners. This was achieved by extracting nodes from the RVE after meshing, reordering them properly, and using equation constraints for
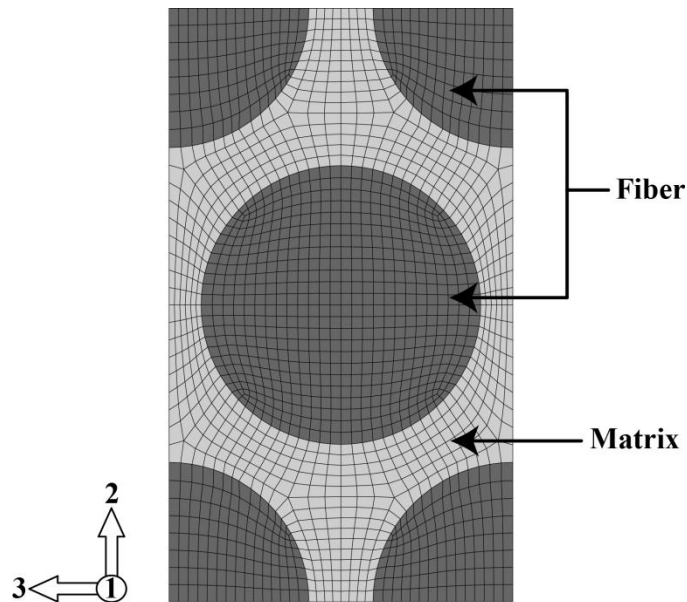
Figure 8: Representative volume element (RVE) with
hexagonal fiber packing for fiber volume fraction of 0.6

36

the node sets. The axial direction of the fibers is defined as the 1-direction (longitudinal). Carbon

fiber properties (AS4) reported by Sun (Sun and Vaidya, 1996) and shown in Table 1 were used

for all simulations. The matrix was assumed to be isotropic with a Poisson's ratio of 0.34.

Table 1: Baseline material properties of the fiber

Material	Type	$E_1(GPa)$	$E_2(GPa)$	$G_{12}(GPa)$	v_{12}	v_{23}
AS4	Transversely isotropic	235	14	28	0.2	0.25

Three parametric studies were conducted. First, the fiber volume fraction was varied from 0.05

to 0.85 with the matrix modulus was fixed at 1% of the fiber-direction fiber modulus,

$E_m = 2.35GPa$. In the second study, the matrix modulus was varied from 1% to 120% of the

fiber modulus in the fiber direction. (A matrix modulus of $0.0204 \times E_{11fiber}$ roughly corresponds to

epoxy 3501-6 (E_m = 4.8 GPa).) Results for the modulus study were obtained for four different

fiber volume fractions of 0.05, 0.25, 0.6 and 0.85. In both of these parametric studies, four

unique composite loading states were examined: ε_{11}, ε_{22}, ε_{12}, and ε_{23}. These loads were achieved
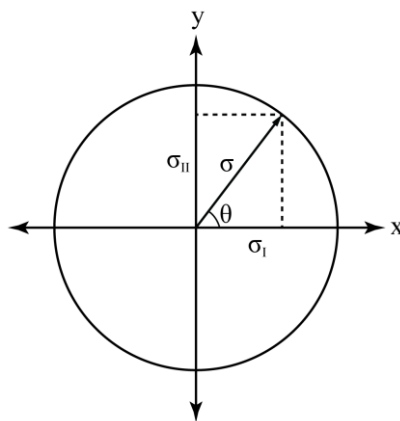
Figure 9: Decomposition of biaxial load into its
components

by fixing displacements of the RVE control nodes such that a strain of 0.01 was applied in each load case. In the third study, five types of biaxial loads were applied: $(\sigma_{22}, \sigma_{33})$, $(\sigma_{12}, \sigma_{22})$, $(\sigma_{12}, \sigma_{23})$, $(\sigma_{12}, \sigma_{13})$, and $(\sigma_{23}, \sigma_{22})$. These loads were applied such that they corresponded to the x- and y-components of the biaxial load represented as the radius of a circle as shown in Fig. 9, with θ varying from 0° to 180°.

The two uniaxial loads required to generate the biaxial load state can be expressed as

$$\begin{aligned} \sigma_I &= \sigma \cos\theta \\ \sigma_{II} &= \sigma \sin\theta \end{aligned} \tag{3.21}$$

where $\sigma = 10 MPa$ was the resultant biaxial load vector magnitude, and σ_I and σ_{II} are the corresponding uniaxial loads. For this third study, the matrix modulus and fiber volume fraction were held constant at $0.01702 \times E_{11fiber}$ ($E_m = 4.0$ GPa) and 0.6, respectively.

3.4. Results and Discussion

As discussed above, three series of simulations were carried out to quantify the dependencies of the interaction energy on material properties, fiber volume fraction, and loading conditions: (i) constant matrix and fiber modulus with varying fiber volume fraction, (ii) varying matrix modulus for four different fiber volume fractions, and (iii) constant material and microstructure properties with varying biaxial loading conditions.

3.4.1. Effect of Fiber Volume Fraction on Interaction Energy

Volume average quantities (stresses, strains and stiffness) of the composite were extracted from the model and then the total strain energy for the composite was calculated using Eq. (3.2). The volume average quantities (stresses, strains and stiffness) of the constituents were also extracted. Constituent strain fluctuations and average stresses and strains were computed and used in Eqs. (3.19) and (3.20) to give Φ_f and Φ_m. The total interaction energy was computed using Eq. (3.17). The interaction energy fraction $(\Delta U / U)$ was computed for all the fiber volume fractions and each load case. The properties of the RVE were transversely isotropic, thus only four (and not all six) load cases are unique. Figure 10 shows $\Delta U / U$ as a function of fiber volume fraction for each load case. Three features of these data are of particular interest. First, the interaction energy is strongly dependent on the load case and it can be a significant fraction of the total energy. It can be more than 30% of the total strain energy for longitudinal shear loading (shear-12), although it was negligible for unidirectional loading in the fiber direction (tension-11). Second, interaction energy increases with increasing fiber volume fraction, up to typical volume fractions. Finally, transverse tension (tension-22) and transverse shear (shear-23) show a peak at a fiber volume fraction of about 0.65, very close to typical fiber volume fractions in aerospace-grade composites.
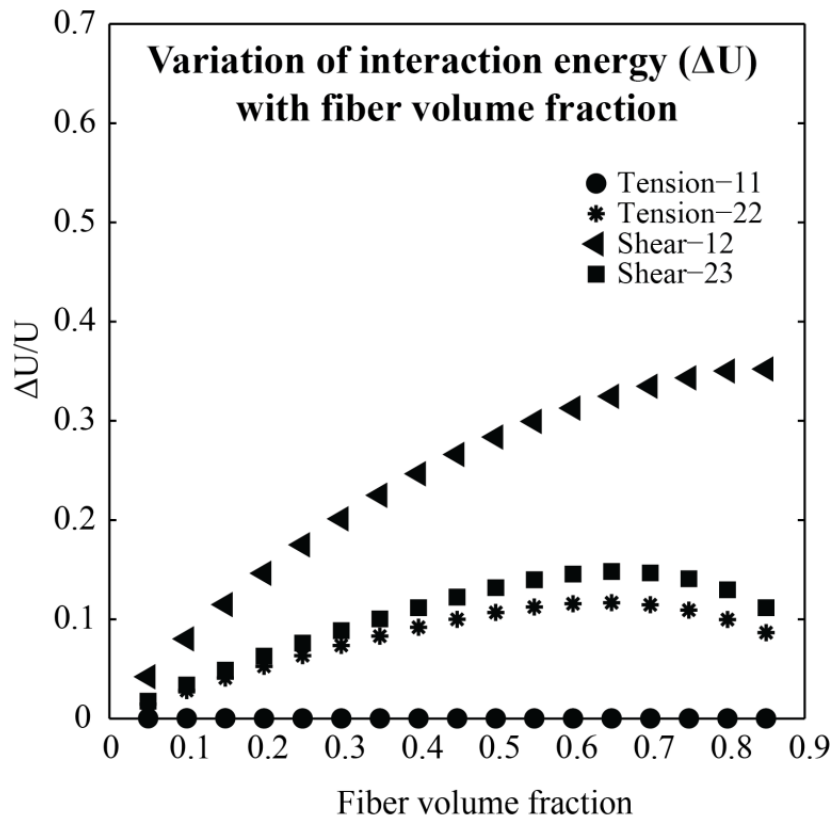
Figure 10: Variation of interaction energy with fiber volume fraction

To qualitatively understand these features consider stresses in an RVE with a fiber volume fraction of 0.6 subject to the four load cases. In case of longitudinal tension, shown in Fig. 11a, the stress distribution is uniform in each constituent throughout the structure, thus strain fluctuations are minimal. Consequently, as shown in Equations (3.19) and (3.20), Φ_f and Φ_m, and correspondingly ΔU, are nearly zero for this load case. In the case of longitudinal shear, shown in Fig. 11b, the stress fluctuation is largest. Consequently, the interaction energy is

maximized for this case, as seen in Fig. 10. This result is critically important because it means that at a typical fiber volume fraction for aerospace grade composites (60%), volume average constituent stresses neglect nearly 30% of the distortion energy in the composite in shear. The transverse tension and transverse shear load cases are shown in Fig. 11c and Fig. 11d, respectively. For both cases the stress fluctuations are significant, so interaction energy will not
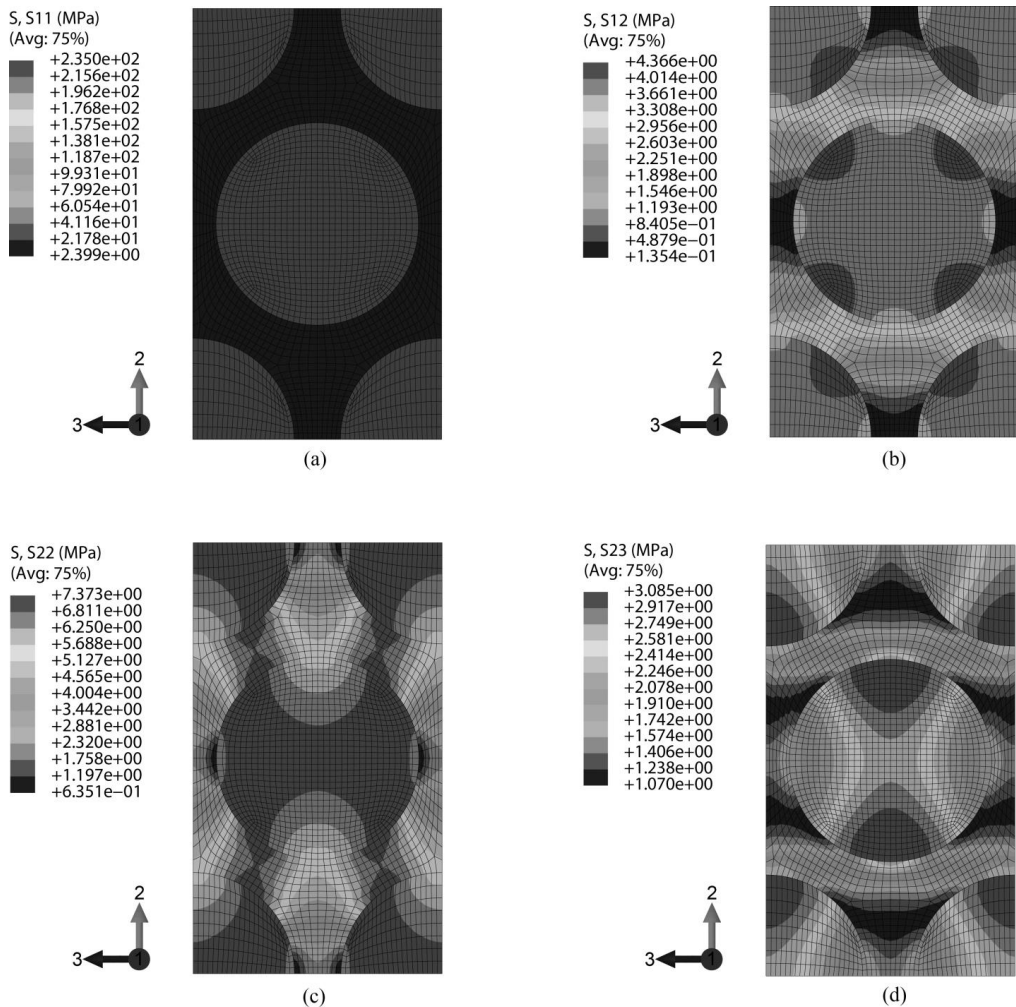
Figure 11: (a) Stress plot for load case tension-11 (b) Stress plot for load case shear-12
(c) Stress plot for load case tension-22 (d) Stress plot for load case shear-23

41

be negligible. Stress distributions for longitudinal shear, transverse shear, and transverse tensionare quantitatively shown in Figure 12. The high probability densities at low strain values result from fiber strains, thus the fluctuations in fiber strain are small. The matrix strain distribution consists of the larger strain values. The distinction is shown in Fig.12 by enclosing fiber and matrix distribution in dashed lines. The matrix strain distribution is widest in longitudinal shear and smallest in transverse tension. Consequently, the interaction energy should be the least for transverse tension and the greatest for longitudinal shear— in agreement with Fig. 10.
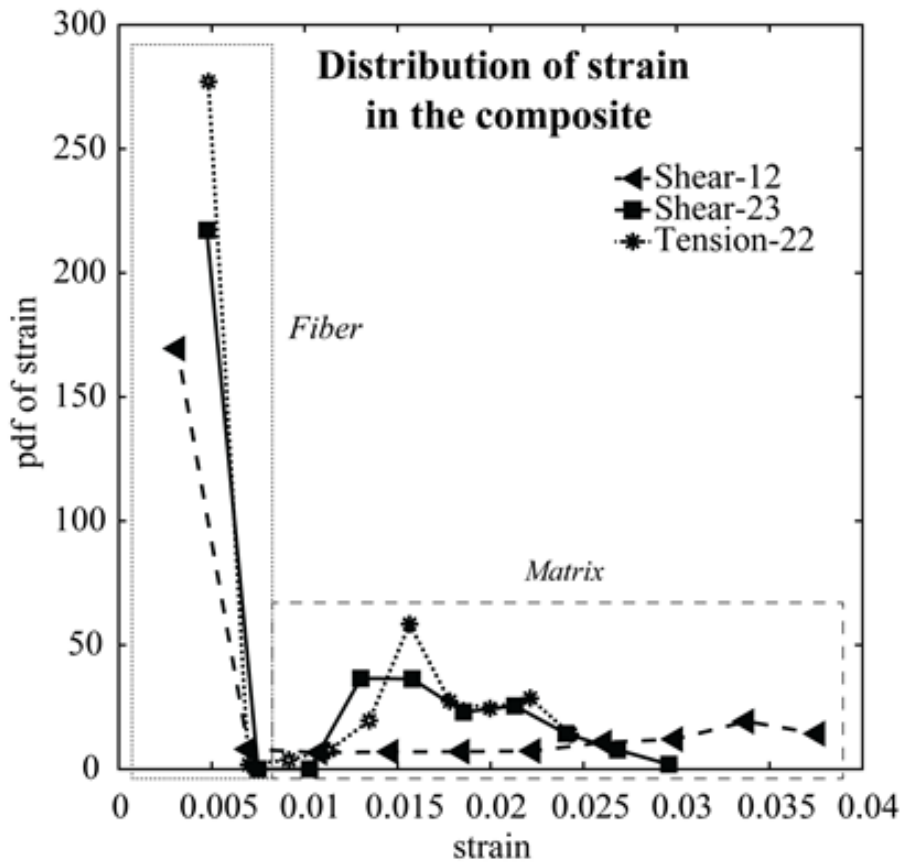
Figure 12: Probability distribution function for strains for different load cases

An important observation to be made from these data is that the matrix strain distribution, and consequently the matrix strain fluctuation, is much broader and at much higher strains than the fiber strain distribution. This suggests that the small strain values of the fiber in conjunction with the even smaller strain fluctuations in fiber render the fiber a minor contributor to the interaction energy in the composite. To confirm this, the relative contribution of each constituent was examined. Figure 13 shows the relative matrix contribution to interaction energy plotted against fiber volume fraction for the four different load cases. The results are notable: up to typical fiber
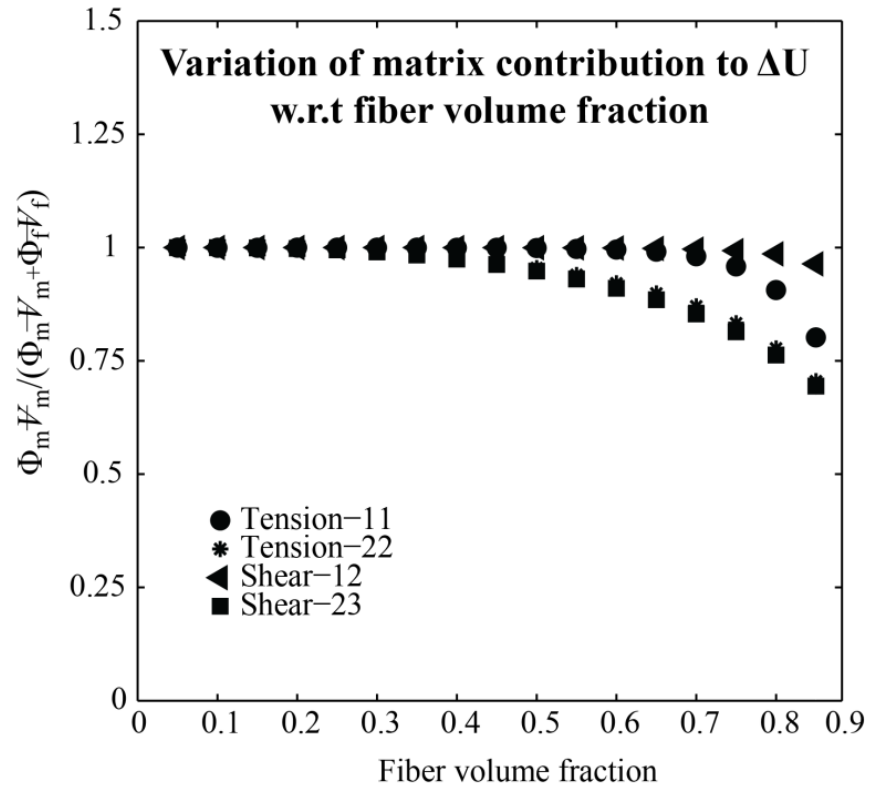
Figure 13: Variation of contribution of matrix to interaction energy
with fiber volume fraction

volume fractions, the matrix accounts for vast majority of interaction energy. For a fiber volume fraction of 0.6, the matrix contributes almost entirety (more than 99%) of the interaction energy of the composite for longitudinal shear loading, the most significant load case. Even for transverse tension and transverse shear, matrix contribution to interaction is about 90%. This result is important because it permits the interaction energy contribution of the fiber to be neglected, such that augmenting matrix failure theories with interaction energies can be the focus of future failure prediction efforts.

Figures 14-22 show the contribution of the various terms in Eq. (3.20) to interaction energy of the matrix constituent. It can be seen that the contribution of terms $C_{11}^m \left\langle \left(\tilde{\varepsilon}_1^m \right)^2 \right\rangle$,
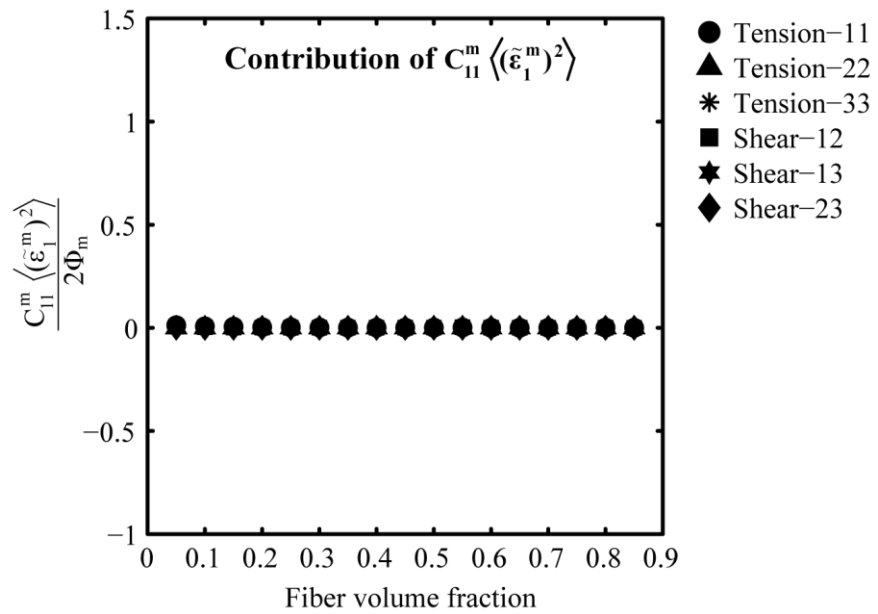
Figure 14: Variation of contribution of $C_{11}^m \left\langle \left(\tilde{\varepsilon}_1^m \right)^2 \right\rangle$ term to interaction energy of the matrix

45
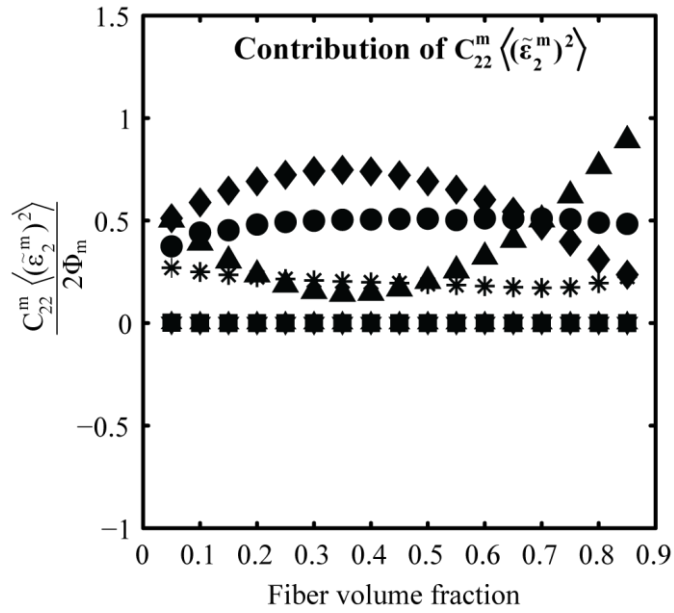
Figure 15: Variation of contribution of $C_{22}^m \left\langle \left(\tilde{\varepsilon}_2^m \right)^2 \right\rangle$ term to interaction energy of the matrix
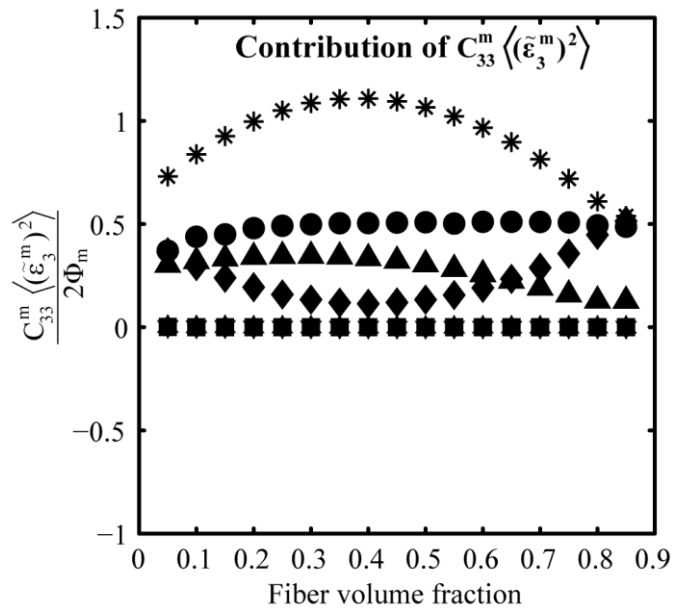
Figure 16: Variation of contribution of $C_{33}^m \left\langle \left(\tilde{\varepsilon}_3^m \right)^2 \right\rangle$ term to interaction energy of the matrix
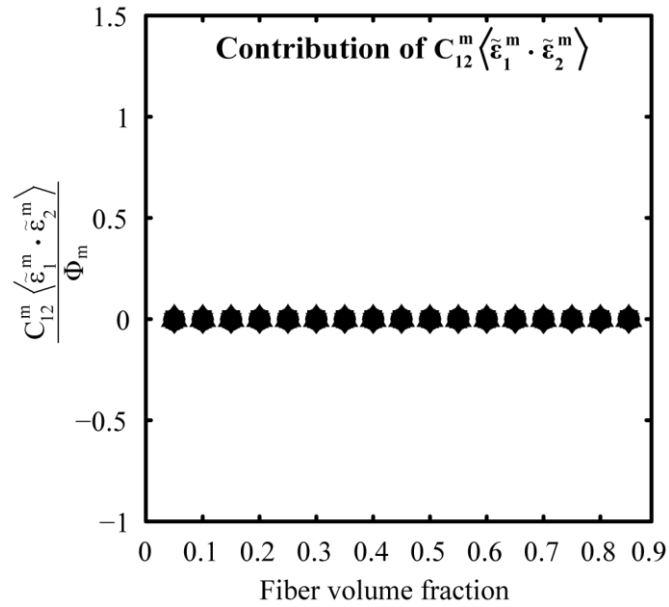
Figure 17: Variation of contribution of $C_{12}^{m}\langle \widetilde{\varepsilon}_{1}^{m} \cdot \widetilde{\varepsilon}_{2}^{m} \rangle$ term to interaction energy of the matrix
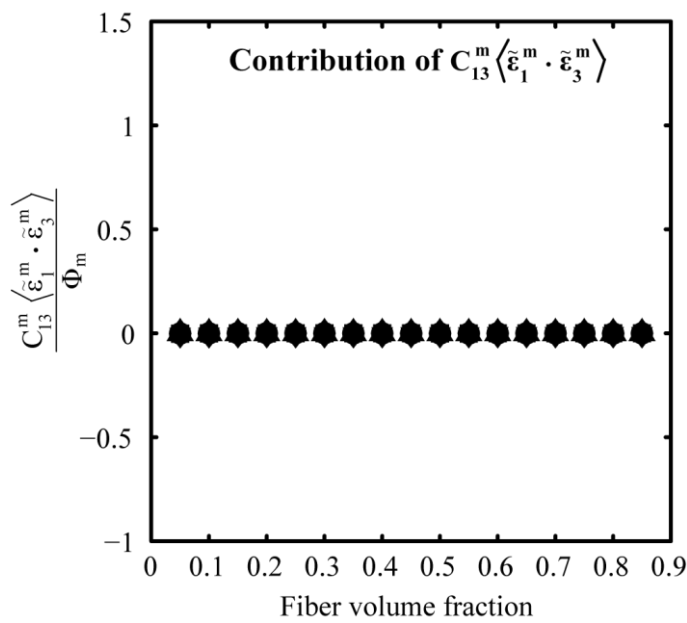
Figure 18: Variation of contribution of $C_{13}^{m}\langle \widetilde{\varepsilon}_{1}^{m} \cdot \widetilde{\varepsilon}_{3}^{m} \rangle$ term to interaction energy of the matrix

47
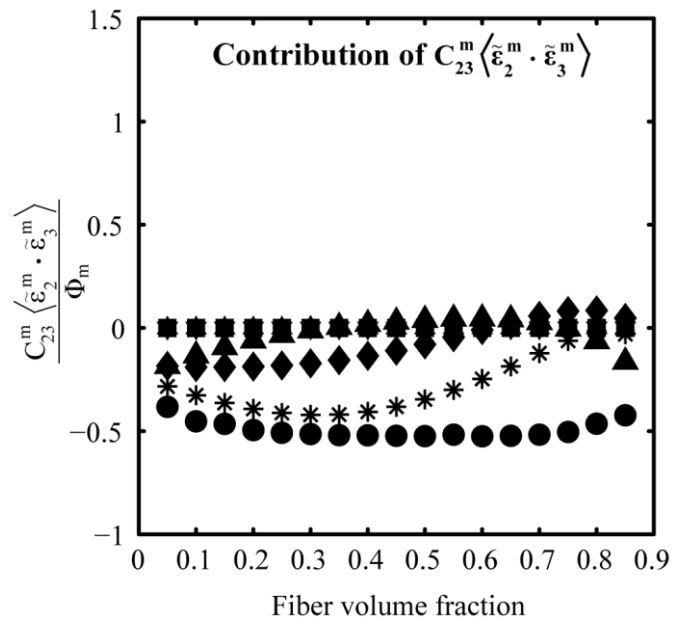
Figure 19: Variation of contribution of $C_{23}^m \langle \tilde{\varepsilon}_2^m \cdot \tilde{\varepsilon}_3^m \rangle$ term to interaction energy of the matrix
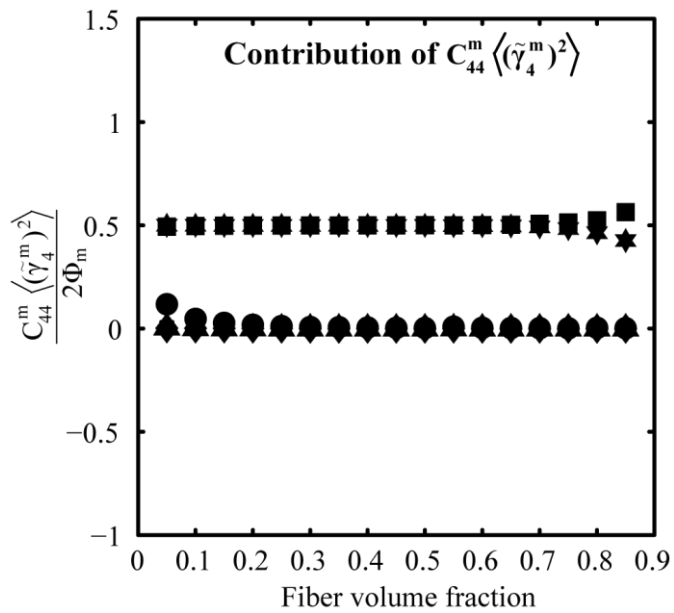
Figure 20: Variation of contribution of $C_{44}^m \langle (\tilde{\gamma}_4^m)^2 \rangle$ term to interaction energy of the matrix
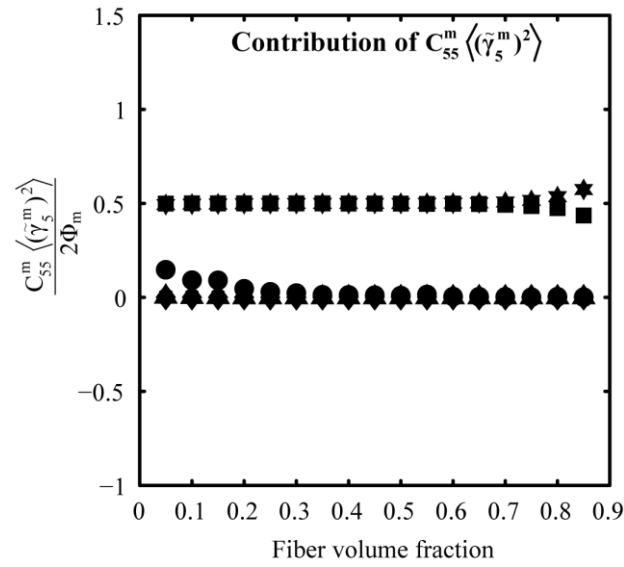
Figure 21: Variation of contribution of $C_{55}^m\left\langle\left(\tilde{\gamma}_5^m\right)^2\right\rangle$ term to interaction energy of the matrix
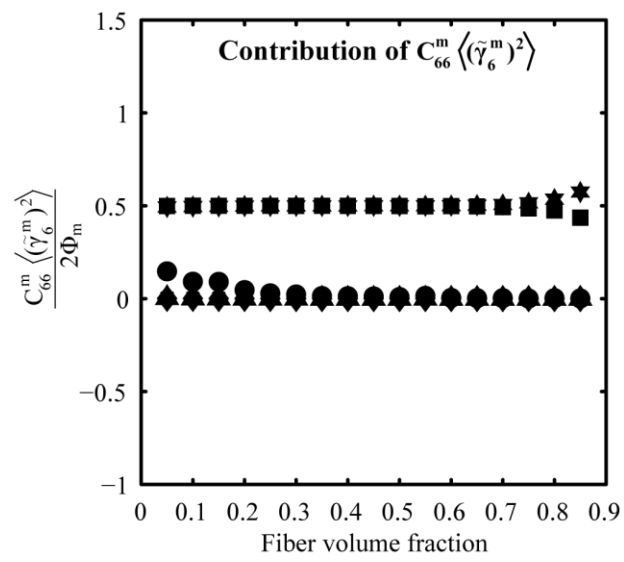
Figure 22: Variation of contribution of $C_{66}^m\left\langle\left(\tilde{\gamma}_6^m\right)^2\right\rangle$ term to interaction energy of the matrix

$C_{12}^m \langle \widetilde{\varepsilon}_1^m \cdot \widetilde{\varepsilon}_2^m \rangle$ and $C_{13}^m \langle \widetilde{\varepsilon}_1^m \cdot \widetilde{\varepsilon}_3^m \rangle$ is always zero irrespective of fiber volume fraction and load

case. The contribution of terms $C_{22}^m \langle (\widetilde{\varepsilon}_2^m)^2 \rangle$ and $C_{33}^m \langle (\widetilde{\varepsilon}_3^m)^2 \rangle$ to interaction energy of the matrix is

always zero irrespective of the fiber volume fraction for shear loading in the longitudinal

directions.

3.4.2. Effect of Relative Matrix Modulus on Interaction Energy

In order to investigate the variation of the interaction energy with matrix modulus, the

matrix modulus was varied from 1% to 120% of the fiber-direction fiber modulus. Results were

obtained for four fiber volume fractions: 0.05, 0.25, 0.60, and 0.85. Figure 23 shows the

variation of relative interaction energy with matrix modulus for the four unique load cases. Fig.

23a shows the variation of interaction energy with matrix modulus in longitudinal tension. For

this load case, the interaction energy for all volume fractions is negligible. For the other three

load cases, shown in Fig. 23b-d, a general trend is observed: an initial increase in matrix

modulus results in a decrease in interaction energy until a minimum is reached, after which

additional increase in matrix modulus results in an increase in interaction energy. The minimum

of the interaction energy occurs when the relevant fiber and matrix stiffnesses are the closest. For

the load case in the transverse direction, shown in Fig. 23b, the interaction energy reaches a

minimum when the matrix modulus is 5% of the fiber-direction fiber modulus, corresponding to

a matrix modulus of 11.75 GPa, which is close to the fiber modulus in the transverse direction of
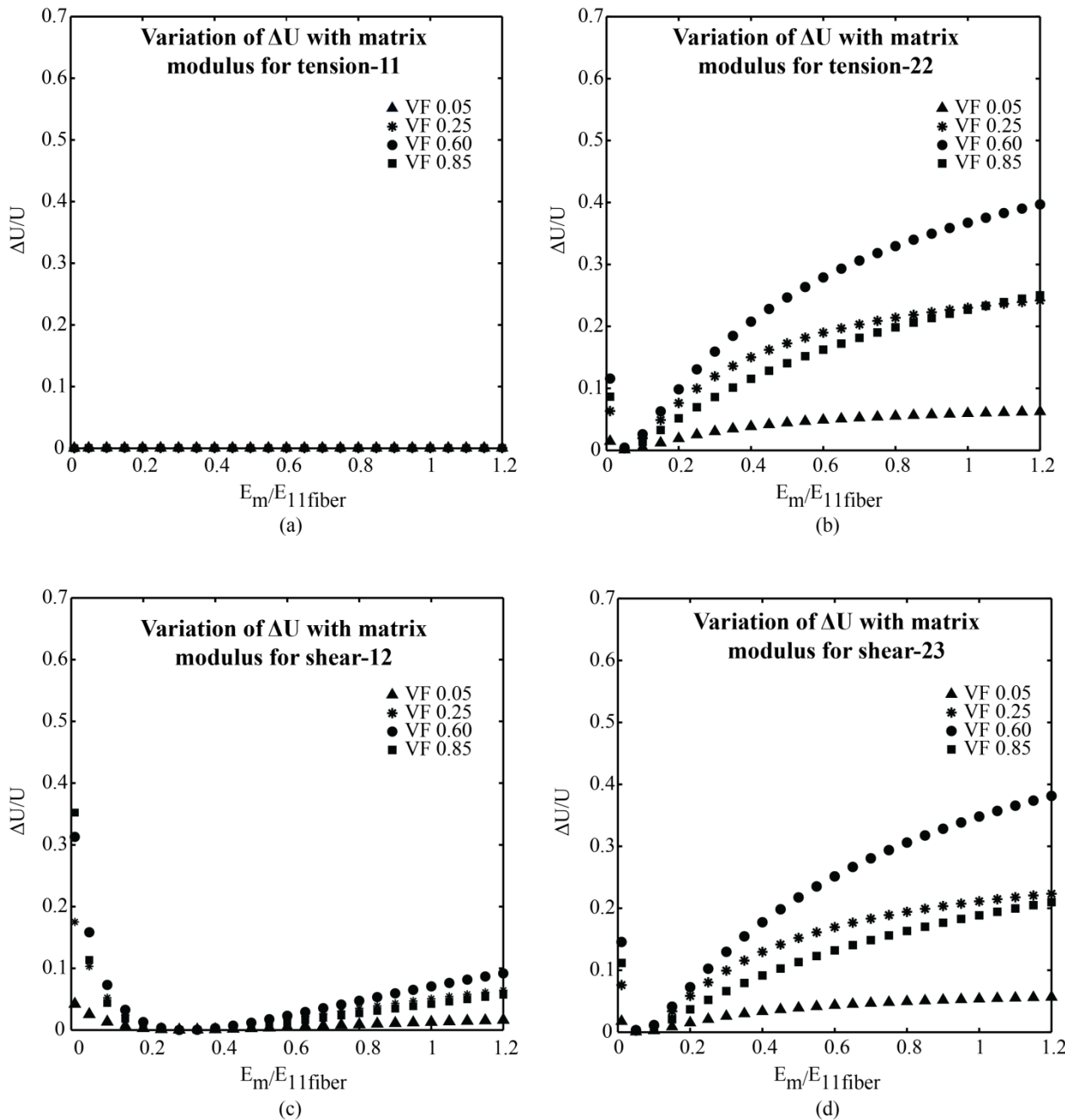
Figure 23: (a) Variation of interaction energy with matrix modulus in load case tension-11 (b) Variation of interaction energy with matrix modulus in load case tension-22 (c) Variation of interaction energy with matrix modulus in load case shear-12 (d) Variation of interaction energy with matrix modulus in load case shear-23

14 GPa. For a load case of shear-12, shown in Fig. 23c, the interaction energy reaches a minimum when the matrix modulus is 30% of the fiber-direction fiber modulus, corresponding to a matrix shear modulus of 26.31 GPa, which is close to the fiber shear modulus in 12-direction of 28 GPa. For a load case of shear-23, shown in Fig. 23d, the interaction energy reaches a minimum when the matrix modulus is 5% of the fiber-direction fiber modulus, corresponding to a matrix shear modulus of 4.38 GPa, which is close to the fiber shear modulus in 23-direction of 5.6 GPa. These results indicate that for near iso-stress loadings the interaction energy increases with increasing difference in the fiber and matrix modulus in the loading directions.

3.4.3. Effect of Combined Loading on Interaction Energy

In actual application, a composite is rarely subjected to uniaxial stresses and so it is important to study the behavior of interaction energy under multi-axial load states. As discussed in sections 3.4.1. and 3.4.2, the interaction energy for tensile loading in the longitudinal is negligible. Thus it was not included in the study of combined loads. The fiber volume fraction and the matrix modulus were held constant at 0.6 and 4.0 GPa, respectively. The biaxial load is represented by the radius of a circle as shown in Fig 9, where θ is the angle made by the radius of the circle with the x-axis which is varied from 0° to 180°.

Figure 24 shows the variation of interaction energy under five types of biaxial loadings: $(\sigma_{22}, \sigma_{33})$, $(\sigma_{12}, \sigma_{22})$, $(\sigma_{12}, \sigma_{23})$, $(\sigma_{12}, \sigma_{13})$, and $(\sigma_{23}, \sigma_{22})$. Under a biaxial longitudinal shear loading $\sigma_{12} - \sigma_{13}$ the interaction energy does not change, remaining constant at 27% of the total strain energy. This gives us an important metric for evaluating interaction energy under

combined longitudinal shear loading. For a particular fiber-matrix combination and fiber volume

fraction, interaction energy for biaxial shear loading is always the same as that for pure
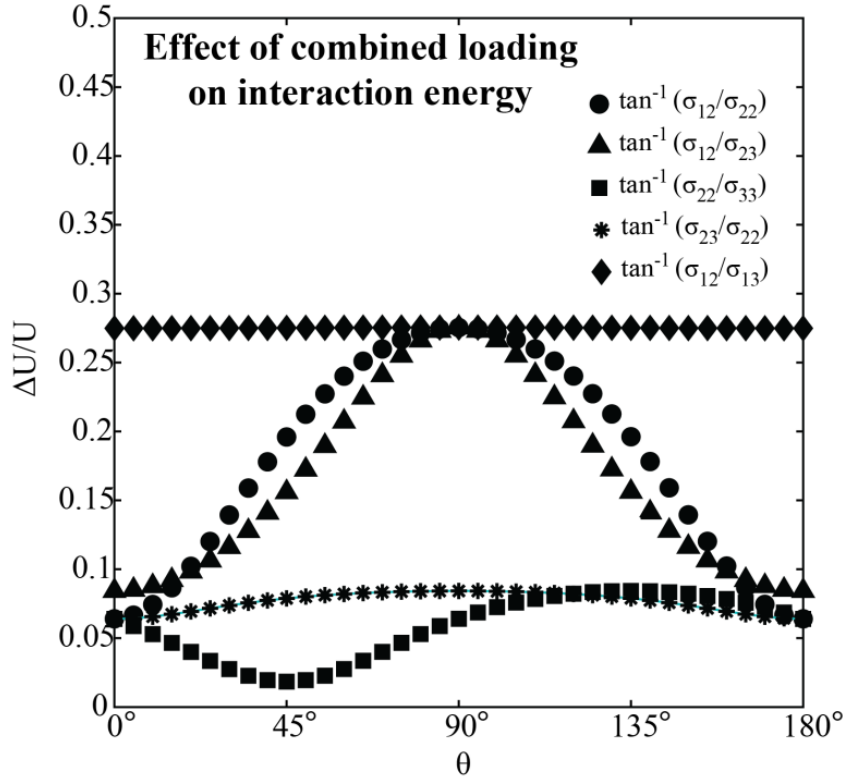
Figure 24: Variation of interaction energy with biaxial loads

longitudinal shear loading. Varying the ratio of σ_{12} to σ_{13} essentially rotates the stress

distributions in the RVE, but does not substantially change their relative quantitative values.

When the RVE was subjected to a transverse normal $(\sigma_{22}, \sigma_{33})$ biaxial loading the interaction

energy reached a minimum at 45°, corresponding to equal biaxial transverse loading. At this

angle a nearly uniform distribution of strains and stresses in the constituents is observed, similar

to Fig. 11a, producing negligible interaction energy. In the remaining three cases, $(\sigma_{12}, \sigma_{23})$, $(\sigma_{12}, \sigma_{22})$, and $(\sigma_{23}, \sigma_{22})$, the maximum interaction energy occurs at 90°, which corresponds to a pure shear loading. This result is remarkable: any deviation from a pure shear loading reduces the interaction energy that would be computed. Thus, the composite shear loading in particular causes interaction energies to become significant, such that the interaction energy could be bounded by evaluating only a small number of load states.

3.5 Summary and Conclusions

Accurate failure prediction is critical in efforts to maximize the promising advantages offered by composite materials. This requires physics-based failure prediction models, which necessarily require accurate understanding of constituent stress and strain. The use of volume average constituent stresses and strains to predict failure is a computationally efficient first step toward this effort, but does not account for the entire strain energy in the composite. In this study, this missing energy, termed the interaction energy, was introduced and expressions to define it were derived. A series of parametric finite element studies were conducted to quantify the relative magnitude of the interaction energy for varying fiber volume fractions, matrix modulus, and loading conditions. Our results showed that for typical carbon-epoxy composites used in the aerospace industry the interaction energy may be as high as 30% of the total strain energy in the composite under shear loading, which is the load state yielding the highest relative interaction energy. Furthermore, for such systems the matrix constituent is the major contributor to interaction energy. This result is important for future efforts to enhance composite failure prediction because it suggests that focus be placed on matrix failure criteria augmentation.

4. Benchmarking of lamina failure tests from WWFE-I and WWFE-II with a three parameter micromechanics based matrix failure theory

This chapter presents an existing three parameter micromechanics based matrix failure theory and its benchmarking with lamina test data from well-known composite failure benchmarks 'World Wide Failure Exercise-I' (WWFE-I) and 'World Wide Failure Exercise-II' (WWFE-II) (Hinton and Soden, 1998; Hinton and Kaddour, 2012). The WWFEs contain a detailed assessment of various leading theoretical approaches for predicting deformation and failure responses of polymer composite laminates under complex states of stress. The theoretical predictions were compared with one another and with experimental tests data. This chapter contains a detailed discussion of the Fertig failure theory which is followed by a brief discussion of the results and benchmarking against the available experimental test data from the WWFEs. A von Mises-maximum principal stress based matrix failure theory is also presented and is applied to one of the lamina failure test cases of the first World Wide Failure Exercise.

4.1 Introduction

For almost fifty years, accurate failure prediction of composites has been an overarching goal for both the scientists and engineers alike. This large span of time saw an abundance of failure modeling techniques introduced, which usually satisfy a particular set of data but fail to explain the generalized failure behavior of composites. This can be attributed to the complicated behavior of composites owing to their heterogeneous material properties and the large number of unknowns encountered during failure prediction. Then, there is the question of the scale at which to characterize failure. It is an ongoing debate whether constituent level failure prediction is

better than lamina or laminate level failure prediction. Finally, failure of composites is very subjective and end product oriented. What might constitute failure for an aerospace grade composite material might be totally different to failure of composite material used in an automobile. Considering the difficulty of the topic, it is not surprising that no theory is universally recognized as being a unified, verified and a complete failure methodology.

4.2 Failure modeling

4.2.1 Constituent level failure modeling

Composite structures are built from composite laminates, which are fabricated by stacking several composite laminae together. The behavior of each lamina is governed by its constituents, i.e. the properties of fibers, the surrounding matrix, the volume fraction of fibers, and fiber morphology. Most composite failure theories operate at the lamina scale by predicting lamina level failure using lamina level homogenized stresses and strains. Damage and failure at the lamina level is then used to predict laminate level failure. A major disadvantage of using lamina level quantities is that it does not allow the use of constituent level physics to explain the failure behavior of composites. Lamina level stress/strains are poor at describing the actual stress/strain state in the constituents. In reality, composite failure is a result of failure of one of its constituents, either the matrix or fiber. Thus it is important to characterize failure at the constituent level as opposed to the lamina level. This kind of failure methodology is called micromechanical failure modeling, which uses volume average quantities of the constituents to predict failure. For any type of composite loading, constituent level, volume average stresses are better at describing the stress/strain state in the constituents. They enable development of

physics-based models which can further expand our understanding of behavior of composites. It is due to these advantages that the failure techniques studied and developed in this work employ constituent level stresses in contrast to lamina level stresses. These constituent level stresses were extracted from a representative volume element (RVE) of an idealized microstructure of a hexagonally packed fiber reinforced composite, shown in Fig. 25. The RVE has periodic boundary conditions enforced on all its sides and was subjected to 6 types of load $\left(\sigma_{11}, \sigma_{22}, \sigma_{33}, \tau_{12}, \tau_{13}, \tau_{23} \right)$, which generated stresses in the fiber and the matrix regions. After
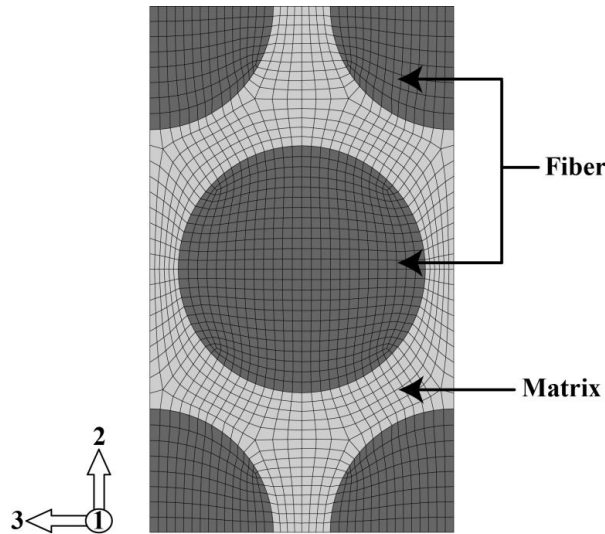
Figure 25: The RVE with hexagonal fiber
packing

extracting stresses from the fiber and the matrix regions, volume average constituent stresses were computed. This was accomplished by computing the mapping X between the composite and constituent stresses, which can be used to compute constituent level stresses for any type of composite load state.

This mapping can be computed as shown below

$$_L X_i^f = \frac{\sigma_i^f}{\sigma_L^c} \qquad \text{and} \qquad _L X_i^m = \frac{\sigma_i^m}{\sigma_L^c} \qquad (4.1)$$

where the subscript L denotes the load case, i ($i = 11,22,\ldots,23$) denotes the six components of the stress vector, f denotes the fiber, m denotes the matrix and c denotes the composite. For example the mapping functions for matrix constituent under a pure σ_{11} composite load state are

$$_1 X_i^m = \frac{\sigma_i^m}{\sigma_1^c} \qquad (4.2)$$

Thus for any composite load state, the stress i in a constituent a is given by

$$\sigma_i^a = \sum_{j=1}^{6} {}_j X_i^a \sigma_j^c \qquad (4.3)$$

4.2.2. The Fertig Failure theory

The Fertig failure theory (Fertig III, 2012) is a micromechanical matrix failure theory that requires three parameters, which all have physical meaning, and utilizes volume-average constituent level stresses to predict failure of a constituent (matrix or fiber here) and thereby of the composite. One particularly attractive feature of this theory lies in its simple calibration to obtain three parameters, which can then be used to predict failure load under any composite state of stress. According to this theory, matrix failure occurs when

$$B_t\{I_t\}^2 + \cfrac{1}{1+\cfrac{\beta}{\tau_0}\{-I_h\}}[B_{s1}I_{s1} + B_{s2}I_{s2}] = 1 \tag{4.4}$$

where B_t, B_{s1}, B_{s2} represent the coefficients of matrix average stress invariants; I_t, I_{s1}, I_{s2}, I_h represent the invariants of matrix stress tensor, τ_0 represents the shear strength of the matrix, and β represents pressure strengthening due to compressive loading (~ 0.35) (Hoppel et al., 1995a). The values of B_i are determined from three composite static failure tests: *transverse tension, transverse compression, and longitudinal shear*, all of which involve failure of the matrix constituent. The invariants are computed from the volume average matrix stresses as follows

$$I_t = \frac{\sigma_{22}^m + \sigma_{33}^m + \sqrt{(\sigma_{22}^m + \sigma_{33}^m)^2 - 4(\sigma_{22}^m\sigma_{33}^m - \sigma_{23}^m\sigma_{23}^m)}}{2} \tag{4.5}$$

$$I_{s1} = \sigma_{12}^{m\,2} + \sigma_{13}^{m\,2} \tag{4.6}$$

$$I_{s2} = \frac{1}{4}(\sigma_{22}^m - \sigma_{33}^m)^2 + \sigma_{23}^{m\,2} \tag{4.7}$$

$$I_h = \sigma_{22}^m + \sigma_{33}^m \tag{4.8}$$

where I_t corresponds to the maximum tensile stress normal to the fiber, I_{s1} is related to the shear in the longitudinal direction, I_{s2} is related to the transverse shear, and I_h represents the pressure on the maximum transverse shear plane.

In order to predict the failure envelopes for lamina failure test cases of the World Wide Failure Exercises, the B_i terms were calibrated for each case by using available lamina strengths which correspond to failure loads. The RVE was first subjected to a transverse failure load and the resultant matrix stresses were used to compute matrix stress invariants using Eqs. (4.5)- (4.8) which were then substituted in Eq. (4.4) to obtain three values of the three unknown co-efficients B_t, B_{s1}, B_{s2}. Similarly, the RVE was subjected to transverse compressive failure load and longitudinal shear failure load to obtain three more values for each load case. The three equations with three unknowns were then expressed as

$$\begin{bmatrix} V_{11} & V_{12} & V_{13} \\ V_{21} & V_{22} & V_{23} \\ V_{31} & V_{32} & V_{33} \end{bmatrix} \begin{bmatrix} B_t \\ B_{s1} \\ B_{s2} \end{bmatrix} = \begin{bmatrix} 1 \\ 1 \\ 1 \end{bmatrix} \tag{4.9}$$

where V_{ij} are the values obtained by subjecting the RVE to failure loads. The three coefficients for each test case were computed by inverting the V_{ij} matrix as shown below

$$\begin{bmatrix} B_t \\ B_{s1} \\ B_{s2} \end{bmatrix} = \begin{bmatrix} V_{11} & V_{12} & V_{13} \\ V_{21} & V_{22} & V_{23} \\ V_{31} & V_{32} & V_{33} \end{bmatrix}^{-1} \begin{bmatrix} 1 \\ 1 \\ 1 \end{bmatrix} \tag{4.10}$$

The fiber failure criterion uses maximum stress failure criterion given by

$$\frac{\sigma_{11}^f}{S_{11}^{f+}} = 1 \qquad \text{or} \qquad \frac{\sigma_{11}^f}{S_{11}^{f-}} = 1 \tag{4.11}$$

where S_{11}^{f+} is the longitudinal tensile strength of the fiber and S_{11}^{f-} is the longitudinal compressive strength of the fiber. It must be noted that the longitudinal strength of the fiber is used here to

express the in situ failure of fibers due various failure mechanism like fiber fracture, fiber pullout, fiber buckling etc.

4.2.3. Matrix failure theory based on von Mises-maximum principal stress

The second matrix failure theory used in this chapter is based on von Mises-maximum principal stress. The failure theory predicts matrix failure when the von Mises stress or the maximum principal stress in the matrix exceeds a critical value. This approach first requires the calculation of matrix stress concentration factor in an ideal microstructure at the point of matrix failure

S, Max. Principal
(Avg: 75%)
+5.117e+01
+4.656e+01
+4.195e+01
+3.734e+01
+3.273e+01
+2.812e+01
+2.351e+01
+1.890e+01
+1.430e+01
+9.686e+00
+5.077e+00
+4.672e−01
−4.142e+00

σ_{Vavg} = 30.3866 MPa
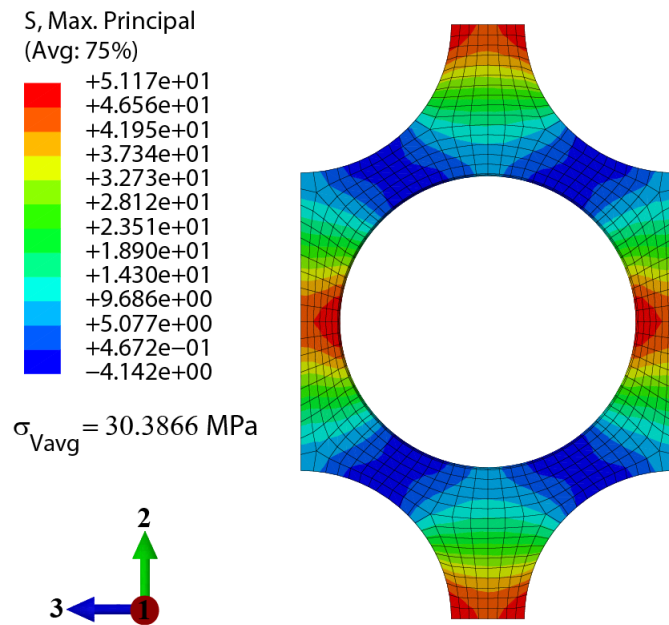
Figure 26: Fluctuations in maximum principal stress
in the matrix

under transverse tension. Figure 26 shows the fluctuations in the maximum principal stress in the matrix constituent when an RVE was subjected to transverse failure load. The matrix stress

concentration factor (α_m) can be computed using the maximum principal stress in the matrix

constituent and the nominal (or volume average) stress in the matrix as follows

$$\alpha_m = \frac{\sigma_{max}^m}{\sigma_{nom}^m} \qquad (4.12)$$

where α_m is the matrix stress concentration factor and σ_{max}^m and σ_{nom}^m are the maximum principal

stress and nominal matrix stress respectively that must be extracted from the RVE. Since α_m uses

peak stress in the matrix it is strongly dependent on the mesh size of the RVE. A coarse mesh in

the RVE may not capture the peak stress in the matrix constituent accurately and lead to

incorrect computation of α_m and this error in computation of α_m may lead to incorrect prediction

failure loads. A mesh convergence study needs to be done to make sure that the mesh size of the

RVE is refined enough to capture the correct maximum principal stress in the matrix constituent.

The matrix failure criterion is taken to be

$$\frac{\sigma_{max\ principal}^m}{S_{+t}^m \alpha_m} = 1 \qquad \text{or} \qquad \frac{\sigma_{VM}^m}{S_{VM}^m} = 1 \qquad (4.13)$$

where $\sigma_{max\ principal}^m$ is the maximum principal matrix stress, σ_{VM}^m is the von Mises stress in the

matrix, S_{+t}^m is the transverse tensile strength of the matrix, S_{VM}^m is the von Mises strength of the

matrix, and α_m is the matrix stress concentration factor. The fiber failure criterion remains

unchanged. In order to predict the failure envelopes for lamina failure test cases of the World

Wide Failure Exercises, three quantities were required to be pre-computed for each of the test

cases. S_{+t}^m was computed by using Eq. (4.3) and the transverse strength of the lamina. α_m was

computed by using Eq. (4.12) . The maximum and the nominal stresses used in Eq. (4.12) were extracted by subjecting the RVEs to transverse failure loads. Finally, the laminae were subjected to longitudinal shear failure loads (or transverse compressive failure loads) and the matrix stresses were computed using Eq. (4.3). These stresses were then used to compute principal stresses in the matrix constituent and the von Mises strength of the matrix constituent S_{VM}^m was then obtained as follows

$$S_{VM}^m = \sqrt{\frac{(\sigma_I - \sigma_I)^2 + (\sigma_{II} - \sigma_{III})^2 + (\sigma_I - \sigma_{III})^2}{2}} \qquad (4.14)$$

where σ_I, σ_{II} and σ_{III} are the principal stresses of the matrix constituent.

4.3. Results

The focus of this chapter is to use the Fertig failure theory to predict failure of composites and benchmark it against lamina failure test data from well-known composite failure benchmarks 'World Wide Failure Exercise-I' (WWFE-I) and 'World Wide Failure Exercise-II' (WWFE-II). The failure exercises contain in total twenty-six carefully selected test cases which include strength envelopes and stress-strain curves for a range of unidirectional and multidirectional laminates. The Fertig failure theory is benchmarked against seven strength envelopes for unidirectional laminae. These are ideal for evaluating failure criteria, whereas laminate level tests are appropriate for evaluating the combination of failure criteria with progressive damage methodology. The details of the test cases are included in Table 2.

Table 2: Lamina failure tests from WWFE-I and WWFE-II

Test case	Lamina layup	Material	Loading
1	0°	E-glass/LY556 epoxy	σ_2 vs. τ_{12}
2	0°	T300/BSL914C carbon/epoxy	σ_1 vs. τ_{12}
3	0°	E-glass/MY750 epoxy	σ_2 vs. σ_1
4	0°	T300/PR319	τ_{12} vs. σ_2 $(\sigma_1 = \sigma_2 = \sigma_3)$
5	90°	E-glass/MY750 epoxy	σ_2 vs. σ_3 $(\sigma_1 = \sigma_3)$
6	0°	S-glass/epoxy	σ_1 vs. σ_3 $(\sigma_2 = \sigma_3)$
7	0°	Carbon/epoxy	σ_1 vs. σ_3 $(\sigma_2 = \sigma_3)$

4.3.1. Failure predictions of the Fertig failure theory

The benchmarking of the Fertig failure theory and its comparison with lamina test data and leading failure theories from the WWFEs is shown below.

Test case 1: GRP lamina under combined transverse and shear loading

The failure envelopes predicted by the Fertig failure theory for test case 1 are shown in Fig. 27.

Figure 27(a) shows the failure envelope when the UD values provided by the WWFE-I authors were used as model inputs. Figure 27(b) shows the failure envelope obtained when different UD values were used as inputs to the model which yielded slightly better results. In both the cases (a) and (b), the theory fits the shape of the test data very well especially in the $(+\sigma_2, \tau_{12})$ quadrant. In case (a), the Fertig failure theory is conservative, especially in the $(-\sigma_2, \tau_{12})$ quadrant. By choosing a different transverse compressive strength than the one given by the originators of the exercise, the theory predicts a failure envelope which is a little less conservative. The test data shows an increase in shear strength with an increase in the transverse compressive load. This feature of the experimental data is not captured by the theory. It is known that material inhomogeneity in a composite gives rise to stress and strain fluctuations in the constituents. We have already shown that the volume average matrix stresses do not capture these stress/strain fluctuations in the constituents of the composite material and thus all the strain energy of a constituent is not accounted for. The bulk of this missing energy (about 30%) is due to fluctuations in the matrix constituent when the composite is a under shear state of stress. Because our failure theory uses volume average constituent level stresses to predict failure of the

65

constituents of the composite material, the matrix failure in this high shear region is not captured well since the missing strain energy in the matrix constituent is ignored. The matrix failure theory needs to be augmented with this missing energy to improve the predictions for this test case.
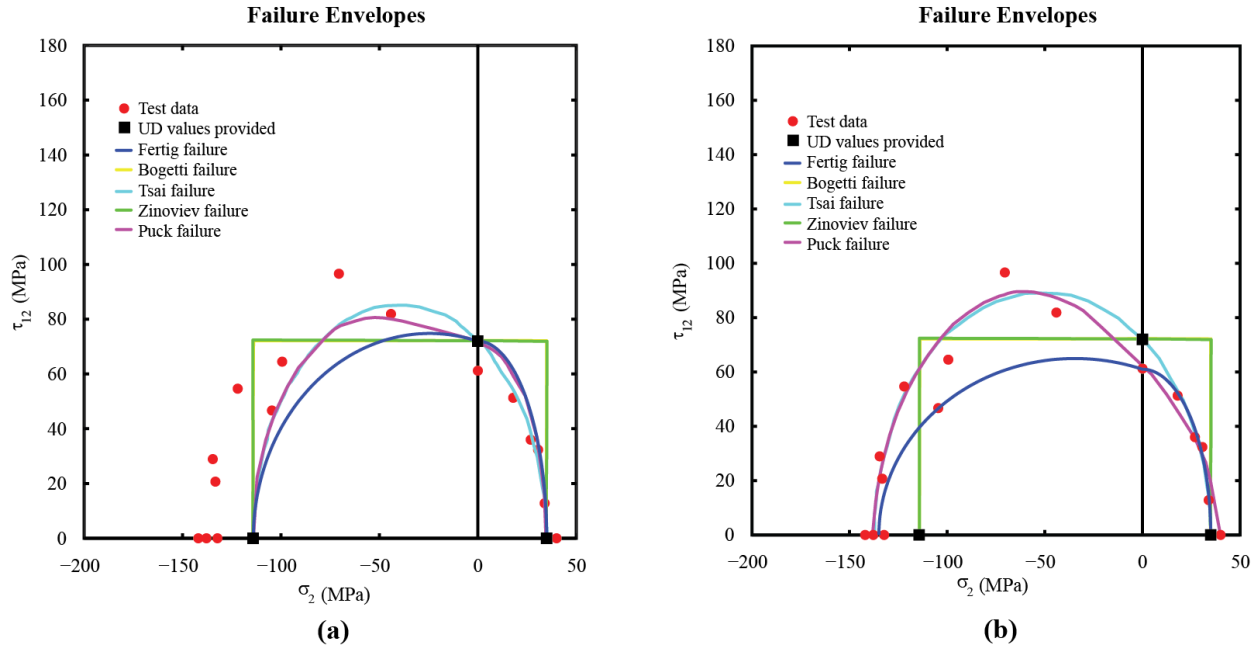
Figure 27: (a) Biaxial failure envelopes for 0° lamina made of GRP (E-glass/LY556) material with UD values provided as model inputs
(b) Biaxial failure envelopes for 0° lamina made of GRP (E-glass/LY556) material with different UD values used as model inputs

<u>Test case 2: CFRP lamina under combined longitudinal and shear loading</u>

The failure envelope predicted by the Fertig failure theory for test case 2 is shown in Fig.28. It can be seen that the theory captures the general shape of the experiments very well except in the high-shear region. As in case of test case 1, a matrix failure theory augmented with the missing energy may improve the predictions for this test case.
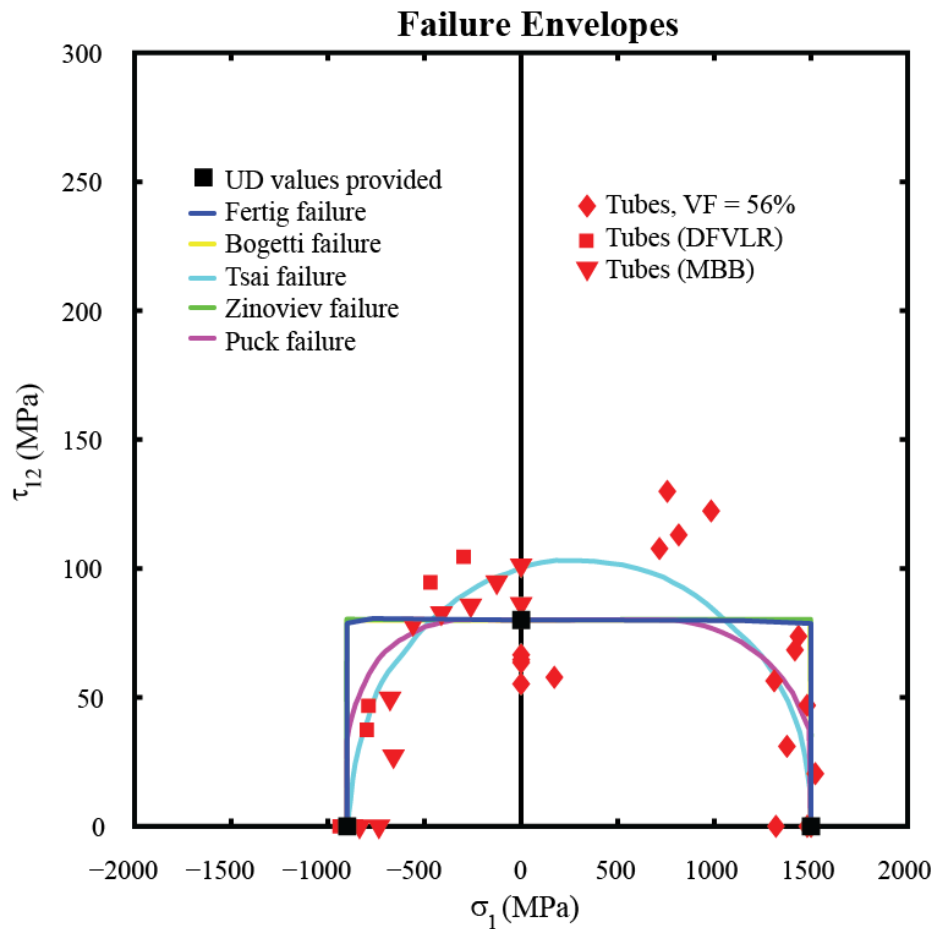
Figure 28: Biaxial failure envelopes for 0° lamina made of CFRP material (T300/BSL914C).

The failure prediction of the Fertig failure theory is shown in Fig. 29. It can be seen that like most of leading theories, the Fertig failure theory is very non conservative in the $(+\sigma_1, -\sigma_2)$ quadrant. The discrepancy between the observed and predicted modes of failure is due to the inability of theory to incorporate matrix stresses (σ_{11}^m) in the fiber direction.
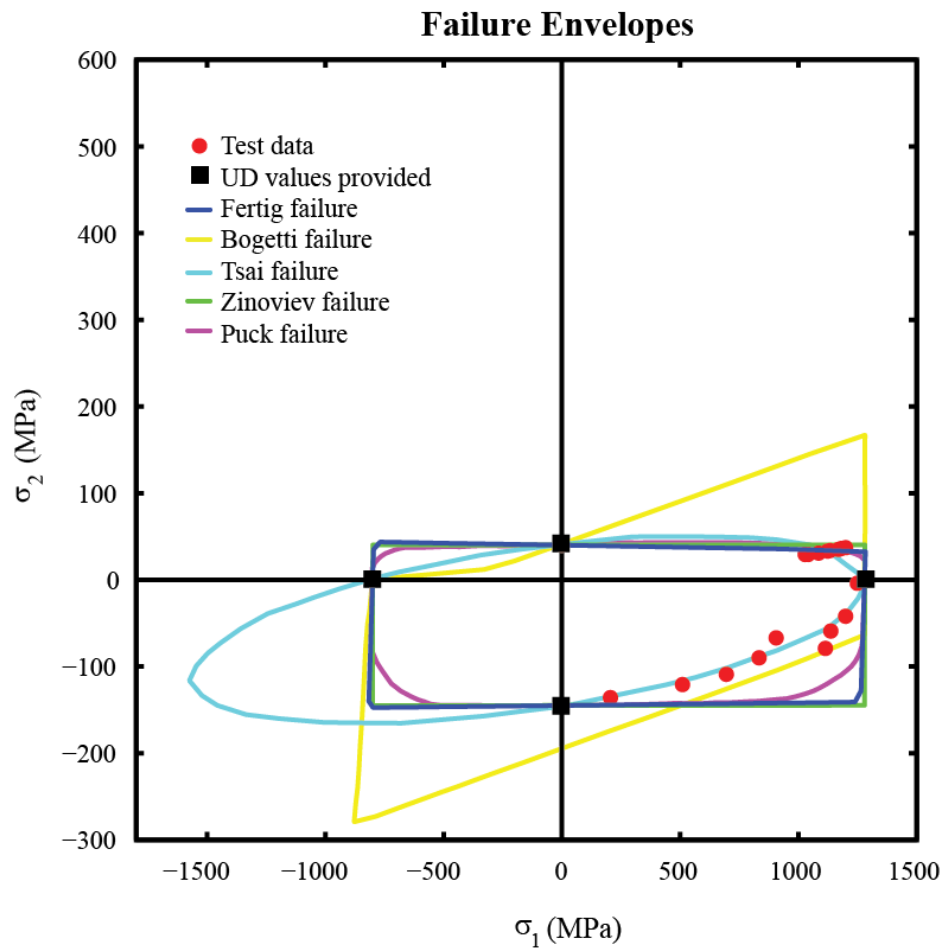
Figure 29: Biaxial failure envelopes for 0° lamina made of GRP material (E-glass/MY750).

The failure envelopes predicted by the von Mises-maximum principal stress failure theory for test case 3 are shown in Fig. 30. It can be seen that the theory captures the shape of the data well, especially in the $(+\sigma_1, -\sigma_2)$ quadrant upto a point after which it is very conservative.
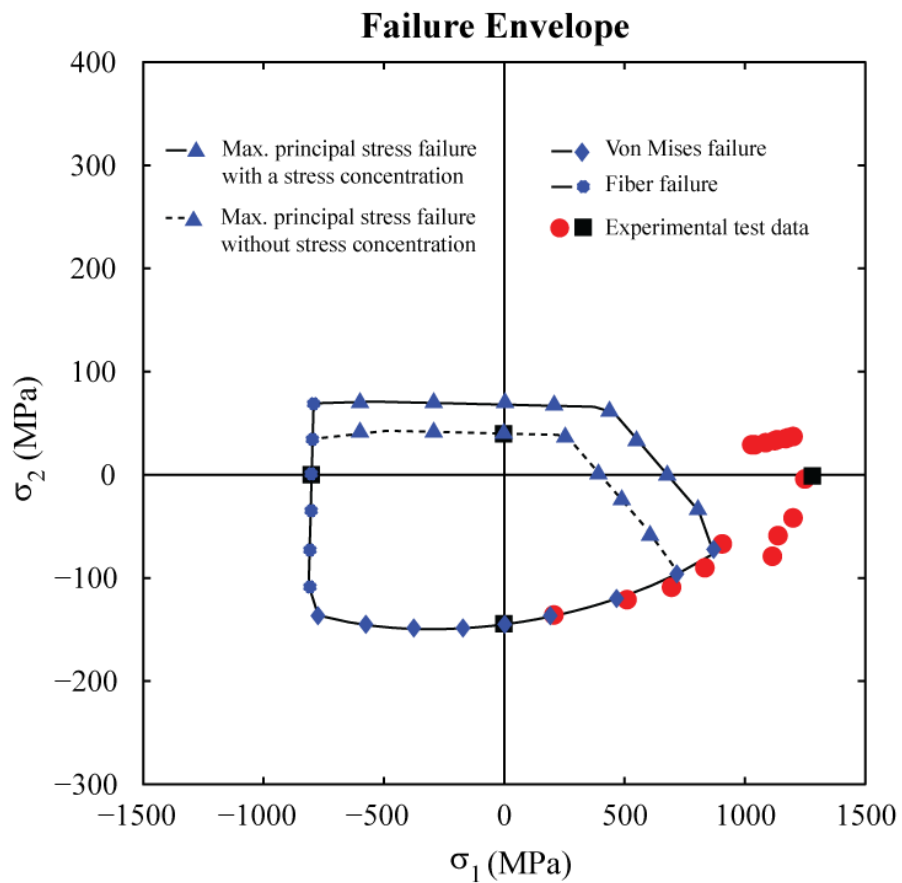
Figure 30: Biaxial failure envelopes for 0° lamina made of GRP material (E-glass/MY750) predicted by Von Mises – Max. principal stress theory

In the absence of the stress concentration factor, the matrix fails much before actual failure as suggested by the experimental data. This failure is captured by the theory when the appropriate stress concentration factor was used. The test data suggests that catastrophic failure of the lamina

occurred just before the load reached the tensile strength of the fiber. This was because even though the matrix had failed, the fiber could hold the composite together but now it was carrying a larger load. Von Mises – maximum principal stress based failure theory was used with a progressive damage scheme to capture this behavior in the fourth quadrant. After matrix cracking, the load carrying capacity of the matrix reduces significantly. To calculate the resultant fiber stresses after matrix failure, the matrix properties were degraded as follows

$$E^m_{new} = 15\% E^m_{original} \tag{4.15}$$

$$\upsilon^m_{new} = 0.01\% \upsilon^m_{original} \tag{4.16}$$

where E^m_{new} and $E^m_{original}$ are the new and original Elastic moduli of the matrix respectively and

υ^m_{new} and $\upsilon^m_{original}$ are the new and original poisons ratio of the matrix respectively. The new resultant fiber stresses were computed from the RVE with hexagonal fiber packing using the procedure discussed in section 4.2. The original fiber failure criterion and new fiber stresses were then used to compute failure load which represents catastrophic composite failure. The failure envelope predicted is shown in Fig. 31 along with the failure loads predicted previously without using any progressive damage scheme. It can be seen that after a particular load, the matrix fails much before what is seen in the experiments and all the load is now transferred to the fibers, the failure of which results in catastrophic composite failure.
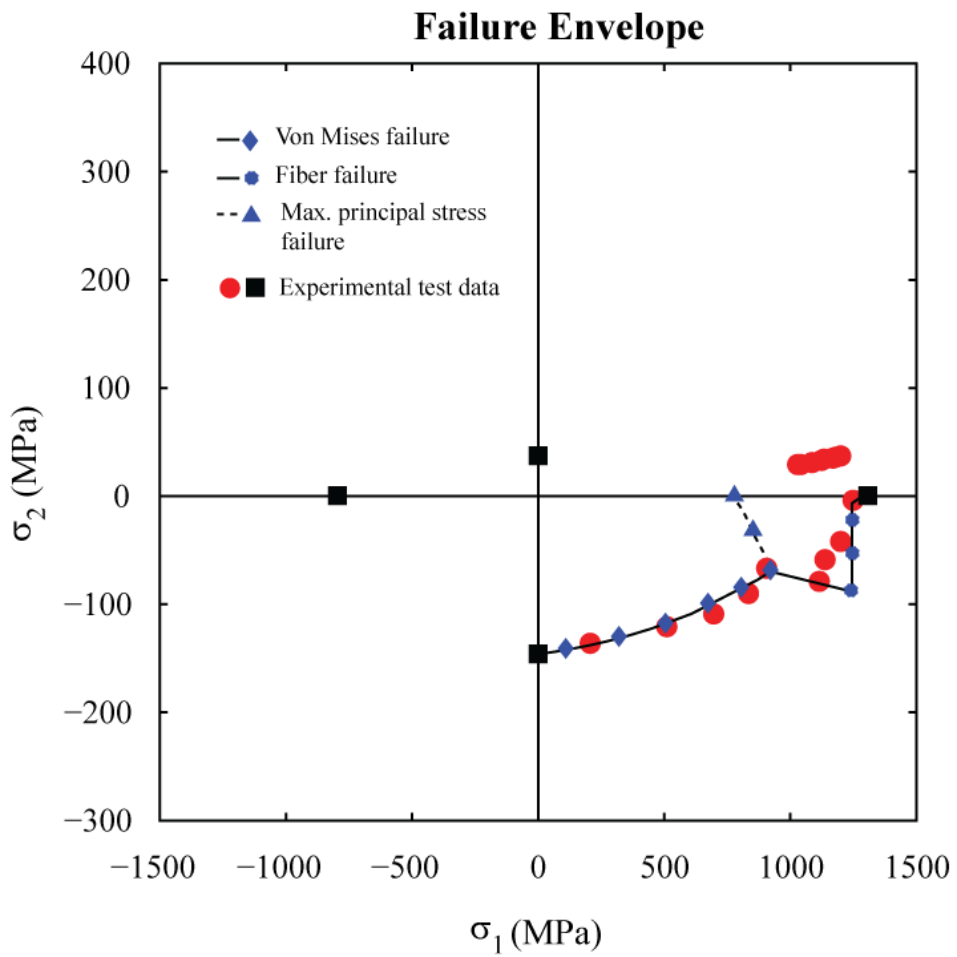
Figure 31: Biaxial failure envelopes for 0° lamina made of GRP material (E-glass/MY750) predicted by Von Mises – Max. principal stress theory with progressive matrix damage

Test case 4: CFRP lamina under combined hydrostatic and shear loading

The failure envelopes predicted by the Fertig failure theory for test case 4 are shown in Fig. 32. Figure 32(a) shows the failure envelope when the UD values provided by the authors were used as model inputs and $\beta=0.1$ and Fig. 32(b) shows the failure envelope when different UD values were used as inputs to the model and $\beta=0.35$. In both the cases (a) and (b), the theory fits the shape of the test data very well. When the shear strength of the 0° tubes is used as one of the model inputs, the theory captures the test data of the 0° very well. When the UD values provided by the
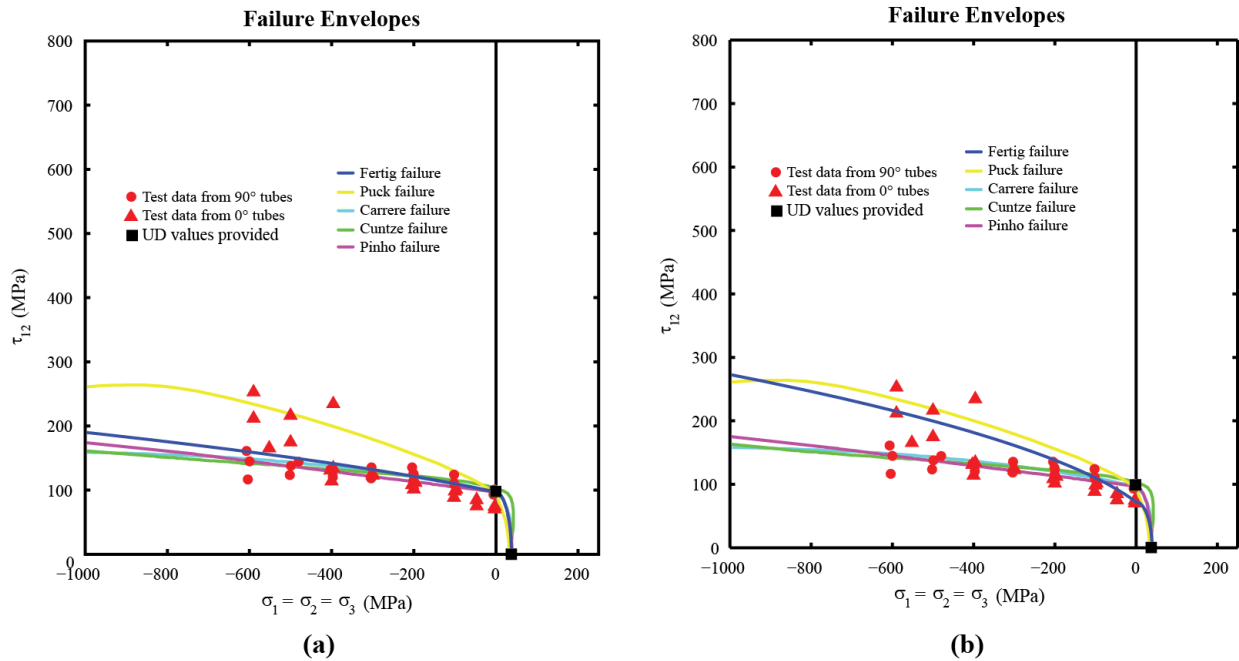
Figure 32: (a) Triaxial failure envelopes for 0° lamina made of CFRP material (T300/PR319) with β=0.01
(b) Triaxial failure envelopes for 0° lamina made of CFRP material (T300/PR319) with β=0.35

originators of the exercise are used, the pressure strengthening term β has to be reduced to 0.1 from 0.35 to capture the failure of 90° tubes.

Test case 5: GRP lamina with combined transverse and through thickness loading

The failure envelope predicted by the Fertig failure theory for test case 5 is shown in Fig. 33. It can be seen that the predictions of the theory captures failure very well.
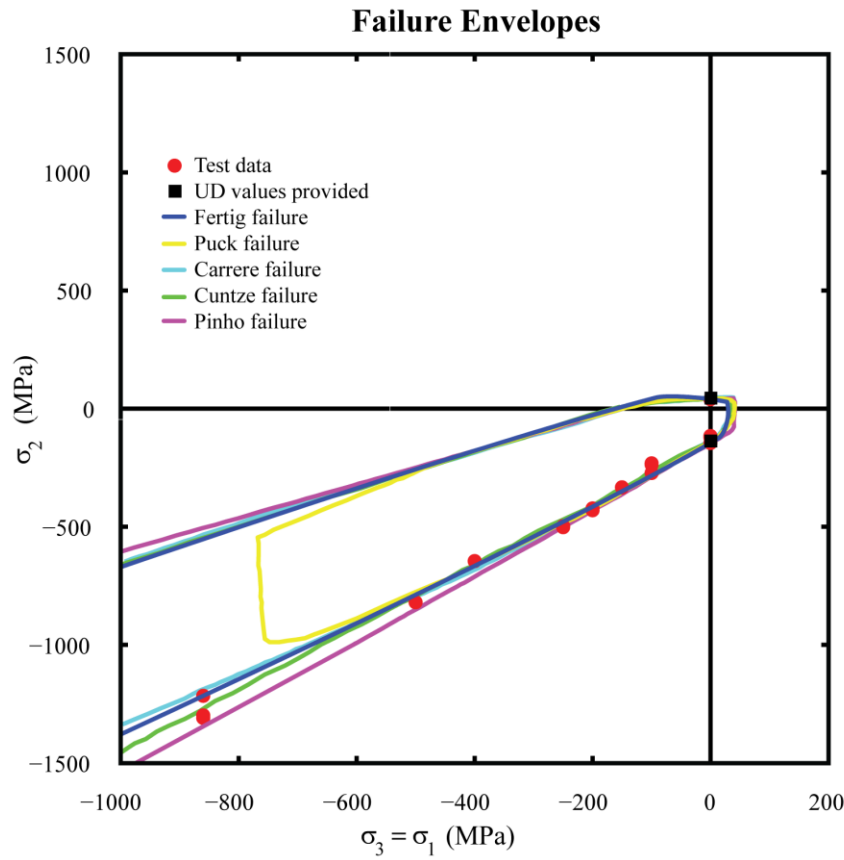
Figure 33: Triaxial failure envelopes for 0° lamina made of GRP material (E-glass/MY750)

Test case 6: GRP lamina with combined through thickness and longitudinal loading

The failure envelope predicted by the Fertig failure theory for test case 6 is shown in Fig. 34. There is a large scatter of data in the $(+\sigma_1, -\sigma_2/-\sigma_3)$ quadrant in which the theory does a good job predicting failure. In the $(-\sigma_1, -\sigma_2/-\sigma_3)$ failure seems to be occurring due to fiber kinking which was concluded by Pinho (Pinho et al., 2013) - "For matrix failure under considerable superposed hydrostatic pressure, the stress state in the specimen after matrix failure can in principle lead to subsequent fibre kinking". Since the fiber failure criterion does not account for fiber kinking, the
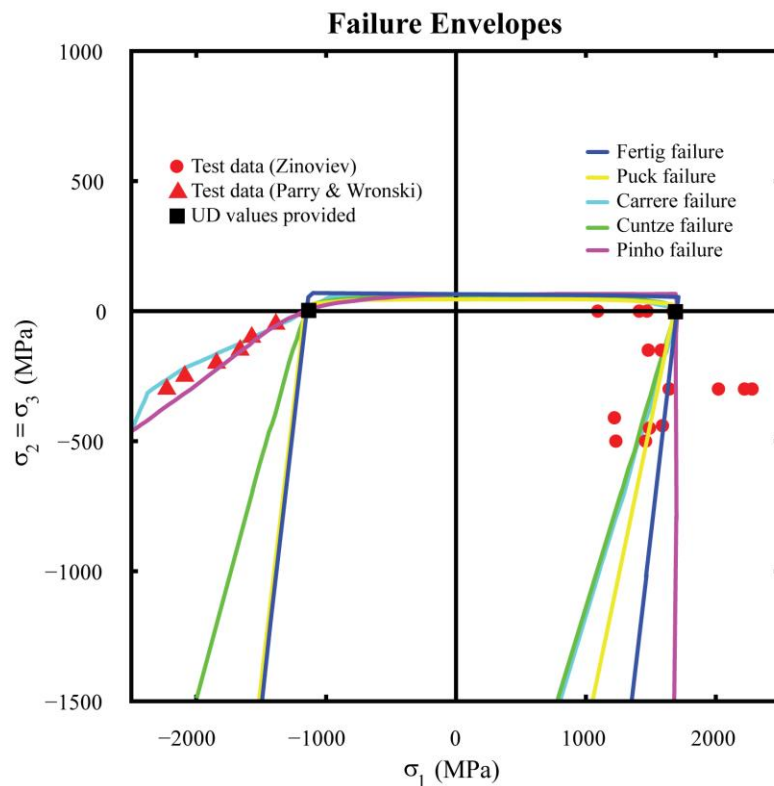
Figure 34: Triaxial failure envelopes for 0° lamina made of GRP material (S-glass/Epoxy)

theory gives more conservative results. It can be seen that two theories – Pinho (Pinho et al., 2012) and Carrerre (Carrere et al., 2012) capture fiber kinking very well.

Test case 7: CFRP lamina with combined through thickness and longitudinal loading

A comparison of failure theories for test case 7 is shown in Fig. 35. The Fertig failure theory captures the overall shape of the data. Similar to case 6, in the $(-\sigma_1, -\sigma_2/-\sigma_3)$ compressive failure was not captured by the theory. Since the fiber failure criterion does not account for fiber
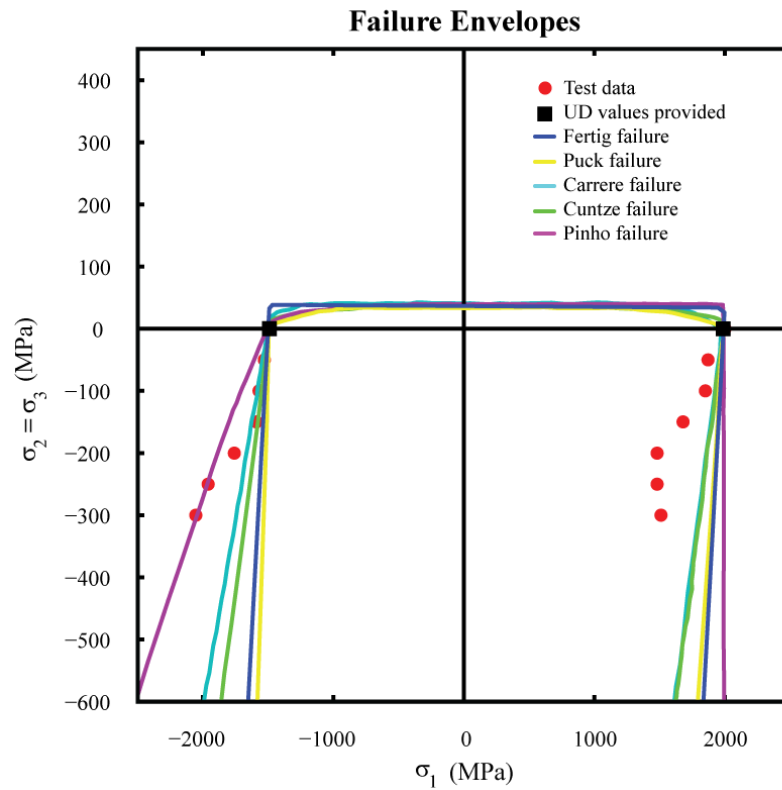
Figure 35: Triaxial failure envelopes for 0° lamina made of CFRP material (Carbon/Epoxy)

kinking, the predictions of the theory are again conservative. It can be seen again, that the Pinho failure theory captures fiber kinking very well.

4.4. Conclusions

An existing three parameter micromechanics based matrix failure theory was presented and its failure load predictions were compared with experimental data from the WWFE exercises. It was concluded for most of the test cases, the predictions of the Fertig failure theory were in close agreement with the test data. The Fertig failure theory over-predicted failure loads for GRP lamina under combined normal and longitudinal compressive loading (test case 3) where the failure was caused by matrix cracking perpendicular to the fibers. The Fertig failure theory could not predict these cracks in the matrix due to the inability of the theory to incorporate the contribution of the longitudinal stress in the matrix constituent $\left(\sigma_{11}^m\right)$ that had caused the cracking. The theory was conservative in predicting the fiber failures under compressive loads in test case 6 and 7 since a simple maximum stress failure criterion was used to predict the strength of fibers under compression. The Fertig failure theory needs to incorporate the effect of fiber buckling to improve failure prediction of the fiber constituent under compressive loads. In general, the predictions of the theory were also similar to the leading failure theories from the WWFE exercises. However, the leading theories from WWFE-I and WWFE-II require substantially more input parameters, which makes calibration very difficult. The advantage of the Fertig failure theory lies in its simplistic calibration, which requires just three parameters that can be obtained from three standard composite failure tests (transverse tension, transverse compression and longitudinal shear). The theory uses volume average matrix stresses to predict

failure loads. It has been shown that these volume average constituent quantities do not capture all the energy. If the failure theory is augmented with this missing energy, the failure predicting capabilities might be improved especially for shear loads.

The second failure methodology presented in this work is based on von Mises – maximum principal stress which uses constituent stresses to predict failure loads. A failure envelope was obtained using this theory for test case 3. The matrix appeared to fail much before catastrophic failure of the lamina that was observed in the test data. After matrix cracking normal to the fiber direction, the fibers were the only load carrying agents left and the lamina was then held together only by the fibers. This behavior of the lamina was predicted by using von Mises – maximum principal stress theory along with a progressive damage scheme for test case 3 where the properties of the matrix were degraded substantially and the failure envelope obtained was better than the predictions of any of the leading failure theories.

5. Matrix failure modeling accounting for interaction energy

In Chapter 2 it was shown that volume average constituent level stresses that are used to predict strengths using a micromechanics-based failure theory do not account for all the energy of the composite. This missing energy, termed interaction energy, is due to the inability of the volume average constituent level stresses to capture the stress/strain fluctuations produced in the constituents due to material inhomogeneity. Since these fluctuations are greatest in the matrix constituent and negligible in the fiber constituent, the bulk of the interaction energy contribution is due to fluctuations within the softer matrix constituent of the composite. Thus only the matrix failure theory was augmented with the interaction energy to improve composite failure load predictions. This chapter presents a methodology to augment the volume average matrix level stresses with appropriate fluctuations of stress in the matrix constituent. These matrix level stresses are energy consistent and are used with the Fertig failure theory to predict failure envelopes for lamina failure test cases of the first and second World Wide Failure Exercise. The results are compared with failure envelopes generated previously with the Fertig failure theory but with volume average matrix level stresses.

5.1 Augmenting the volume average matrix level quantities

The modelling technique presented in this chapter aims at developing a constituent-level stress measure that conserves energy by using respective stress/strain fluctuations in the matrix constituent as shown below

$$\bar{\sigma}_{ij}^{m} = \left\langle \sigma_{ij}^{m} \right\rangle + \operatorname{sign}\left(\left\langle \sigma_{ij}^{m} \right\rangle \right) \Psi \sqrt{\tilde{\sigma}_{ij}^{m2}} \qquad (5.1)$$

$$\overline{\varepsilon}_{ij}^{m} = \left\langle \varepsilon_{ij}^{m} \right\rangle + \text{sign}\left(\left\langle \sigma_{ij}^{m} \right\rangle\right)\Psi\sqrt{\tilde{\varepsilon}_{ij}^{m2}} \qquad (5.2)$$

where $\left\langle \sigma_{ij}^{m} \right\rangle$ and $\left\langle \varepsilon_{ij}^{m} \right\rangle$ are volume average matrix level stresses and strains respectively,

$\sqrt{\left\langle \tilde{\sigma}_{ij}^{m2} \right\rangle}$ and $\sqrt{\left\langle \tilde{\varepsilon}_{ij}^{m2} \right\rangle}$ are stress and strain fluctuations in the matrix respectively, $\overline{\sigma}_{ij}^{m}$ and $\overline{\varepsilon}_{ij}^{m}$ are

energy consistent matrix level stresses and strains respectively and Ψ is fluctuation energy

constant that minimizes the average error in the total energy. The fiber level stresses are not

augmented since the stress/strain fluctuations in the fiber constituent are negligible. A RVE of

hexagonal fiber packing must be subjected to unit biaxial/tri-axial loading according to the load

configuration being analyzed. The volume average fiber and matrix level quantities and volume

average stress/strain fluctuation squared quantities of the matrix constituent are extracted from

this Representative Volume Element (RVE). Average stress and strain fluctuations cannot be

directly computed by conventional averaging technique as that would yield zero. To obtain

consistent quantities for augmentation, volume average squared quantities are extracted and their

square roots are added to the respective volume average matrix quantities. Direct use of the

energy consistent stresses gives rise to excess strain energy and so the fluctuation energy

constant Ψ needs to be incorporated such that the new quantities do not over predict the strain

energy. A detailed procedure for approximating the fluctuations is presented in the following text

for Test case-1 of the first World Wide Failure Exercise. The fluctuations of the matrix

constituent for all the other test cases were obtained similarly.

5.1.1 Approximating the volume average stress fluctuations of the matrix constituent for a GRP lamina under combined normal and shear loading (Test case-1 of WWFE-I)

An RVE with hexagonal fiber packing was subjected to combined normal and shear loading. For extracting fluctuations and calibration, a unit biaxial load was applied such that it corresponded to the x- and y-components of the biaxial load represented as the radius of a circle as shown in Fig. 36 and θ is varied from 0° to 360°. The two uniaxial loads required to generate the normal and shear loading can be expressed as

$$\sigma_I = \sigma \cos \theta \tag{5.3}$$

$$\sigma_{II} = \sigma \sin \theta \tag{5.4}$$

where σ is the resultant bi-axial load and, σ_I and σ_{II} are the corresponding uniaxial loads. Volume average quantities (stresses and strains) of the fiber and matrix constituents and volume average fluctuation squared quantities (stresses and strains) of the matrix constituent were extracted from this RVE. Figure 37 shows plots of the stress fluctuations, the volume average stresses and the energy consistent stresses of the matrix constituent.
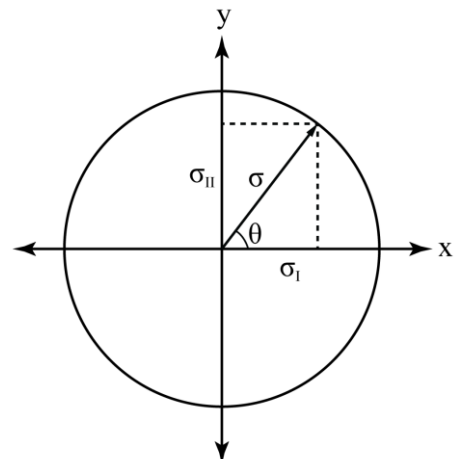
Figure 36: Decomposition of biaxial load into its components
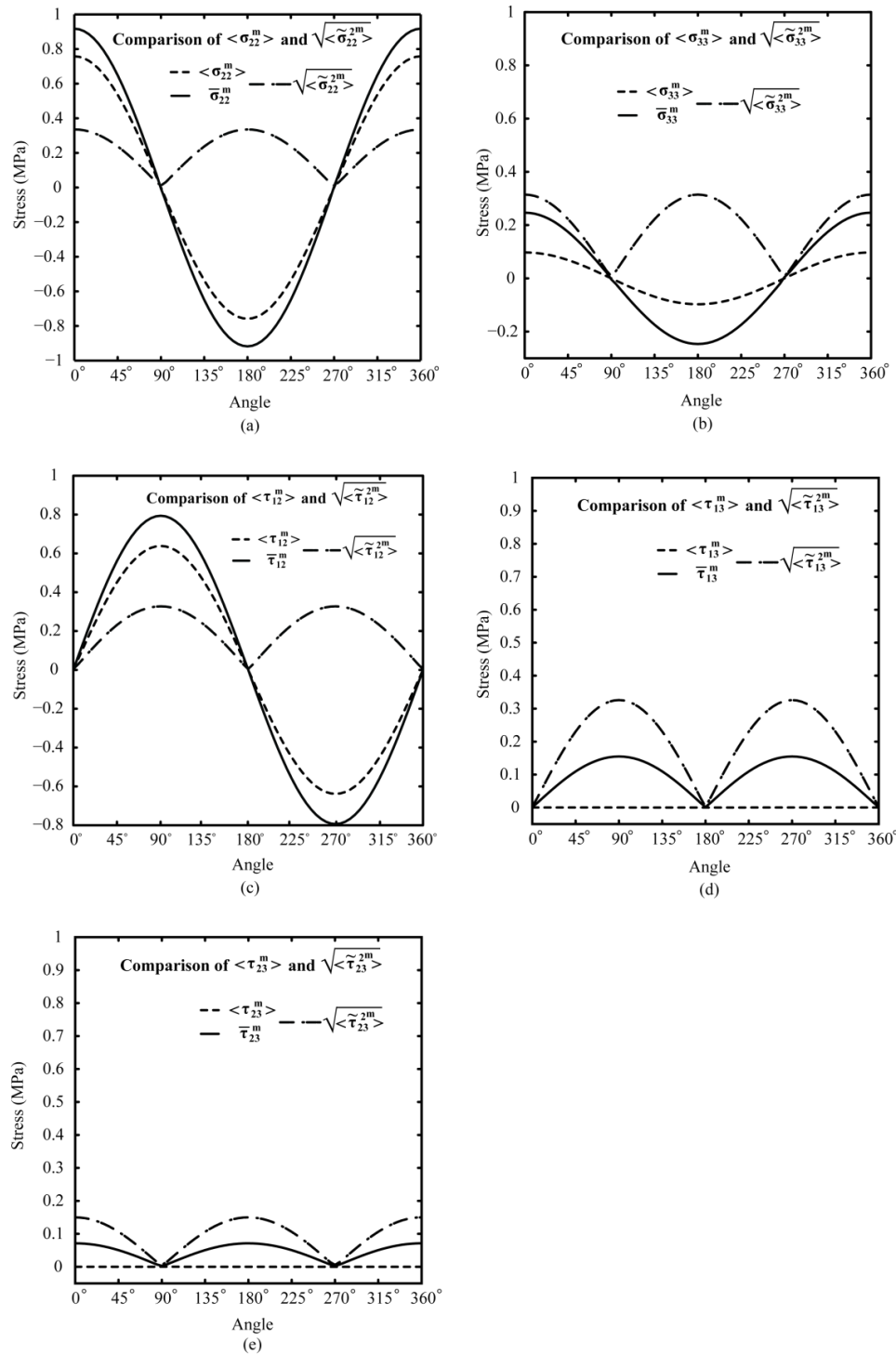
Figure 37: Comparison of volume average stresses and volume average stress fluctuations and the energy conserving stresses of the matrix constituent for GRP lamina under combined transverse normal and shear loading

The stress fluctuations observed in the matrix constituent can be categorized into two types: TYPE-I and TYPE-II. TYPE-I fluctuations can be determined from volume average stresses of the matrix constituent directly using the expression

$$\sqrt{\left\langle \widetilde{\sigma}_{ij}^{m\,2} \right\rangle} = F_{ij} \left\langle \sigma_{ij}^{m} \right\rangle \tag{5.5}$$

(no summation over repeated indices) where $\sqrt{\left\langle \widetilde{\sigma}_{ij}^{m\,2} \right\rangle}$ is volume average stress fluctuation of the matrix constituent, F_{ij} is a constant and $\left\langle \sigma_{ij}^{m} \right\rangle$ is the volume average stress of the matrix constituent. The constant F_{ij} was determined using the volume average stress fluctuations and the volume average stresses of the matrix constituent that were extracted from the RVE under unit biaxial load. In Fig. 37, volume average stress fluctuations in plots (a), (b) and (c) are TYPE-I fluctuations. TYPE-II fluctuations cannot be directly determined from the corresponding volume average matrix stresses and because the volume average stress is zero. These fluctuations are computed using either of the expressions

$$\sqrt{\left\langle \widetilde{\sigma}_{ij}^{m\,2} \right\rangle} = L\left(A_{ij}\left|\cos\theta\right| + B_{ij}\right) \tag{5.6}$$

$$\sqrt{\left\langle \widetilde{\sigma}_{ij}^{m\,2} \right\rangle} = L\left(A_{ij}\left|\sin\theta\right| + B_{ij}\right) \tag{5.7}$$

where $\sqrt{\left\langle \widetilde{\sigma}_{ij}^{m\,2} \right\rangle}$ is the volume average stress fluctuation of the matrix constituent, L is magnitude of the biaxial/tri-axial load, θ is the angle at which load is applied and A_{ij}, B_{ij} are constants. Again, A_{ij} and B_{ij} were calibrated using the volume average stress fluctuations of the matrix constituent of the RVE under unit biaxial load. For the load case under consideration,

82

volume average stress fluctuations in plots (d) and (e) are TYPE-II fluctuations. Table 3 shows the types of fluctuations that were observed in the various stress components when an RVE was subjected to biaxial/tri-axial states of stress that corresponded to the loading configurations of the lamina failure tests of the World Wide Failure Exercises. The fluctuation in the longitudinal normal stress component of the matrix constituent was not analyzed because it was concluded in Chapter 3 that these fluctuations do not give rise to any interaction energy.

Table 3: Type of fluctuations observed due to different loading configurations in the WWFEs

Test case	Material	Loading	Stress components TYPE-I fluctuations	Stress components TYPE-II fluctuations
1	E-glass/LY556 epoxy	σ_2 vs. τ_{12}	$\sigma_{22}^m, \sigma_{33}^m, \tau_{12}^m$	$\tau_{13}^m*, \tau_{23}^m$
2	T300/BSL914C carbon/epoxy	σ_1 vs. τ_{12}	τ_{12}^m	$\sigma_{22}^m, \sigma_{33}^m, \tau_{13}^m*, \tau_{23}^m$
3	E-glass/MY750 epoxy	σ_1 vs. σ_2	σ_{22}^m	$\sigma_{22}^m, \tau_{12}^m, \tau_{13}^m, \tau_{23}^m$
4	T300/PR319	τ_{12} vs. σ_2 $(\sigma_1 = \sigma_2 = \sigma_3)$	$\sigma_{22}^m, \sigma_{33}^m, \tau_{12}^m$	$\tau_{13}^m*, \tau_{23}^m$
5	E-glass/MY750 epoxy	σ_2 vs. σ_3 $(\sigma_1 = \sigma_3)$	-	$\sigma_{22}^m, \sigma_{33}^m, \tau_{12}^m, \tau_{13}^m, \tau_{23}^m$
6	S-glass/epoxy	σ_1 vs. σ_3 $(\sigma_2 = \sigma_3)$	$\sigma_{22}^m, \sigma_{33}^m$	$\tau_{12}^m, \tau_{13}^m, \tau_{23}^m$
7	Carbon/epoxy	σ_1 vs. σ_3 $(\sigma_2 = \sigma_3)$	$\sigma_{22}^m, \sigma_{33}^m$	$\tau_{12}^m, \tau_{13}^m, \tau_{23}^m$

*Although the fluctuations in the τ_{13}^m component of the matrix stress is of TYPE-II, it was approximated as TYPE-I fluctuation using fluctuations in the τ_{12}^m component of the matrix constituent.

A comparison of the constants F_{ij} and A_{ij}, B_{ij} for various lamina failure test cases of the World

Wide Failure Exercises is shown in Table 4, Table 5 and Table 6 respectively.

Table 4: Comparison of values of F_{ij} for various test cases of the WWFEs

Constants	Test case						
	1	2	3	4	5	6	7
F_{22}	0.445	-	0.435	0.143	-	0.154	0.075
F_{33}	3.245	-	-	0.140	-	0.154	0.075
F_{12}	0.513	0.452	-	0.528	-	-	-
F_{13}	0.513	0.452	-	0.528	-	-	-

Table 5: Comparison of values of A_{ij} for various test cases of the WWFEs

Constants	Test case						
	1	2	3	4	5	6	7
A_{22}	-	0.008	-	-	0.373	-	
A_{33}	-	0.006	0.309	-	0.532	-	
A_{12}	-	-	0.004	-	0.002	0.004	0.004
A_{13}	-	-	0.003	-	0.0004	0.004	0.004
A_{23}	0.144	0.004	0.145	0.111	0.103	0.128	0.068

Table 6: Comparison of values of B_{ij} for various test cases of the WWFEs

Constants	Test case						
	1	**2**	**3**	**4**	**5**	**6**	**7**
B_{22}	-	0.001	-	-	0.026	-	
B_{33}	-	0.006	0.004	-	0.006	-	
B_{12}	-	-	0.0005	-	0.003	0.0003	0.002
B_{13}	-	-	0.0003	-	0.003	0.0003	0.0002
B_{23}	0.006	0.001	0.004	0.006	0.052	0.003	0.001

The value from Tables 4, 5 and 6 suggest that all the constants F_{ij}, A_{ij} and B_{ij} are strongly

dependent on the type of loading and the material properties of the composite material.

5.1.2 Computing the fluctuation energy constant (Ψ)

Strain energy of the composite was computed using volume average quantities of the

fiber constituent and energy consistent quantities of the matrix constituent. In all the load cases it

was seen that direct augmentation of the matrix level quantities resulted in an over prediction of

the strain energy of the composite. The fluctuation energy constant (Ψ) was introduced not only

to prevent this over prediction of energy of the composite but also to minimize the average error

in the interaction energy. The interaction energy was computed using the volume average

composite quantities, volume average fiber level quantities and energy consistent quantities of

the matrix constituent which can be shown as

$$\Delta U = \frac{1}{2}\langle \sigma_{ij}^{C} \rangle \langle \varepsilon_{ij}^{C} \rangle V_{C} - \left(\frac{1}{2}\langle \sigma_{ij}^{f} \rangle \langle \varepsilon_{ij}^{f} \rangle V_{f} + \frac{1}{2}\left(\langle \sigma_{ij}^{m} \rangle + sign\left(\langle \sigma_{ij}^{m} \rangle\right)\Psi\sqrt{\tilde{\sigma}_{ij}^{m2}} \right)\left(\langle \varepsilon_{ij}^{m} \rangle + sign\left(\langle \varepsilon_{ij}^{m} \rangle\right)\Psi\sqrt{\tilde{\varepsilon}_{ij}^{m2}} \right)V_{m} \right) \quad (5.8)$$

An iterative process was used to compute Ψ such that the mean error in the interaction energy was zero. The different values of Ψ that were computed for the various lamina failure test cases are provided in Table 7.

Table 7: Values of Ψ for different test cases of the WWFEs

Test case	Material	Loading	Ψ
1	E-glass/LY556 epoxy	σ_2 vs. τ_{12}	0.4750
2	T300/BSL914C carbon/epoxy	σ_1 vs. τ_{12}	0.4110
3	E-glass/MY750 epoxy	σ_1 vs. σ_2	0.5360
4	T300/PR319	τ_{12} vs. σ_2 $(\sigma_1 = \sigma_2 = \sigma_3)$	0.3520
5	E-glass/MY750 epoxy	σ_2 vs. σ_3 $(\sigma_1 = \sigma_3)$	0.3620
6	S-glass/epoxy	σ_1 vs. σ_3 $(\sigma_2 = \sigma_3)$	0.4230
7	Carbon/epoxy	σ_1 vs. σ_3 $(\sigma_2 = \sigma_3)$	0.1070

It can be seen from table 7 that Ψ is a function of loading type, material properties of the composite, and the type of fiber packing in the RVE. Table 8 shows the values of Ψ that were obtained for composites with different material properties and same fiber volume fraction subjected to combined normal and longitudinal shear loading.

Table 8: Values of Ψ for different materials subjected to same loading configuration

Material	Ψ
E-glass/LY556 epoxy	0.4750
T300/BSL914C carbon/epoxy	0.5050
E-glass/MY750 epoxy	0.4730
T300/PR319	0.4750
E-glass/MY750 epoxy	0.4730
S-glass/epoxy	0.4780
Carbon/epoxy	0.4250

A comparison of interaction energy computed using volume average matrix stresses and energy consistent matrix level stresses from Eqs. (5.1) and (5.2) is shown in Figures 38-44.
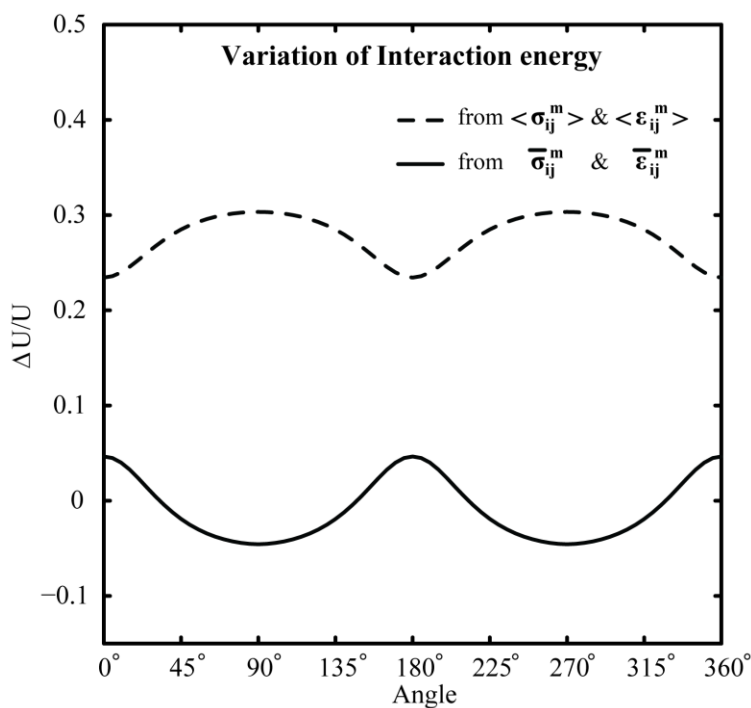

Figure 38: Interaction energy for test case-1
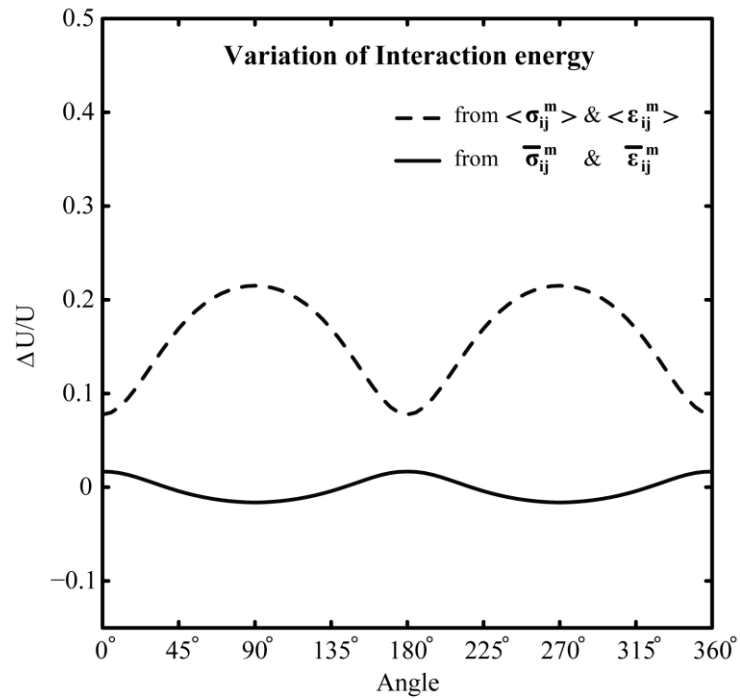
Figure 39: Interaction energy for test case-2
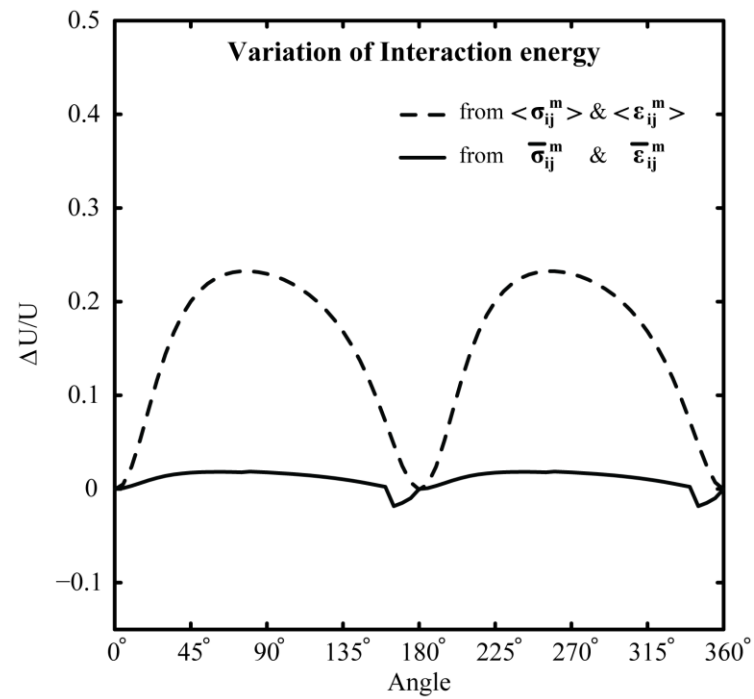
Figure 40: Interaction energy for test case-3
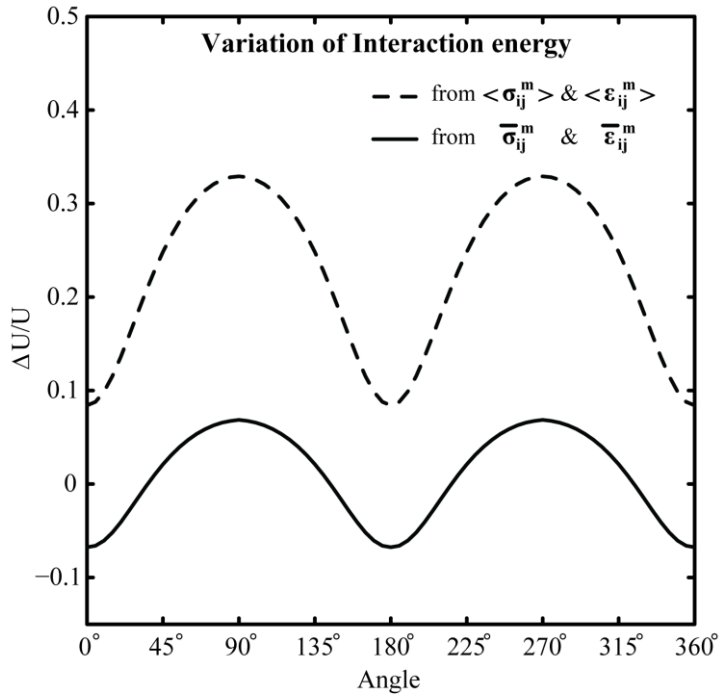
Figure 41: Interaction energy for test case-4
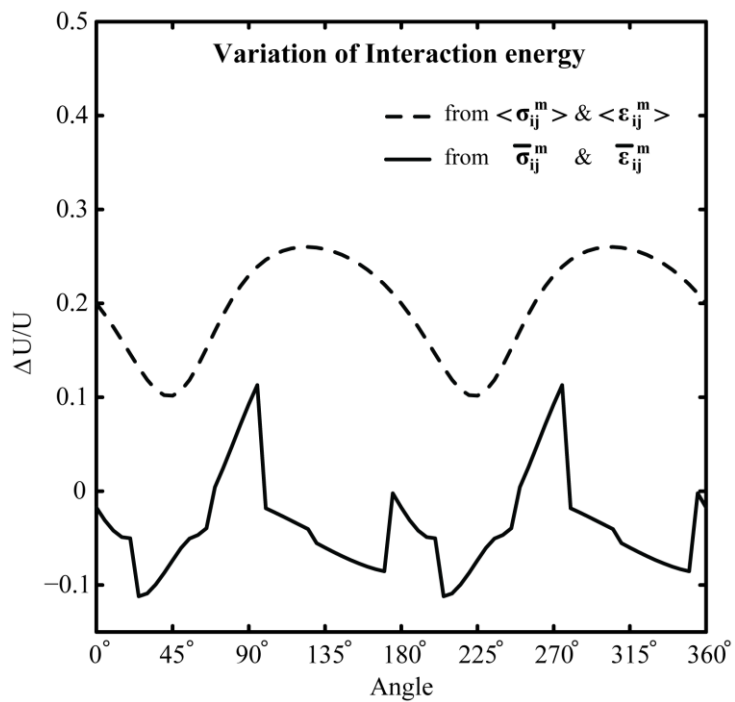
Figure 42: Interaction energy for test case-5
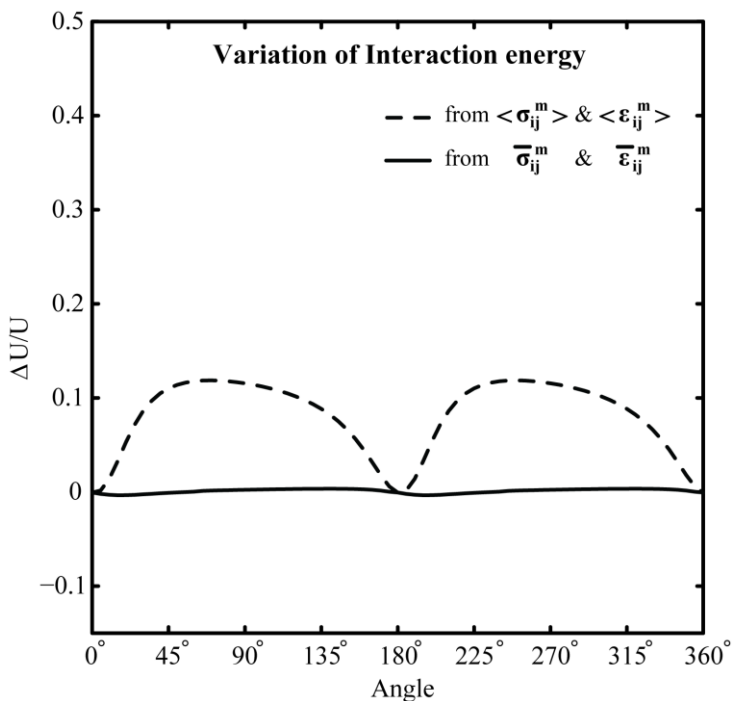
Figure 43: Interaction energy for test case-6
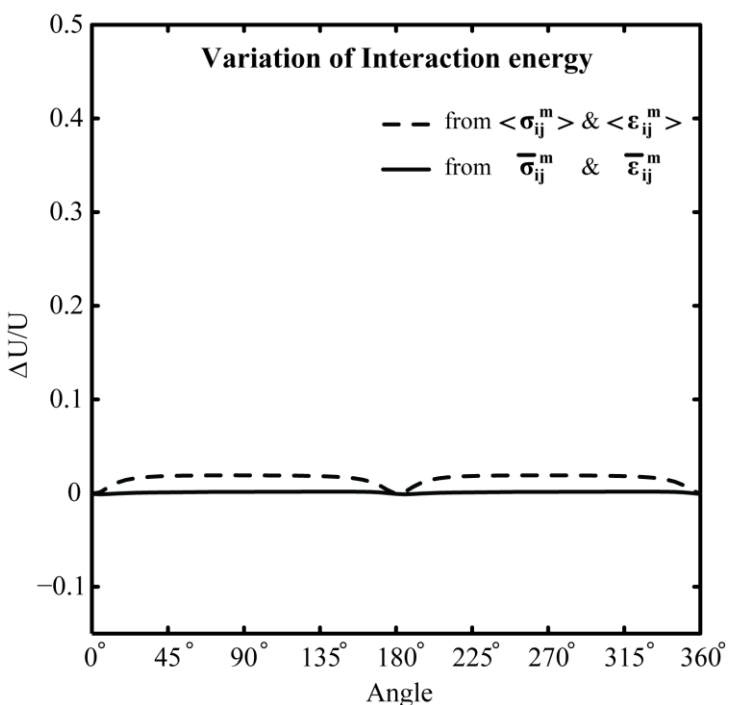
Figure 44: Interaction energy for test case-7

5.2 Modified Fertig failure theory

After calibration, Eqs. (5.5), (5.6) and (5.7) can be used to compute stress fluctuations of the matrix constituent for any type and magnitude of loading, material properties and type of distribution of fibers in the matrix. Using these stress fluctuations, augmented stresses of the matrix constituent can be determined using Eqs. (5.1) and (5.2). The modified Fertig failure theory uses energy consistent constituent stresses of the matrix constituent to predict matrix level failure. For the sake of clarity and continuity the modified approach is outlined below. Failure in the matrix constituent occurs when

$$B_t\{I_t\}^2 + \frac{1}{1 - \frac{\beta}{\tau_0}\{-I_h\}}\left[B_{s1}I_{s1} + B_{s2}I_{s2}\right] = 1 \tag{5.9}$$

where B_t, B_{s1}, B_{s2} represent the coefficients of the stress invariants of the matrix constituent; I_t, I_{s1}, I_{s2}, I_h represent the invariants of matrix stress tensor, τ_0 represents the shear strength of the matrix, and β represents pressure strengthening due to compressive loading, the value of which is chosen to be 0.35 (Hoppel et al., 1995b). The values of B_i are determined from three composite static failure tests: *transverse tension, transverse compression, and in-plane shear*, all of which involve failure of the matrix constituent. The invariants are computed from the augmented volume average matrix stresses as follows

91

$$I_t = \frac{\overline{\sigma}_{22}^m + \overline{\sigma}_{33}^m + \sqrt{\left(\overline{\sigma}_{22}^m + \overline{\sigma}_{33}^m\right)^2 - 4\left(\overline{\sigma}_{22}^m \overline{\sigma}_{33}^m - \overline{\sigma}_{23}^m \overline{\sigma}_{23}^m\right)}}{2} \tag{5.10}$$

$$I_{s1} = \overline{\sigma}_{12}^{m\,2} + \overline{\sigma}_{13}^{m\,2} \tag{5.11}$$

$$I_{s2} = \frac{1}{4}\left(\overline{\sigma}_{22}^m - \overline{\sigma}_{33}^m\right)^2 + \overline{\sigma}_{23}^{m\,2} \tag{5.12}$$

$$I_h = \overline{\sigma}_{22}^m + \overline{\sigma}_{33}^m \tag{5.13}$$

where $\overline{\sigma}_{ij}^m$ are energy consistent stresses of the matrix constituent, I_t corresponds to the maximum tensile stress normal to the fiber, I_{s1} is related to the in-plane shear, I_{s2} is related to the transverse shear, and I_h represents the pressure on the maximum transverse shear plane. The fiber failure criterion is outlined below

$$\frac{\sigma_{11}^f}{S_{11}^{f+}} = 1 \qquad \text{or} \qquad \frac{\sigma_{11}^f}{S_{11}^{f-}} = 1 \tag{5.12}$$

where σ_{11}^f is the volume average longitudinal stress of the fiber constituent, S_{11}^{f+} is the longitudinal tensile strength of the fiber and S_{11}^{f-} is the longitudinal compressive strength of the fiber. The different values of B_t, B_{s1}, B_{s2} that were obtained by using volume average stresses of the matrix constituent and energy consistent matrix level stresses are listed in Table 9.

Table 9: Comparison of B$_i$ parameters obtained by using volume average and energy consistent matrix level stresses

Test cases	B_t $\left(mm^2/N\right)$		B_{s1} $\left(mm^2/N\right)^2$		B_{s2} $\left(mm^2/N\right)^2$	
	$\left\langle \sigma_{ij}^m \right\rangle$	$\overline{\sigma}_{ij}^m$	$\left\langle \sigma_{ij}^m \right\rangle$	$\overline{\sigma}_{ij}^m$	$\left\langle \sigma_{ij}^m \right\rangle$	$\overline{\sigma}_{ij}^m$
1	0.001274	0.000832	0.000487	0.000303	0.000994	0.001114
2	0.001835	0.001408	0.000351	0.000244	0.000396	0.000458
3	0.000925	0.000606	0.000459	0.000287	0.000837	0.000912
4	0.000882	0.000643	0.000266	0.000164	0.000928	0.000591
5	0.000969	0.000622	0.000459	0.000287	0.000608	0.000796
6	0.000324	0.000213	0.000473	0.000292	0.000612	0.000583
7	0.000878	0.000399	0.000472	0. 000091	0.000682	0.000120

Table 10 contains the ratios of the parameters obtained by using volume average matrix level

stresses and energy consistent matrix level stresses.

Table 10: Comparison of ratios of the parameters obtained by using volume average matrix level stresses and energy consistent matrix level stresses.

Test cases	B_t $\left(mm^2/N\right)$	B_{s1} $\left(mm^2/N\right)^2$	B_{s1} $\left(mm^2/N\right)^2$
1	1.5313	1.6073	0.8923
2	1.3033	1.4385	0.8646
3	1.5264	1.5993	0.9178
4	1.3717	1.6220	1.5702
5	1.5579	1.5993	0.7638
6	1.5211	1.6199	1.0497
7	2.2005	5.1868	5.6833

5.3 Results

The failure load predictions obtained for lamina failure test cases of the World Wide Failure Exercises by using the Fertig failure theory with energy consistent stresses of the matrix constituent are presented in this section. The new failure plots are compared with available test data and the original predictions obtained with volume average matrix stresses.

Test case 1: GRP lamina under combined normal and shear loading

The failure predictions obtained by using energy consistent and volume average matrix stresses in the Fertig failure theory for a GRP lamina under combined normal and shear loadi
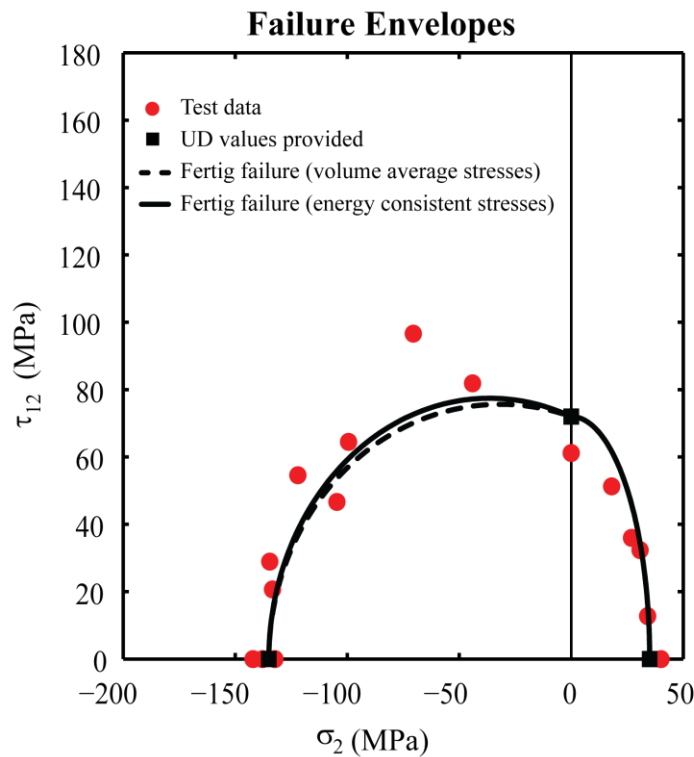

Figure 45: Comparison of failure load predictions for GRP
lamina under combined normal and shear loading

ng are shown in Fig. 45. The failure envelopes were the same in the $(+\sigma_{22}, \tau_{12})$ quadrant.

However, in the $(-\sigma_{22}, \tau_{12})$ quadrant, the failure envelope obtained by using energy consistent

matrix stresses was slightly better in capturing the high shear failure loads that the volume

average stresses failed to capture. Figure 46 shows the distribution of stresses in the RVE under

unit normal and shear load for two loading angles: 45 ° (first quadrant) and 135 ° (second

quadrant). Results show that the spread of the stress distribution in the transverse direction is

greater for the RVEs loaded at an angle of 45° in the first quadrant as compared to the one

loaded at an angle of 135 ° in the second quadrant. However, the shear stress distribution is

larger for the RVE loaded at an angle of 135° in the first quadrant as compared to the one

loadedat 45° in the second quadrant. Since maximum interaction energy occurs due to

fluctuations in the shear stress, augmented stresses are more accurate in the second quadrant in

this test case.
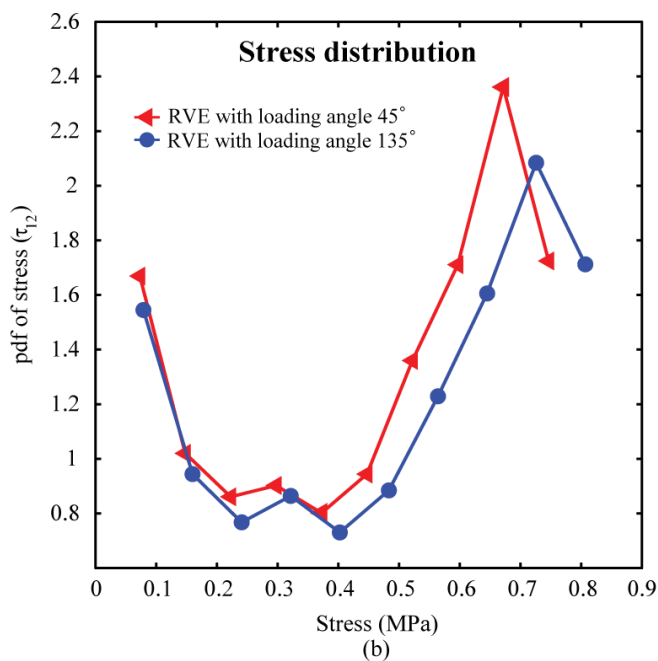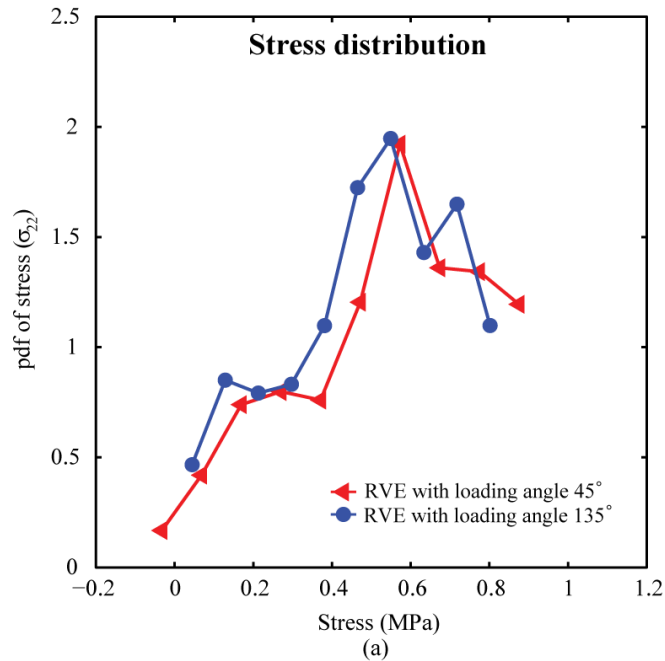
Figure 46: Comparison of stress distributions

Test case 2: CFRP lamina under combined longitudinal and shear loading

The failure predictions obtained by using volume average and energy consistent matrix stresses in the Fertig failure theory for a CFRP lamina under combined longitudinal and shear loading are shown in Fig. 47. The results suggest that the energy consistent matrix level stresses produced a no improvement in predicting failure loads for this load case. There is a large scatter of data especially in case of high shear failure loads which not captured by any failure theory of the first World Wide Failure Exercise.
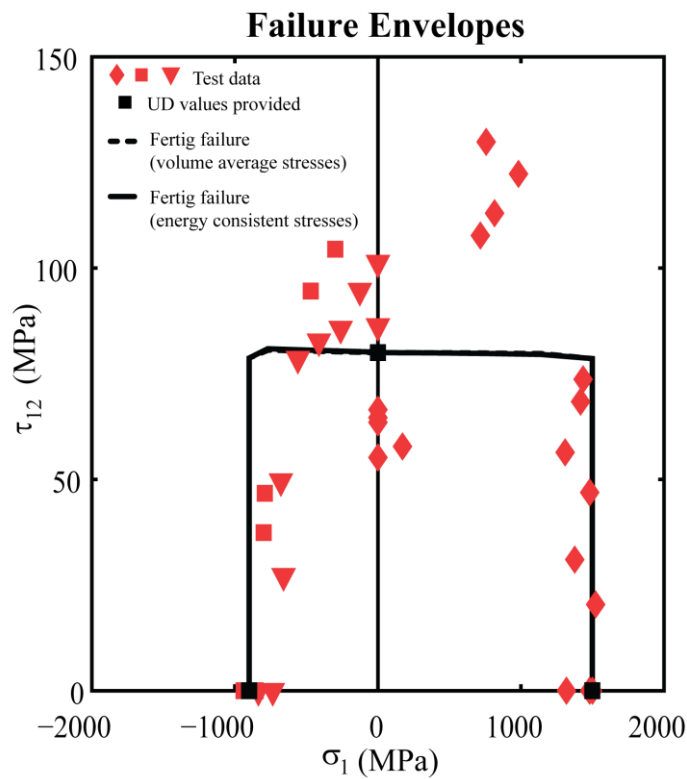
Figure 47: Comparison of failure load predictions for CFRP lamina under combined longitudinal and shear loading

Test case 3: GRP lamina under combined normal and longitudinal loading

The failure predictions obtained by using volume average and energy consistent matrix stresses in the Fertig failure theory for a GRP lamina under combined normal and longitudinal loading are shown in Fig. 48. Like test case 2, the energy consistent matrix level stresses failed to produce any significant improvement in the failure load predictions.
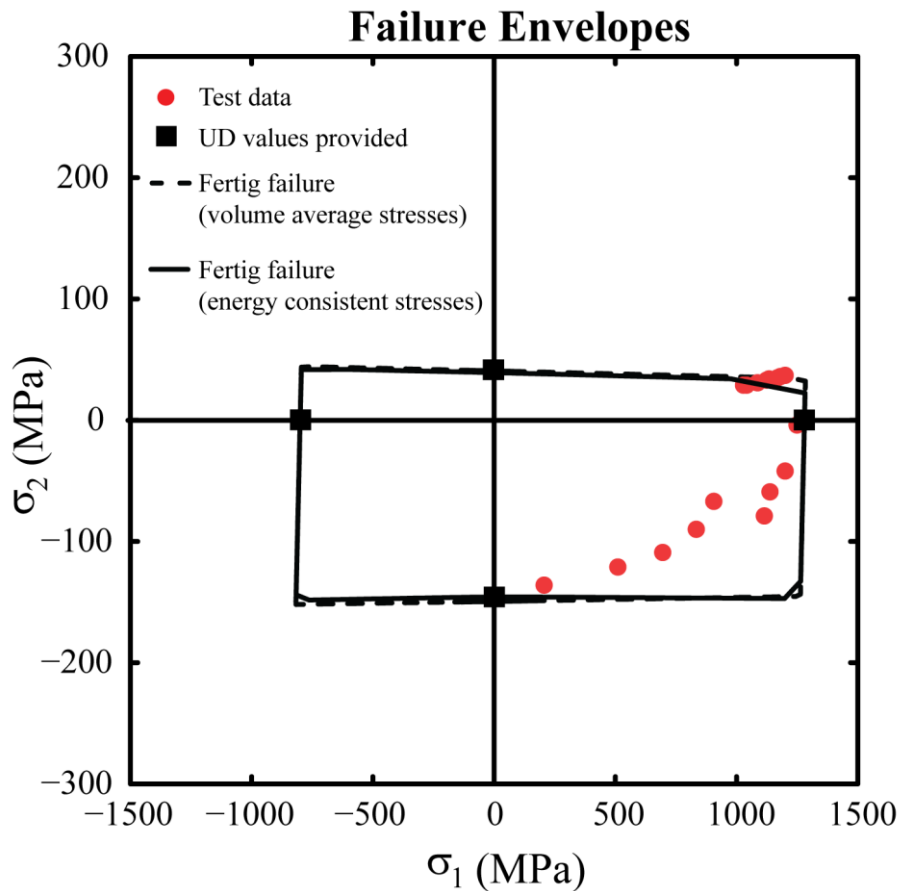

Figure 48: Comparison of failure load predictions for GRP lamina
under combined longitudinal and shear loading

The failure predictions obtained by using volume average and energy consistent matrix level stresses in the Fertig failure theory for a CFRP lamina under combined hydrostatic and shear loading are shown in Fig. 49. Overall the use of energy consistent matrix level stresses only slightly changed the failure envelope.
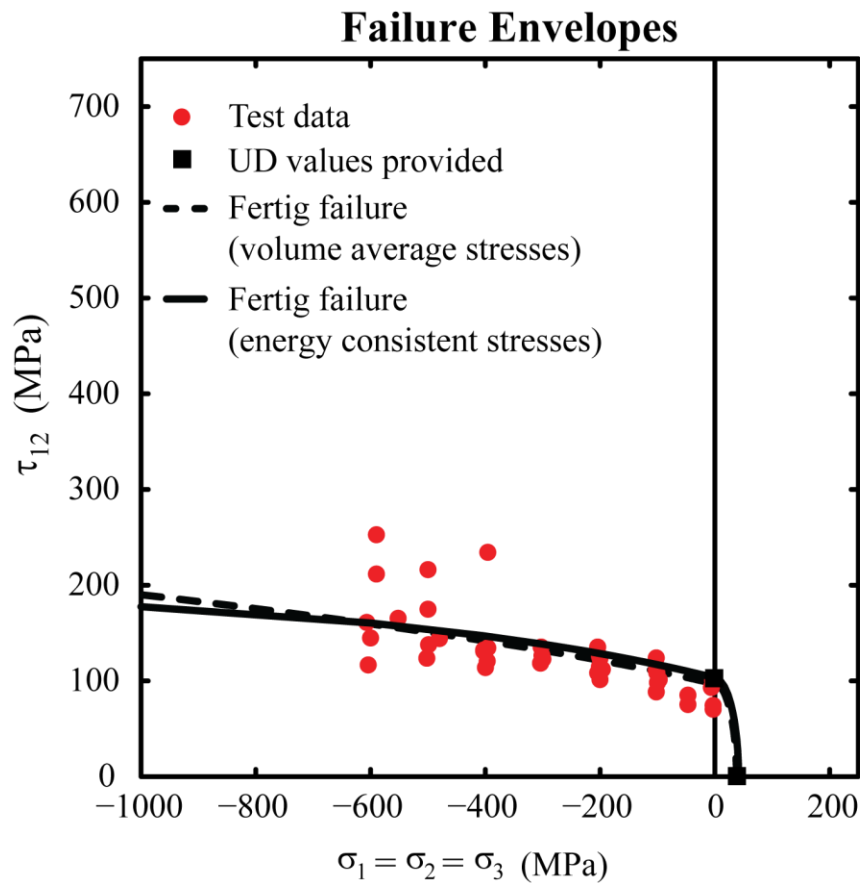

Figure 49: Comparison of failure load predictions for CFRP lamina under combined hydrostatic and shear loading

Test case 5: GRP lamina with combined normal and through thickness loading

The failure predictions obtained by using volume average and energy consistent matrix stresses in the Fertig failure theory for a GRP lamina under combined normal and through thickness loading are shown in Fig. 50. The use of energy consistent stresses produced a more conservative failure envelope as compared to that produced by volume average stresses of the matrix constituent.
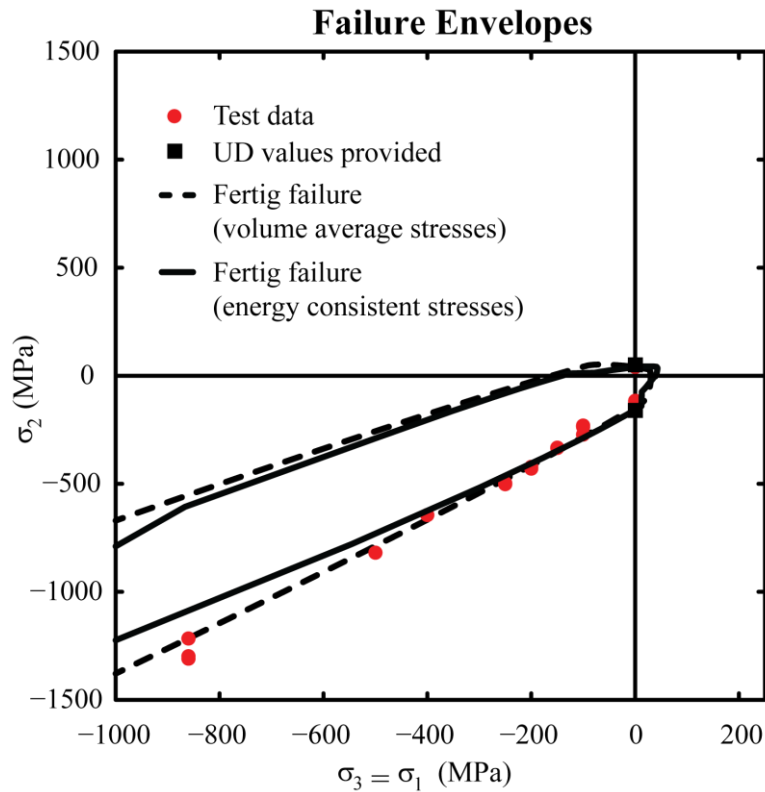
Figure 50: Comparison of failure load predictions for GRP lamina
under combined transverse and through thickness loading

Test case 6: GRP lamina with combined through thickness and longitudinal loading

The failure predictions obtained by using volume average and energy consistent matrix stresses in the Fertig failure theory for a GRP lamina under combined through thickness and longitudinal loading are shown in Fig. 51. The Fertig failure theory with energy consistent stresses for the matrix constituent predicted slightly higher matrix strengths under transverse and through thickness tension as compared to that predicted by using volume average stresses.
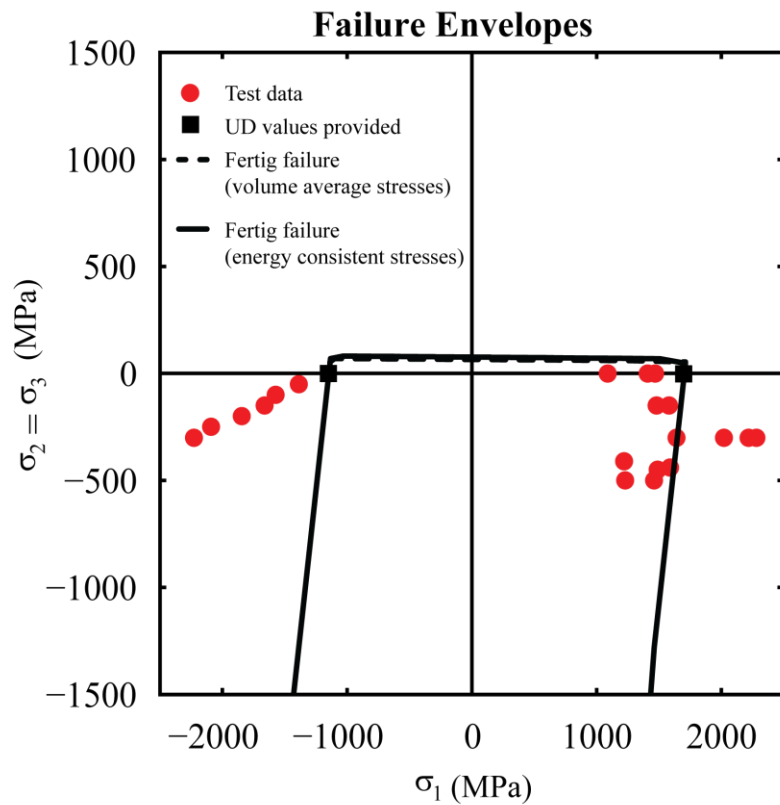
Figure 51: Comparison of failure load predictions for GRP lamina under combined through thickness and longitudinal loading

<u>Test case 7: CFRP lamina with combined through thickness and longitudinal loading</u>

The failure predictions obtained by using volume average and energy consistent matrix level stresses in the Fertig failure theory for a CFRP lamina under combined through thickness and longitudinal loading are shown in Fig. 52. Like test 6, the Fertig failure theory with energy consistent stresses for the matrix constituent did not lead to any improvement in the failure load predictions for this test case.
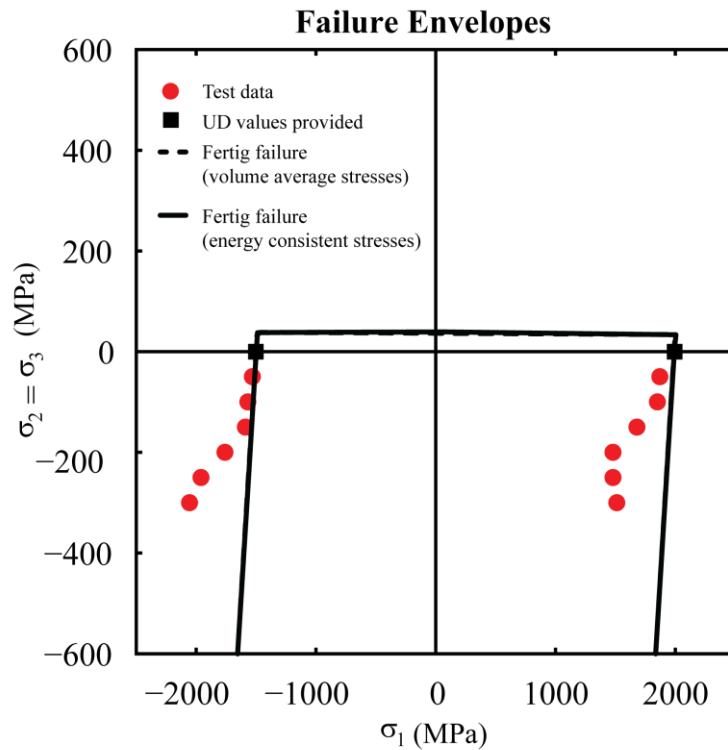

Figure 52: Comparison of failure load predictions for CFRP lamina for combined through thickness and longitudinal loading

5.4 Discussion

Volume average matrix constituent quantities do not capture the stress/strain fluctuations that arise in the constituents of a composite under different types of loading thereby giving rise to interaction energy. These fluctuations are greatest in the matrix constituent and are negligible in the fiber constituent of the composite material. Consequently, bulk of the Interaction energy contribution is due to the matrix constituent. Thus only the volume average stresses and strains of the matrix constituent need to be augmented with the fluctuations in stresses and strains respectively to improve failure load predictions. In this chapter a method of capturing the fluctuations in the matrix constituent was presented and the volume average quantities of the matrix quantities were augmented with these fluctuations. The new energy consistent stresses of the matrix constituent were then used with the Fertig failure theory to obtain failure load predictions for various lamina failure tests of the first and second World Wide Failure Exercise. The results were then compared with experimental test data and with the failure envelopes that were previously obtained using volume average matrix stresses in the Fertig failure theory.

The results show that for most of the test cases the energy consistent matrix stresses did not improve failure load predictions. In test case 5, the energy consistent matrix stresses led to prediction of a more conservative failure envelope as compared to that which was predicted using volume average matrix stresses. Even though the improvement in the strength predictions was by a very small amount in a couple of test cases (test cases 2 and 6), the matrix stresses used in failure load predictions were energy consistent and hence more accurate than their volume average counterparts. Lastly, now that the new stress metric is energy consistent, we know that any discrepancy in the failure load predictions and the experimental test data is not due to inaccurate stresses but because of the deficiencies in the failure theory itself. Thus one problem

has been solved and now we may direct our efforts towards other modifications to the failure theory to improve strength predictions in unidirectional fiber reinforced composite materials.

6. Conclusions and Recommendations

6.1. Summary and Conclusions

This study has detailed the motivation for creation of robust and reliable tools to predict failure in unidirectional fiber reinforced polymers based on micromechanical modeling using energy consistent volume average constituent level stresses. It was shown that volume average quantities (stresses/strains) of the constituents do not account for all the energy of the composite due to their inability to capture the stress/strain fluctuations of the constituents. This study showed that the missing energy, termed interaction energy, is dependent on the fiber volume fraction, material properties of the composite and the type of loading on the composite. The interaction energy was nearly 30% for composites with carbon fibers and epoxy matrix due to longitudinal shear loads and negligible for longitudinal tensile loads. Under transverse loads the interaction energy was about 12% and under transverse shear loads it was 15%.

A three parameter micromechanics based Fertig failure theory was used to asses failure loads for lamina failure tests of the first and the second World Wide Failure Exercises. This theory used volume average constituent level stresses to predict failure of the composite and thereby predict failure of the lamina. For almost all the test cases, the predictions of the theory were in close agreement with the test data. The theory assumes that the longitudinal stresses in the matrix constituent do not contribute in any failure mechanism which led to over-prediction of strengths under combined tensile longitudinal and compressive transverse loads for glass/epoxy composites. A maximum stress failure criterion was used to assess fiber failure due to which fiber failure due to fiber kinking mechanism was not predicted in two of the test cases. Some test cases were identified where failure loads could be improved by augmenting the matrix failure

theory with interaction energy. A von Mises – maximum principal stress failure criteria was also used to obtain failure envelope for one of the test cases where the Fertig failure theory over predicted the failure loads. A progressive damage scheme was used in which the properties of the matrix constituent in the failed lamina was degraded significantly thereby reducing the load carrying capacity of the matrix. The resultant loads carried by fibers were calculated using micromechanics. Results with this progressive modeling scheme were compared with one of the test cases where both the Fertig failure theory and the von Mises-Maximum principal stress failure theory. The failure envelope predicted by the von Mises-maximum principal stress theory described the mechanism of failure accurately and it was better than any of the leading failure theories. It was concluded that this theory with a similar progressive damage scheme would yield good results in the remaining test cases.

A new methodology was formulated to capture the stress-strain fluctuations of the matrix constituent and the volume average quantities of the matrix constituent were augmented with respective fluctuations. The energy consistent stresses were used along with the Fertig failure theory to predict failure envelopes for the lamina failure test cases of the first and second World Wide Failure Exercise. The results were then compared with experimental test data and the failure enveloped predicted by the same theory using un-augmented volume average stresses. The comparisons showed that the failure enveloped improved failure load predictions slightly for some of the test cases. Even though the improvement of the failure load predictions was not by a significant amount, the problem of interaction energy has been solved. It is well known that volume average constituent quantities do not capture the stress/fluctuations in the constituents of the composite material. Some of these fluctuations, which may play a role in failure mechanisms, self-equilibrate and produce no corresponding volume average stress/strain in the

constituent. The methodology that was developed in this thesis to compute energy consistent quantities (stresses and strains) provides a means to capture these stress/strain fluctuations and thereby improve the assessment of failure in composite.

6.2. Recommendations for future work

The failure theories that were ranked highest by the authors of the World Wide Failure Exercises can be categorized into two types. First – theories which were very simple in implementation and use and yet provided reasonably good results and second – theories which were complicated and involved a large number of parameters but gave very accurate predictions. The Fertig failure theory is micromechanics based theory which requires just three parameters that can be calibrated from three simple failure tests on unidirectional laminae. Moreover it incorporates physics to assess failure of the constituents of the composite. It is not as complicated as some of the leading failure theories and can be calibrated very easily. Comparisons showed that the predictions of the theory were in good agreement not only with the experimental data but also with the predictions of the leading failure theories of the world wide failure exercises. One of the test cases revealed that the theory needs to consider the effects of longitudinal stress of the matrix component to assess failure of the matrix constituent. Currently, failure of the fiber constituent is assessed using a maximum stress failure criterion which is why the theory could not predict fiber failure due to fiber kinking in a couple of test cases. The theory assumes linear elastic behavior of the constituents of the composite material and it would be interesting to look at the results when non-linear matrix behavior is incorporated. Only lamina failure test cases were analyzed since a progressive damage scheme for predicting cascading

laminate failure was not adopted. The use of energy consistent stresses coupled with non-linear behavior of the matrix and a progressive scheme will make the Fertig failure theory a powerful approach in the field of failure load predictions of FRPs.

Only unidirectional fiber reinforced composites were analyzed in this work but the modeling technique presented in the thesis can be extended to any kind of composite material. Lamina failure for only a select number of loading configurations was considered in this study exercise and the energy consistent stresses may yield improvements in some of the untested configurations.

References

Bogetti, T.A., Hoppel, C.P., Harik, V.M., Newill, J.F., and Burns, B.P. (2004a). Predicting the nonlinear response and progressive failure of composite laminates. Compos. Sci. Technol. *64*, 329–342.

Bogetti, T.A., Hoppel, C.P., Harik, V.M., Newill, J.F., and Burns, B.P. (2004b). Predicting the nonlinear response and failure of composite laminates: correlation with experimental results. Compos. Sci. Technol. *64*, 477–485.

Burke, R.C. (1983). Astronautics and Aeronautics.

Carrere, N., Laurin, F., and Maire, J. (2012). Micromechanical-based hybrid mesoscopic 3D approach for non-linear progressive failure analysis of composite structures. J. Compos. Mater. *46*, 2389–2415.

Carrere, N., Laurin, F., and Maire, J. (2013). Micromechanical-based hybrid mesoscopic three-dimensional approach for non-linear progressive failure analysis of composite structures—Part B: Comparison with experimental data. J. Compos. Mater. *47*, 743–762.

Christensen, R. (1997). Stress based yield/failure criteria for fiber composites. Int. J. Solids Struct. *34*, 529–543.

Cuntze, R. (2004). The predictive capability of failure mode concept-based strength criteria for multi-directional laminates—part B. Compos. Sci. Technol. *64*, 487–516.

Cuntze, R. (2012). The predictive capability of failure mode concept-based strength conditions for laminates composed of unidirectional laminae under static triaxial stress states. J. Compos. Mater. *46*, 2563–2594.

Cuntze, R. (2013). Comparison between experimental and theoretical results using Cuntze's "failure mode concept" model for composites under triaxial loadings—Part B of the second world-wide failure exercise. J. Compos. Mater. *47*, 893–924.

Cuntze, R., and Freund, A. (2004). The predictive capability of failure mode concept-based strength criteria for multidirectional laminates. Compos. Sci. Technol. *64*, 343–377.

Deuschle, H.M., and Kröplin, B.-H. (2012). Finite element implementation of Puck's failure theory for fibre-reinforced composites under three-dimensional stress. J. Compos. Mater. *46*, 2485–2513.

Deuschle, H.M., and Puck, A. (2013). Application of the Puck failure theory for fibre-reinforced composites under three-dimensional stress: Comparison with experimental results. J. Compos. Mater. *47*, 827–846.

Fertig III, R.S. (2012). Bridging the gap between physics and large-scale structural analysis: a novel method for fatigue life prediction of composites.

Garnich, M., and Hansen, A. (1997). A multicontinuum approach to structural analysis of linear viscoelastic composite materials. J. Appl. Mech. *64*, 795–803.

Gerstle, F., and Reedy, E. (1985). On the application of the maximum stress failure criterion to off-axis and angle-ply laminates. J. Compos. Mater. *19*, 505–512.

Gol'denblat, I., and Kopnov, V. (1965). Strength of glass-reinforced plastics in the complex stress state. Polym. Mech. *1*, 54–59.

Gotsis, P., Chamis, C.C., and Minnetyan, L. (1998). Prediction of composite laminate fracture: micromechanics and progressive fracture. Compos. Sci. Technol. *58*, 1137–1149.

Hart-Smith, L. (2002). Expanding the capabilities of the Ten-Percent Rule for predicting the strength of fibre–polymer composites. Compos. Sci. Technol. *62*, 1515–1544.

Hashin, Z. (1980). Failure criteria for unidirectional fiber composites. J. Appl. Mech. *47*, 329–334.

Hashin, Z. (1983). Analysis of composite materials—a survey. J. Appl. Mech. *50*, 481–505.

Herakovich, C.T. (2012). Mechanics of composites: A historical review. Mech. Res. Commun. *41*, 1–20.

Hill, R. (1963). Elastic properties of reinforced solids: some theoretical principles. J. Mech. Phys. Solids *11*, 357–372.

Hinton, M., and Kaddour, A. (2012). The background to the Second World-Wide failure exercise. J. Compos. Mater. *46*, 2283–2294.

Hinton, M., and Soden, P. (1998). Predicting failure in composite laminates: the background to the exercise. Compos. Sci. Technol. *58*, 1001–1010.

Hoppel, C.P., Bogetti, T.A., and Gillespie, J.W. (1995a). Literature Review-Effects of hydrostatic pressure on the mechanical behavior of composite materials. J. Thermoplast. Compos. Mater. *8*, 375–409.

Hoppel, C.P., Bogetti, T.A., and Gillespie, J.W. (1995b). Literature Review-Effects of hydrostatic pressure on the mechanical behavior of composite materials. J. Thermoplast. Compos. Mater. *8*, 375–409.

Huang, Z.-M. (2004). A bridging model prediction of the ultimate strength of composite laminates subjected to biaxial loads. Compos. Sci. Technol. *64*, 395–448.

Huang, Y., Xu, L., and Ha, S.K. (2012). Prediction of three-dimensional composite laminate response using micromechanics of failure. J. Compos. Mater. *46*, 2431–2442.

Kaddour, A., and Hinton, M. (2013). Maturity of 3D failure criteria for fibre-reinforced composites: Comparison between theories and experiments: Part B of WWFE-II. J. Compos. Mater. *47*, 925–966.

Kaddour, A., Hinton, M., Smith, P., and Li, S. (2013). The background to the third world-wide failure exercise. J. Compos. Mater. *47*, 2417–2426.

Knox, C.E. (1982). Fiberglass reinforcement. In Handbook of Composites, (Springer), pp. 136–159.

Kuraishi, A., Tsai, S.W., and Liu, K.K. (2002). A progressive quadratic failure criterion, part B. Compos. Sci. Technol. *62*, 1683–1695.

Liu, K.-S., and Tsai, S.W. (1998). A progressive quadratic failure criterion for a laminate. Compos. Sci. Technol. *58*, 1023–1032.

Mayes, J.S., and Hansen, A.C. (2004). Composite laminate failure analysis using multicontinuum theory. Compos. Sci. Technol. *64*, 379–394.

Mukhopadhyay, S., and Sakthivel, J. (2005). Spider Silk–Providing New Insights in the Field of High Performance Materials. J. Ind. Text. *35*, 91–113.

Nahas, M. (1986). Yield and ultimate strengths of fibre composite laminates. Compos. Struct. *6*, 283–294.

Nelson, E.E., Hansen, A.C., and Mayes, J.S. (2012). Failure analysis of composite laminates subjected to hydrostatic stresses: A multicontinuum approach. J. Compos. Mater. *46*, 2461–2483.

Nicholson, P.T., and Shaw, I. (2000). Ancient Egyptian materials and technology (Cambridge University Press).

De Oliveira, J.Á., Paciornik, S., and d' Almeida, J. (2009). Microstructural analysis of composite tubes through digital microscopy. J. Compos. Mater. *43*, 1857–1868.

Pinho, S., Darvizeh, R., Robinson, P., Schuecker, C., and Camanho, P. (2012). Material and structural response of polymer-matrix fibre-reinforced composites. J. Compos. Mater. *46*, 2313–2341.

Pinho, S., Vyas, G., and Robinson, P. (2013). Material and structural response of polymer-matrix fibre-reinforced composites: Part B. J. Compos. Mater. *47*, 679–696.

Puck, A., and Schürmann, H. (1998). Failure analysis of FRP laminates by means of physically based phenomenological models. Compos. Sci. Technol. *58*, 1045–1067.

Puck, A., and Schürmann, H. (2002). Failure analysis of FRP laminates by means of physically based phenomenological models. Compos. Sci. Technol. *62*, 1633–1662.

Rotem, A. (1998). Prediction of laminate failure with the Rotem failure criterion. Compos. Sci. Technol. *58*, 1083–1094.

Rowell, R.M. (2012). Handbook of wood chemistry and wood composites (CRC press).

Soden, P., Kaddour, A., and Hinton, M. (2004). Recommendations for designers and researchers resulting from the world-wide failure exercise. Compos. Sci. Technol. *64*, 589–604.

Sun, C.T., and Vaidya, R.S. (1996). Prediction of composite properties, from a representative volume element. Compos. Sci. Technol. *56*, 171–179.

Talley, C.P. (2004). Mechanical properties of glassy boron. J. Appl. Phys. *30*, 1114–1115.

Timot, S.W. (1961). Electrically conducting fibrous carbon.

Tsai, S.W., and Wu, E.M. (1971). A general theory of strength for anisotropic materials. J. Compos. Mater. *5*, 58–80.

Vollrath, F., Holtet, T., Thogersen, H.C., and Frische, S. (1996). Structural organization of spider silk. Proc. R. Soc. Lond. B Biol. Sci. *263*, 147–151.

Zhou, Y.-X., and Huang, Z.-M. (2012). A bridging model prediction of the ultimate strength of composite laminates subjected to triaxial loads. J. Compos. Mater. *46*, 2343–2378.

Zinoviev, P.A., Grigoriev, S.V., Lebedeva, O.V., and Tairova, L.P. (1998). The strength of multilayered composites under a plane-stress state. Compos. Sci. Technol. *58*, 1209–1223.

Zinoviev, P.A., Lebedeva, O.V., and Tairova, L.P. (2002). A coupled analysis of experimental and theoretical results on the deformation and failure of composite laminates under a state of plane stress. Compos. Sci. Technol. *62*, 1711–1723.

Appendix A: Periodic boundary conditions

The naming convention as shown in Fig. X was adopted to derive the periodic boundary conditions for the Representative Volume Element (RVE) which is a cuboid where CN1, CN2,…, CN8- are node sets that contain the nodes on the eight corners (vertices) of the cuboid, ES1, ES2, ES3, ES4, LS1, LS2, LS3 and LS4 are node sets that contain the nodes on the edges of the cuboid. These node sets do not contain the nodes on the corners of the cuboid. FS1, FS2,…, FS6 are node sets that contain the nodes on the six faces of the cuboid. These node sets do not contain the nodes on the edges and the corners of the cuboid.
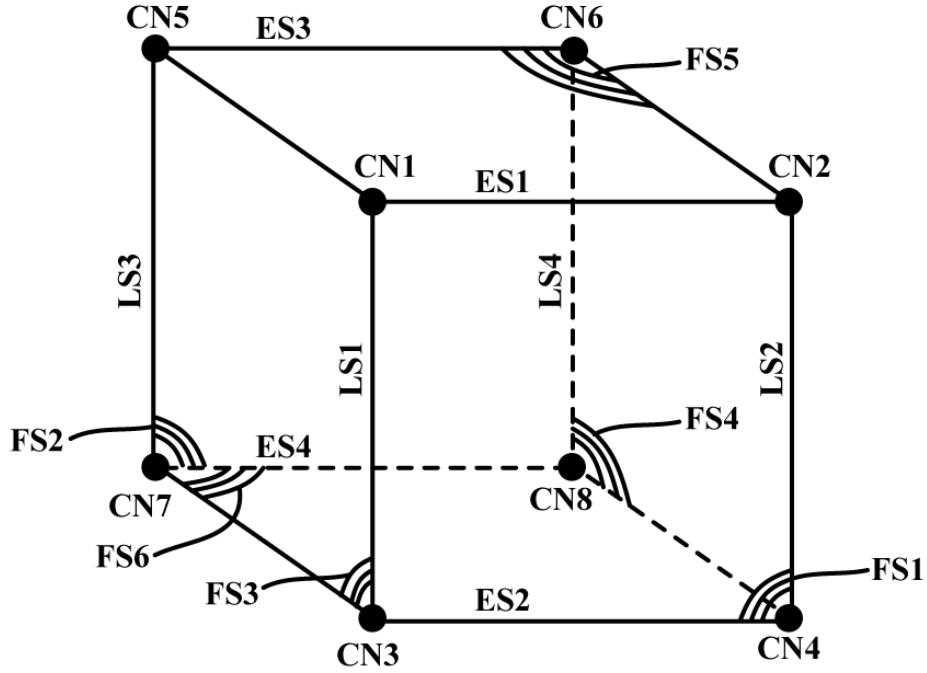
Figure 53: Naming convention for node sets of the Representative Volume Element

The equation constraints for nodes on the corners are

$$u_i^{CN6} - u_i^{CN2} - u_i^{CN7} = 0$$

$$u_i^{CN3} - u_i^{CN4} - u_i^{CN7} = 0$$

$$u_i^{CN5} - u_i^{CN6} - u_i^{CN7} = 0$$

$$u_i^{CN2} - u_i^{CN6} - u_i^{CN4} = 0$$

where $i = 1,2,3$ denotes the directions and u denotes the displacements of corner nodes in the i-direction.

The equation constraints for nodes on the edges are

$$u_i^{LS1} - u_i^{LS2} - u_i^{CN7} = 0$$

$$u_i^{LS2} - u_i^{LS4} - u_i^{CN4} = 0$$

$$u_i^{LS3} - u_i^{LS2} + u_i^{CN4} - u_i^{CN7} = 0$$

$$u_i^{LS5} - u_i^{LS6} - u_i^{CN7} = 0$$

$$u_i^{LS7} - u_i^{LS6} + u_i^{CN6} - u_i^{CN7} = 0$$

$$u_i^{LS6} - u_i^{LS8} - u_i^{CN6} = 0$$

$$u_i^{ES1} - u_i^{ES2} - u_i^{CN6} = 0$$

$$u_i^{ES3} - u_i^{ES4} - u_i^{CN6} = 0$$

$$u_i^{ES2} - u_i^{ES4} - u_i^{CN4} = 0$$

where $i = 1,2,3$ denotes the directions and u denotes the displacements of corner and edge nodes in the i-direction. The equation constraints for nodes on the faces are

$$u_i^{FS1} - u_i^{FS2} - u_i^{CN4} = 0$$

$$u_i^{FS3} - u_i^{FS4} - u_i^{CN7} = 0$$

$$u_i^{FS5} - u_i^{FS6} - u_i^{CN6} = 0$$

where $i = 1,2,3$ denotes the directions and u denotes the displacements of corner and face nodes in the i-direction.

Appendix B: Influence coefficients for the fiber and matrix constituents of composites of

the World Wide Failure Exercises

1. Fibers

1.1 E-glass

$$
X_{E-glass} = \begin{bmatrix}
1.5718 & -0.1726 & -0.1730 & 0.0005 & -0.0001 & 0.0000 \\
-0.0024 & 1.1548 & -0.0634 & 0.0020 & 0.0000 & 0.0000 \\
-0.0024 & -0.0629 & 1.1540 & 0.0004 & -0.0002 & 0.0000 \\
0.0001 & 0.0005 & 0.0002 & 1.2274 & 0.0000 & 0.0000 \\
0.0000 & 0.0000 & -0.0001 & 0.0000 & 1.2266 & 0.0005 \\
0.0000 & 0.0000 & 0.0000 & 0.0000 & 0.0005 & 1.2167
\end{bmatrix}
$$

1.2 T-300

$$X_{T300} = \begin{bmatrix} 1.6478 & -0.2151 & -0.2154 & 0.0002 & -0.0001 & 0.0000 \\ -0.0010 & 1.1024 & -0.0639 & 0.0009 & -0.0001 & 0.0000 \\ -0.0010 & -0.0635 & 1.1019 & 0.0001 & -0.0004 & 0.0000 \\ 0.0000 & 0.0003 & 0.0002 & 1.2225 & 0.0000 & 0.0000 \\ 0.0000 & 0.0000 & -0.0002 & -0.0000 & 1.2217 & 0.0004 \\ 0.0000 & 0.0000 & 0.0000 & -0.0001 & 0.0002 & 1.1654 \end{bmatrix}$$

1.3 S-glass

$$X_{S-glass} = \begin{bmatrix} 1.6261 & -0.1887 & -0.1891 & 0.0004 & -0.0002 & 0.0000 \\ -0.0023 & 1.1630 & -0.0637 & 0.0018 & -0.0003 & 0.0001 \\ -0.0023 & -0.0633 & 1.1622 & 0.0005 & -0.0007 & 0.0000 \\ 0.0000 & 0.0005 & 0.0001 & 1.2412 & 0.0000 & 0.0000 \\ 0.0000 & 0.0000 & -0.0002 & -0.0000 & 1.2404 & 0.0005 \\ 0.0000 & 0.0000 & 0.0000 & -0.0001 & 0.0003 & 1.2257 \end{bmatrix}$$

1.4 AS4

$$X_{AS4} = \begin{bmatrix} 1.6518 & -0.2118 & -0.2122 & 0.0002 & -0.0001 & 0.0000 \\ -0.0008 & 1.1151 & -0.0643 & 0.0010 & -0.0001 & 0.0000 \\ -0.0008 & -0.0639 & 1.1146 & 0.0001 & -0.0004 & -0.0000 \\ 0.0000 & 0.0003 & 0.0002 & 1.2285 & 0.0000 & -0.0000 \\ -0.0000 & -0.0000 & -0.0002 & -0.0000 & 1.2278 & 0.0004 \\ 0.0000 & -0.0000 & 0.0000 & -0.0001 & 0.0002 & 1.1786 \end{bmatrix}$$

2.   Matrix

2.1 LY556

$$X_{LY556} = \begin{bmatrix} 0.0686 & 0.2812 & 0.2819 & 0.0016 & -0.0002 & 0.0000 \\ 0.0039 & 0.7479 & 0.1032 & 0.0007 & -0.0001 & 0.0000 \\ 0.0039 & 0.1026 & 0.7491 & 0.0008 & -0.0001 & 0.0000 \\ 0.0000 & 0.0002 & -0.0002 & 0.6295 & 0.0000 & 0.0000 \\ 0.0000 & 0.0000 & 0.0000 & 0.0000 & 0.6308 & -0.0001 \\ 0.0000 & 0.0000 & 0.0000 & 0.0000 & 0.0000 & 0.6470 \end{bmatrix}$$

2.2 BSL914C

$$X_{BSL914C} = \begin{bmatrix} 0.0297 & 0.3222 & 0.3227 & 0.0010 & -0.0005 & 0.0000 \\ 0.0015 & 0.8467 & 0.0957 & 0.0001 & -0.0002 & 0.0000 \\ 0.0015 & 0.0951 & 0.8474 & 0.0004 & -0.0001 & 0.0000 \\ 0.0000 & 0.0002 & -0.0002 & 0.6668 & 0.0000 & -0.0001 \\ 0.0000 & 0.0000 & 0.0000 & 0.0000 & 0.6679 & -0.0001 \\ 0.0000 & 0.0000 & 0.0000 & 0.0000 & -0.0001 & 0.7523 \end{bmatrix}$$

2.3 MY750

$$X_{MY750} = \begin{bmatrix} 0.0761 & 0.2811 & 0.2818 & 0.0013 & -0.0006 & 0.0000 \\ 0.0042 & 0.7592 & 0.0974 & 0.0006 & -0.0003 & 0.0000 \\ 0.0042 & 0.0968 & 0.7604 & 0.0007 & -0.0003 & 0.0000 \\ 0.0000 & 0.0002 & -0.0002 & 0.6396 & 0.0000 & -0.0001 \\ 0.0000 & 0.0000 & -0.0001 & 0.0000 & 0.6408 & -0.0001 \\ 0.0000 & 0.0000 & 0.0000 & 0.0000 & 0.0000 & 0.6633 \end{bmatrix}$$

2.4 PR319

$$X_{PR319} = \begin{bmatrix} 0.0071 & 0.3023 & 0.3029 & 0.0013 & -0.0006 & 0.0000 \\ 0.0004 & 0.7687 & 0.1006 & 0.0005 & -0.0003 & 0.0000 \\ 0.0004 & 0.1000 & 0.7697 & 0.0006 & -0.0003 & 0.0000 \\ 0.0000 & 0.0002 & -0.0002 & 0.6316 & 0.0000 & -0.0001 \\ 0.0000 & 0.0000 & -0.0001 & 0.0000 & 0.6329 & -0.0001 \\ 0.0000 & 0.0000 & 0.0000 & 0.0000 & 0.0000 & 0.6695 \end{bmatrix}$$

2.5 Epoxy

$$X_{Epoxy} = \begin{bmatrix} 0.0238 & 0.3173 & 0.3177 & 0.0011 & -0.0005 & 0.0000 \\ 0.0012 & 0.8275 & 0.0963 & 0.0002 & -0.0002 & 0.0000 \\ 0.0012 & 0.0958 & 0.8283 & 0.0004 & -0.0001 & 0.0000 \\ 0.0000 & 0.0002 & -0.0002 & 0.6577 & 0.0000 & -0.0001 \\ 0.0000 & 0.0000 & 0.0000 & 0.0000 & 0.6589 & -0.0001 \\ 0.0000 & 0.0000 & 0.0000 & 0.0000 & -0.0001 & 0.7326 \end{bmatrix}$$